INSIGHTS FROM MURINE MODELS OF NEUROFIBROMATOSIS TYPE I: THE ETIOLOGY AND APPROPRIATE THERAPEUTIC WINDOWS FOR PERIPHERAL NERVE SHEATH TUMORS

by

Lou Chang

A dissertation submitted in partial fulfillment
of the requirements for the degree of
Doctor of Philosophy
(Cell and Developmental Biology)
in the University of Michigan
2011

Doctoral Committee:

Associate Professor Yuan Zhu, Chair
Professor Eric Fearon
Assistant Professor Scott Barolo
Assistant Professor Diane Fingar
Assistant Professor Ivan Patrick Maillard

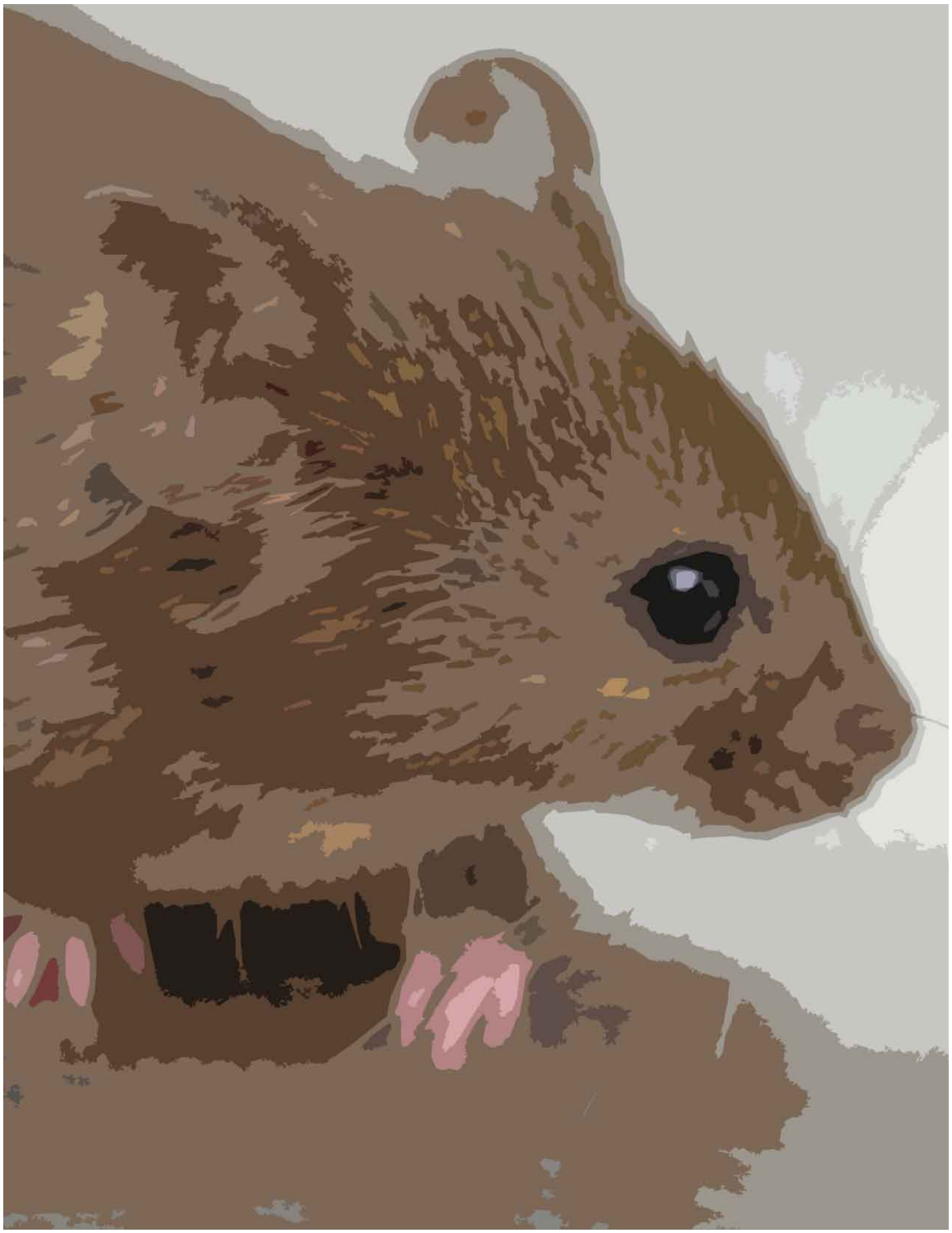

DEDICATION

This thesis is dedicated to all the family and patients afflicted with Neurofibromatosis Type I. One day there will be a cure.

ACKNOWLEDGEMENTS

I would like to thank Dr. Huarui Zheng for his collaboration and discussions regarding my thesis topic. He has contributed invaluable data that greatly strengthened the scientific merit of this work. Figure 6 and 25 of this thesis should be attributed to Dr. Zheng. All the current and past members of the Zhu Lab must be acknowledged for their unwavering support and encouragement. I am especially grateful to Jessica Lee, Neha Patel, Daniel Treisman, Seçkin Ackgül and Yinghua Li for their collaboration in various experiments.

This body of work would not be possible if not for Dr. Yuan Zhu, who has provided extensive guidance, support and vigorous scientific discussions during my training. His knowledge of the field, scientific rigor and work ethic provided me a model of a successful scientist. I sincerely feel that his tutelage has helped me become a better scientist and a more disciplined, responsible individual. Figures 4 and 7 should be attributed to Dr. Zhu.

I would like to acknowledge Dr. David Lucas for our discussions on the histopathology of peripheral nerve sheath tumors and other sarcomas; the Microscopy Image Analysis Laboratory, especially Dorothy Sorenson and Sasha Meshinchi, for their preparation of TEM sections and training; the Morrison Lab, especially Dr. Nancy Joseph, for training in cell culture and flow cytometry, and participation in generation of data based on these techniques; Center for Statistical Consultation and Research, especially Joe Kazemi, for training in mixed models and statistical software packages.

Finally, I want to thank Jaime Chandler, my sister and my parents for loving me despite my eccentricities. Their psychosocial contribution to this thesis has been immeasurable. My sister, 昌加佳, is responsible for the frontispiece.

TABLE OF CONTENTS

LIST OF FIGURES

LIST OF TABLES

LIST OF ABBREVIATIONS

BLBP	Brain lipid binding protein
BP	Brachial plexus
BrdU	5'-Bromodeoxyuridine
CALM	café-au-lait macule
CKO	Conditional knockout
CMT	Charcot-Marie-Tooth
CN	Cutaneous Nerve
DRG	Dorsal root ganglia
EM	Electron microscopy
ERK	Extracellular-signal-regulated kinase
FACS	Fluorescence-activated cell sorting
GDP	Guanosine diphosphate
GEM	Genetically engineered mouse
GFAP	Glial fibrillary acidic protein
GTP	Guanosine triphosphate
H&E	Hematoxylin and eosin
Hyperplasia/NF	Hyperplasia with focal neurofibroma
IHC	Immunohistochemical
KO	Knockout
LOH	Loss of heterozygosity
MPNST	Malignant peripheral nerve sheath tumor
mSC	Myelinating Schwann Cell
mTOR	Mammalian target of rapamycin
mTORC1	Mammalian target of rapamycin complex 1
NCC	Neural crest cell

NIH	National Institute of Health
nmSC	Non-myelinating Schwann Cell
NF1	Neurofibromatosis type 1
NPcis	*Nf1*/*p53* cis chromosome
NPtrans	*Nf1*/*p53* trans chromosomes
P22	Postnatal day 22
P90	Postnatal day 90
$p75^{NGFR}$	p75 low-affinity nerve growth factor receptor
PCC	Pheochromocytoma
pNF	Plexiform Neurofibroma
PNS	Peripheral nervous system
PNST	Peripheral nerve sheath tumor
R26R-LacZ	Rosa26-LacZ reporter
RB	Retinoblastoma
S6	Ribosomal protein S6
SN	Sciatic Nerve
anmSC	Abnormal non-myelinating Schwann cell
dSC	Dissociating Schwann cell
uSC	Unassociated Schwann cell
TEM	Transmission electron microscopy
TN	Trigeminal Nerve
TSC	Tuberous Sclerosis Complex
TUNEL	Terminal deoxynucleotidyl transferase-mediated deoxyuridine triphosphate nick-end labeling
WHO	World Health Organization

CHAPTER I

Introduction and Literature Review

Clinical Features of Neurofibromatosis Type I

Neurofibromatosis type I (NF1), also known as von Recklinghausen disease, is one of the most common monoallelic genetic disorders in humans, afflicting between 1 in 3000 to 4000 newborns (McClatchey, 2007). The incidence of this disease does not vary depending on sex or ethnicity (Friedman, 1999). The NF1 disease is caused by a germline mutation in a single gene termed *NF1*, and the disease displays an autosomal dominant pattern of inheritance. Despite this familial manner of inheritance, approximately 50% of all documented cases occur from *de novo* mutations, likely due to the *NF1* gene having large genomic footprint and an elevated rate of *NF1* germ cell mutations (estimated 1 X 10^{-4} per gamete per generation) (Huson et al., 1988). As there is a significant proportion of the population suffering from this disease and a lack of an effective cure, development of effective therapeutic strategies is the ultimate goal of current NF1 research.

Table 1 - NIH Diagnostic Criteria for Neurofibromatosis Type I (Patients must have two or more of these features).

Six or more café-au-lait macules: **over 5 mm in greatest diameter in pre-pubertal individuals** **over 15 mm in greatest diameter in post-pubertal individuals**
Two or more neurofibromas of any type or one plexiform neurofibroma
Freckling in the axillary or inguinal regions (Crowe's sign)
Optic glioma
Two or more Lisch nodules (iris harmatomas)
A distinctive bony lesion such as a sphenoid dysplasia or thinning of long bone cortex
A first-degree relative with NF1 by the above criteria

NF1 patients display variable expressivity of disease features, prompting the National Institute of Health (NIH) to develop a set of diagnostic criteria that encompasses the most common characteristic features of NF1 (Table 1) (Gutmann et al., 1997). While only some clinical features may develop, disease manifestations are highly associated with age of the patient. Café-au-lait macules (CALMs), symptomatic optic glioma and distinctive bony lesions uniformly appear at birth, axillary freckling by age 4, and Lisch nodules at age 10 (DeBella et al., 2000). Symptomatic plexiform neurofibromas are often diagnosed before the age of 5 (Waggoner et

al., 2000), while dermal neurofibromas tend to manifest during puberty and pregnancy (Theos and Korf, 2006). This well-established timing of symptoms associated with NF1 patients suggests that the NF1 gene may be involved in various developmental processes.

A devastating characteristic of NF1 is a predisposition to developing peripheral nerve sheath tumors (PNSTs). Together, PNSTs account for the majority of morbidity and mortality associated with NF1 (Rasmussen et al., 2001). Benign tumors or neurofibromas can broadly be characterized into two categories: dermal neurofibromas and plexiform neurofibromas (pNFs) (Woodruff, 1999). Both types of neurofibromas are thought to arise from the peripheral nerves and are heterogeneous masses comprised of the normal cellular compartment found in peripheral nerves: Schwann cells, fibroblasts, mast cells, pericytes and neuronal processes. Dermal neurofibromas are the most common form of neurofibromas and are present in most NF1 patients by the end of puberty (Friedman and Birch, 1997). These benign dermal or subcutaneous tumors are well-circumscribed with a nodular growth pattern. While these tumors often cause nuisance or psychological stress to NF1 patients, they pose little threat to their health as dermal neurofibromas are not believed to have the potential to undergo malignant transformation (Zhu and Parada, 2002). pNFs can be detected in over 50% of NF1 patients by whole-body MRI (Mautner et al., 2008), but traditionally only has a 30% rate of diagnosis based on symptoms (Korf, 1999). These tumors are far more insidious for several reasons: (1) they can grow in functionally critical locations, cutting off blood supply or impinging normal organ function, (2) their rapid diffuse growth patterns along the nerve sheath, potentially compromising normal nerve function, and most importantly (3) their propensity for malignant transformation into malignant peripheral nerve sheath tumors (MPNSTs). Natural history studies have found the growth pattern of pNFs to be variable and unpredictable (Friedman, 1999), but tumor growth rates tend to exceed body weight gain and to be faster in younger patients (Dombi et al., 2007), stressing that therapies should be developed for these young patients. An intriguing observation is the presumably congenital pNFs have the potential to undergo malignant transformation while the pubescent dermal neurofibromas do not. These observations suggest that these two neurofibroma subtypes may have different cells-of-origin and/or tumor differentiation states.

MPNSTs are the primary cause of death for NF1 patients (Evans et al., 2002), who as a result have a decreased life expectancy of 15 years (Rasmussen et al., 2001). Individuals afflicted

with NF1 have a lifetime risk between 7 to 13% of developing MPNSTs (Evans et al., 2002), and those with pre-existing pNFs have nearly a 20-fold increased incidence of malignant transformation (Tucker et al., 2005). Of diagnosed MPNSTs, more than 80% are high grade tumors, corresponding to the Whole Health Organization (WHO) grade III-IV (Woodruff, 1999). While surgical resection is the only treatment method to show improved survival, the often sensitive location and invasive growth pattern of MPNSTs often precludes the possibility of complete resection (Ducatman et al., 1986). Combined with resistance to therapeutic modalities such as chemotherapy and radiotherapy, the 5-year survival of patients with MPNSTs is estimated to be between 42-54% (Hagel et al., 2007; McCaughan et al., 2007).

NF1 patients are far more likely to develop PNSTs than the general population. Dermal neurofibromas can arise in the general population, but are usually solitary; in contrast, NF1 patients can have a range between tens to hundreds of these benign tumors (Easton et al., 1993; Pasmant et al., 2010). Plexiform neurofibromas have been described as pathognomonic to NF1 patients, but this has been challenged by case studies describing solitary pNFs in individuals who do not meet the NIH criteria for Nf1 (Fisher et al., 1997; Lin et al., 2004). Regardless, the incidence of plexiform neurofibromas in the general population is so low that an accurate assessment of relative risk is currently not possible. Despite MPNSTs accounting for 10% of diagnosed sarcomas, sporadic MPNSTs are diagnosed in only about 0.001% of the general population (Ducatman et al., 1986). The median age of diagnosis for MPNSTs is 26 for NF1 patients and 62 in sporadic MPNSTs (Ducatman et al., 1986). NF1 patients are 113 to 160 times more likely to develop MPNSTs compared to the general population (Brems et al., 2009; King et al., 2000). This translates into NF1 patients accounting for half of all new MPNSTs diagnoses. The epidemiology of NF1-associated tumors is sharply different from other common epithelial cancers in terms of tumor contribution from sporadic and familial patients, where the incidence of tumors in the sporadic population is typically several thousand-fold higher. Colorectal cancer, for example, has a 5% incidence in individuals over the age of 70 in the general population (Kinzler and Vogelstein, 1996). Together, these statistics suggests that a single mutation in the *NF1* gene transforms the peripheral nerve, a tumor resistant organ, into one that is highly susceptible to peripheral nerve sheath tumors.

Molecular and Genetic characterization of *NF1* and neurofibromin

The discovery of the *NF1* gene in 1990 facilitated molecular characterization of the NF1 disease and presented the first step towards an understanding of the pathogenesis of peripheral nerve sheath tumors (Cawthon et al., 1990; Viskochil et al., 1990; Wallace et al., 1990). The *NF1* gene occupies approximately 350,000 base pairs on chromosome 17 in humans and on chromosome 11 in mice. This gene encodes a 2818 amino acid long protein with a molecular weight of 317 kDa called Neurofibromin (Gutmann et al., 1991).

Although the function of the Neurofibromin protein is not yet fully characterized, a domain has been identified that shares significant homology with GTPase-activating protein (GAP) family members and has been demonstrated to have GAP activity (Ballester et al., 1990; Buchberg et al., 1990; Martin et al., 1990; Xu et al., 1990). Ras-GAP proteins negatively regulate the Ras pathway by stimulating Ras-GTPase activity to convert active Ras-GTP to inactive Ras-GDP (Trahey et al., 1988). The Ras signal transduction pathway is a major messenger that mediates signal input from receptor tyrosine kinases and frequently found to be aberrant in cancers (Vigil et al., 2010). Elevated Ras-GTP levels and active Ras effector molecules were found in Neurofibromin deficient cells (Basu et al., 1992; DeClue et al., 1992), suggesting Neurofibromin functions as a Ras-GAP *in vivo*. Moreover, NF1 patients share many clinical features associated with a class of developmental disorders called RASopathies. RASopathies are caused by germline mutations in genes that encode proteins in the Ras pathway, manifesting as facial deformity, cardiac malformation, mental retardation, and elevated cancer risk (Tidyman and Rauen, 2009). While PNSTs are a unique feature of NF1, these other symptoms implicate the Ras-GAP domain of Neurofibromin as responsible for its tumor suppressing activity.

Ras-mediated signaling has two primary effector pathways: (1) the mitogen-activated protein kinase/extracellular-signal regulated kinase (MAPK/ERK) and (2) the phosphatidylinositol 3 kinase (PI3K)/AKT pathway (Cichowski and Jacks, 2001). Elevated ERK and AKT activities are a common feature of human tumors, including PNSTs (Shaw and Cantley, 2006). These signaling pathways have a variety of cellular effects, but intriguingly, they both can activate the mammalian target of rapamycin (mTOR) signaling hub. mTOR Complex 1 (mTORC1), the rapamycin-sensitive mTOR complex, has been demonstrated to be essential to AKT-mediate proliferation and oncogenic susceptibility (Bhaskar and Hay, 2007; Levine et al., 2006). This pathway has also been demonstrated to be essential in the stimulation of protein and ribosome

biosynthesis, leading to growth and proliferation (Sarbassov et al., 2005). AKT and ERK elicit their activation of mTORC1 by phosphorylating and inactivating Tuberous Sclerosis Complex 2 (TSC2). Active TSC2 forms a complex with Tuberous Sclerosis Complex 1 (TSC1) and together they act as a GTPase-activating protein (GAP) for Ras-homolog enriched in brain (Rheb). Since Rheb in its GTP-bound form stimulates mTORC1 kinase activity, TSC1/TSC2 negatively regulates mTORC1 by converting Rheb into the GDP-bound form. Consistent with this model of AKT and ERK mediated mTORC1 activity, increased mTORC1 activity has been documented in a variety of human tumors (Bhaskar and Hay, 2007; Sabatini, 2006), including those deficient in *NF1* (Johannessen et al., 2008; Johannessen et al., 2005). These observations suggest that mTORC1 may play a critical role in PNST development, and since rapamycin and its analogs have been approved and used as immunosuppressive medication for organ transplant patients, the mTORC1 signal transduction pathway represents a potential therapeutic avenue for treating *NF1*-deficient tumors.

The majority of mutant germline *NF1* alleles sequenced from patients are characterized by small mutations that truncate Neurofibromin, while a minority of these mutant alleles reveals a deletion spanning large portions of the *NF1* locus (Messiaen et al., 2000). There have been very few well established phenotype-genotype correlations based on individual germline mutations, where patients that have a specific microdeletion or large deletions tend to have more severe disease manifestations (Pasmant et al., 2010; Tonsgard et al., 1997). As these germline mutations are all inactivating, and somatic mutations have been detected in many of the major disease features such as CALMs (De Schepper et al., 2008), neurofibromas (Colman et al., 1995) and MPNSTs (Upadhyaya et al., 2008), *NF1* has been described as a tumor suppressor. However, due to the heterogeneous nature of cells PNSTs are comprised of, loss of heterozygosity (LOH) where the wildtype allele is lost, can only be detected in a subset of tumors, often corresponding to tumor grade (Upadhyaya et al., 2008).

Malignant transformation of benign PNSTs to MPNSTs is characterized by the accumulation of additional oncogenic somatic mutations. The two most commonly documented mutation sites, the *p53* locus (Legius et al., 1994; Menon et al., 1990) and the *CDKN2A* locus (Kourea et al., 1999b; Nielsen et al., 1999), have both been identified exclusively in MPNSTs but not benign neurofibromas. The *CDKN2A* locus encodes two independent tumor suppressor genes, $p16^{INK4a}$ and $p14^{ARF}$, that share two common exons, albeit in different reading frames. The

protein encoded by *p14*^{ARF} antagonizes mdm2-mediated degradation of P53, and thus is a positive regulator of P53 activity (Sherr, 2001). Together these observations suggest that malignant transformation is linked to compromise in the P53-mediated tumor suppressor pathway. The protein encoded by *p16*^{INK4a} functions as an inhibitor of CDK4 kinases, and thus is a positive regulator of the Retinoblastoma (Rb) tumor suppressor pathway. The observations of MPNST-specific mutations in *p27*^{KIP1} (Kourea et al., 1999a), another Rb pathway component, and copy number loss of Rb1 in 25% of MPNSTs (Mantripragada et al., 2009) suggest that Rb-mediated tumor suppression may also be dismantled during malignant transformation. The difference between tumors that possess *p53* or CDKN2a loci mutation has not been documented, and it is not known if mutations at both sites are required for malignant transformation.

Together, the molecular and genetic features of NF1-associated peripheral nerve sheath tumors suggest a step-wise model of peripheral nerve sheath tumorigenesis. First, biallelic inactivation of *NF1* results in elevated activity in Ras and its downstream MAPK/ERK and/or PI3K/AKT pathways. This triggers neurofibroma initiation and expansion of the cellular components of the peripheral nerve, ultimately resulting in plexiform neurofibromas. Next, *NF1*-deficient cells proliferate and may acquire somatic mutations in key tumor suppressor genes such as *P53*, resulting in malignant transformation to form MPNSTs.

Insights from previous murine models of Neurofibromatosis type I

Genetically engineered mouse (GEM) models of Neurofibromatosis type I were first generated in 1994 with the germline transmission of an *Nf1* knockout (ko) [*Nf1*^{ko}] allele (Brannan et al., 1994; Jacks et al., 1994). Mice heterozygous for *Nf1* [*Nf1*$^{ko/+}$] failed to generate PNSTs commonly associated with NF1 patients. Instead, these mice have greater incidence of pheochromocytoma and myeloid leukemia, both tumors that have greater relative risk in NF1 patients. Mice homozygous for mutant *Nf1* [*Nf1*$^{ko/ko}$] were embryonically lethal due to abnormal cardiac development, preventing the effects of *Nf1*-deficiency from being assessed *in vivo* postnatally (Brannan et al., 1994; Jacks et al., 1994). The lack of a corresponding PNST phenotype in *Nf1* heterozygous mice is speculated to be due to insufficient somatic mutations (Rangarajan and Weinberg, 2003; Van Dyke and Jacks, 2002). The relatively short life span and small pool of target cells in mice may not permit enough time to inactivate the wildtype *Nf1* allele in the appropriate cell types. Even though these early attempts failed at the primary goal

of modeling human PNSTs, they highlighted a role of *NF1* in cardiac development and provided the impetus to investigate cardiac defects in NF1 patients, which eventually was discovered in a subset of afflicted individuals (Friedman et al., 2002).

The next attempt to model PNSTs made use of chimeric mice composed of *Nf1* wildtype [$Nf1^{+/+}$] and *Nf1*-deficient [$Nf1^{-/-}$] cells. The majority of these mice developed multiple benign neurofibromas, with tumor burden corresponding to increased percentage of *Nf1*-deficient cells (Cichowski et al., 1999). Chimeric mice with the higher percentages of *Nf1*-deficient cells were not viable. This study provided direct evidence that bi-allelic inactivation of *Nf1* is necessary for neurofibroma formation, but did not elucidate which cell types the tumor arose from.

As *Nf1* chimeras failed to generate MPNSTs, another mouse model incorporating *Nf1*/*p53* compound mutants was developed (Cichowski et al., 1999; Vogel et al., 1999). The genomic loci of *Nf1* and *p53* are both on chromosome 11 in mice and are genetically linked. Mouse chromosomes are all acrocentric (Waterston et al., 2002) and unlike humans, loss of their entire chromosomes is the prevalent method by which LOH occurs (Luongo et al., 1994). To exploit these differences between mouse and human chromosomes, GEM models carrying both *Nf1* and *p53* mutations on the same chromosome (NPcis) and opposite chromosomes (NPtrans) were generated. A LOH event of the chromosome 11 carrying wildtype *Nf1* and *p53* alleles in NPcis mice would generate double deficient cells, while LOH in NPtrans mice would produce only either *Nf1*-deficient or *p53* deficient cells. Correspondingly, NPcis mice developed an array of sarcomas predominantly diagnosed as MPSNTs while NPtrans mice did not. Histological analysis of NPcis mice did not reveal the formation of any neurofibromas. These studies underscore the role of P53 in promoting malignancy in PNSTs. Unfortunately, due to the stochastic nature of LOH, it is unknown which cells types sarcomas arise from and whether these sarcomas mimic MPNSTs in humans. Despite these shortcomings, the NPcis mice are currently the leading murine model used to investigate MPNSTs. Indeed, preclinical trials for rapamycin have been performed on NPcis mice carrying sarcomas and were found to have a temporary cytostatic effect on tumor growth (Johannessen et al., 2008).

The next breakthrough in NF1 mouse modeling came with the generation of an *Nf1* allele flanked by loxP sites (flox) [$Nf1^{flox}$] (Zhu et al., 2001). By crossing mice carrying the $Nf1^{flox}$ allele to mice carrying *Krox20*-Cre Recombinase (Voiculescu et al., 2000), a transgene expressed in the developing neural crest lineage cells, *Nf1* could be specifically deleted from the peripheral

nerves and avoid embryonic lethality from cardiac defects (Zhu et al., 2002). Theoretically there exist two genetic configurations of *Nf1* alleles that should be able to generate *Nf1*-deficiency in the peripheral nerves while avoiding embryonic lethality: [*Krox20*-Cre; $Nf1^{flox/ko}$] ($Nf1^{Kx}$CKO1) and [*Krox20*-Cre; $Nf1^{flox/flox}$] ($Nf1^{Kx}$CKO2). Notably, neither genetic configuration was capable of generating tumors resembling dermal neurofibroma. $Nf1^{Kx}$CKO1 mice, those carrying one germline *Nf1* knockout allele, formed tumors histologically resembling pNFs between 10 and 12 months in cranial nerves and spinal roots. $Nf1^{Kx}$CKO2 mice, where *Nf1* is only deficient in the peripheral nerves, had a mild phenotype with few if any tumors, and only hyperplasia. This surprising observation suggests that *Nf1*-deficiency in the peripheral nerves alone is not sufficient for robust pNFs generation in this genetic setting. The most salient difference between the $Nf1^{Kx}$CKO1 and $Nf1^{Kx}$CKO2 mice lie in the cells that have not undergone recombination, which are genotypically *Nf1* heterozygous or *Nf1* wildtype, respectively. The authors posit that *Nf1*-deficient peripheral nerve cells must interact with *Nf1* heterozygous environmental cells for neurofibromas to form. This requirement for *Nf1* heterozygosity in pNFs formation would explain the rarity of pNFs in the general population. Even if peripheral nerve cells became *NF1*-deficient, those cells would be resident in a wildtype environment, precluding tumor development. A possible alternative explanation was that difference between $Nf1^{Kx}$CKO1 and $Nf1^{Kx}$CKO2 mice was due to Cre-mediated recombination efficiency. If there already exists a germline knockout allele only a single flox allele need to be recombined in $Nf1^{Kx}$CKO1 mice and may thus generate more *Nf1*-deficient cells than in $Nf1^{Kx}$CKO2 mice accounting for the more severe phenotype (Carroll and Ratner, 2008). These competing explanations will be addressed in Chapter III of this thesis.

Mast cells are the leading candidate for the *Nf1* heterozygous cells that interact with *Nf1*-deficient cells to promote tumor development (Zhu et al., 2002). Mast cells are hematopoietically derived and are normally resident in the peripheral nerves (Staser et al., 2010). Thus they would not undergo Cre-mediated *Nf1* deletion, and are at the correct location to interact with *Nf1*-deficient cells. Notably, mast cell infiltration is enriched in neurofibromas from both humans (Korf, 1999) and mice (Zhu et al., 2002). Mast cells provide an attractive therapeutic target, as (1) there already exists a variety of drugs that inhibit mast cell function and (2) potential therapies would be targeting a cell lacking accumulated somatic genetic insults (Kenny et al., 2007). Heterozygous *Nf1* mast cells were found to interact with heterozygous fibroblast *in vitro*, resulting in increased collagen production. This interaction was inhibited by

inactivating the c-abl pathway through imatinib (Yang et al., 2006). Hematopoietic transplant from *Nf1* wildtype bone marrow into irradiated *Nf1*^{Kx}CKO1 mice and *Nf1 h*eterozygous bone marrow into irradiated *Nf1*^{Kx}CKO2 mice reversed the *Nf1*^{Kx}CKO1 and *Nf1*^{Kx}CKO2 phenotypes, where mice developed pNFs only if they possessed *Nf1* heterozygous bone marrow (Yang et al., 2008). Using genetic techniques they further refined the identity of the contributory *Nf1* heterozygous bone marrow to a c-kit dependent cell type. This study clearly demonstrates that an *Nf1* heterozygous hematopoietic cell type is critical in providing a permissive tumor microenvironment for neurofibroma formation in the *Krox20* based GEMs.

While advances have been made in the field of Neurofibromatosis type I, there are still few promising therapeutic approaches to managing peripheral nerve sheath tumors aside from surgical resection. From this literature review it is apparent that there are outstanding questions in the NF1 field, and I will attempt to address some of these in my thesis. First, the various GEM approaches described do not provide a clear etiology for peripheral nerve sheath tumors, other than highlighting the neural crest lineage as the source of *Nf1*-deficient cells in neurofibromas. The value of identifying the cell-of-origin is that a better understanding of the cellular etiology of plexiform neurofibromas formation may help direct therapeutic development and may permit earlier diagnosis of these unpredictable tumors. Second, while *Nf1* heterozygous mast cells contribute to neurofibroma development, it is unknown whether mast cell inhibition can be used to prevent neurofibroma formation or malignant transformation. Thus, the overarching objective of this thesis is to utilize murine mouse models of Neurofibromatosis Type I in indentifying promising therapeutic avenues to combating this disease.

CHAPTER II

The Etiology of Neurofibromas: A Window of Opportunity

Schwann Cells as Cell-of-Origin for Neurofibromas

Identification of the cell-of-origin for neurofibromas has historically been problematic, primarily due to the heterogeneous cell types that comprise these tumors. In fact, "neurofibromatosis" is a misnomer that can be traced to the assumption that the tumor cells are primarily neurons and fibroblasts. This can partially be accounted for by the fact that collagen is heavily deposited in neurofibromas and collagen secretion by Schwann cells has only been appreciated within the last 30 years (Carey et al., 1983). Indeed, the majority of the cells in neurofibromas are usually Schwann cells, accounting for 60-80% of tumor cells, with fibroblasts accounting for 10%-20% (Peltonen et al., 1988).

Support for Schwann cells as the cell-of-origin was strengthened with the finding that neurofibroma-derived Schwann cells are angiogenic and invasive while fibroblasts were not (Sheela et al., 1990). Molecular analysis of *NF1* mRNA and Neurofibromin protein from fibroblasts and Schwann cells isolated from neurofibromas reveal that Schwann cells lose *NF1* expression while fibroblasts retain it (Rutkowski et al., 2000; Serra et al., 2000). Although the observation that neural-crest targeted deletion of *Nf1* in mice generate benign PNSTs was thought to definitely prove the Schwann cell-of-origin hypothesis for neurofibromas (Zhu et al., 2002), it was found that fibroblasts also arise from this lineage (Joseph et al., 2004). Together these observations strongly, but not conclusively, implicate Schwann cells as the cell-of-origin for neurofibromas. The looming question that will be addressed in this chapter is how does *Nf1*-deficiency cause Schwann cells to become tumorigenic?

Schwann Cells and Their Neural Crest Origin

Schwann cells are the primary glia of the PNS and exist to support nerve function (Nave and Trapp, 2008). These cells come in two distinct varieties: myelinating Schwann cells (mSCs) that ensheath large caliber (>1µm) axons in a one-to-one ratio, and nonmyelinating Schwann cells (nmSCs) that ensheath one or typically more small caliber (<1µm) axons (Figure 1). The most salient difference between these two cell types is, tautologically, the synthesis of myelin

and production of a myelin sheath. Myelin sheaths are lipid rich, multi-lamallar structures that possess dielectric properties which prevents electrical current from leaving the axon. Ensheathment of peripheral axons by mSC is not complete, with specialized gaps called nodes of Ranvier existing between adjacent Schwann cells. These nodes, in conjunction with the insulation provided by myelin, are critical for rapid action potential propagation in vertebrates through salutatory conduction. Action potentials, thus, propagate slower in nmSCs. Both mSC and nmSCs serve to protect axon function and survival. Axon caliber has been demonstrated to increase in response to ensheathment by Schwann cells (Windebank et al., 1985). Many peripheral demyelinating neuropathies such as Charcot-Marie-Tooth disease (CMT) are characterized by initial Schwann cell dysfunction with progressive axonal loss (Nave et al., 2007). Schwann cells are the critical mediators of peripheral nerve regeneration by forming tracks by which axons can grow along and re-innervate target tissue after damage (Chen et al., 2007). Schwann cells, thus, play a critical role in the proper function and homeostasis of peripheral nerves.

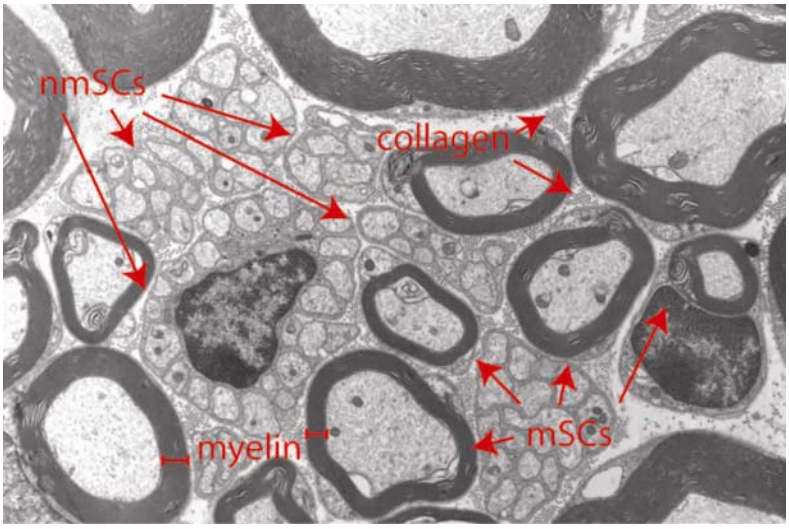

Figure 1 - Transmission electron microscopy (TEM) cross section of normal peripheral nerve. This was imaged is a cross section from a murine sciatic nerve.

For the purposes of this thesis, I will be describing Schwann cell development in the murine sciatic nerve, as it is the system in which glia development in the PNS has best been characterized. Schwann cells arise from the neural crest lineage through a multi-stage differentiation process (Figure 2) (Jessen and Mirsky, 2005). Between embryonic day 12 and 13 (E12 and E13), neural crest cells (NCCs) undergo lineage-restricted differentiation to form Schwann cell precursors (SCPs) which have the potential to become both types of mature Schwann cells (Dong et al., 1999; Jessen et al., 1994) and fibroblasts (Joseph et al., 2004). SCPs retain self-renewal capacity and multilineage differentiation potential and are thus sometimes referred to as neural crest stem cells (NCSCs) (Morrison et al., 1999). Between embryonic day 15

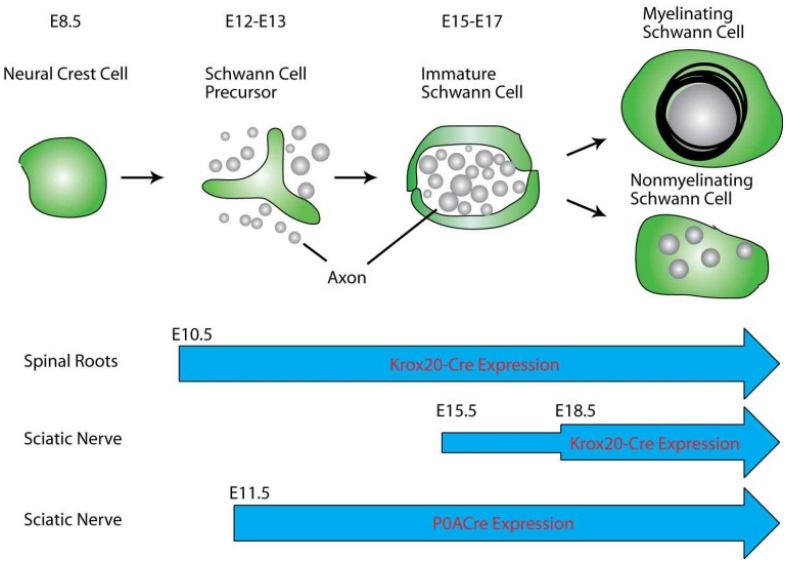

Figure 2 - Schwann cell development in mice and summary of *P0* and *Krox20* Cre Recombinase expression by time and location. Adapted from Jessen and Mirsky, 2005.

and 17 (E15 and E17), SCPs further specify into immature Schwann cells, which begin to ensheath axons and secrete a basal lamina. The fate of immature Schwann cells depends on the caliber of axons in which they ensheath. Immature Schwann cells associated with large caliber (>1µm) axons will release other axons to form a one-to-one Schwann cell to axon ratio and differentiate into mSCs. This process thought to be mediated through Neuregulin-1 signaling (Taveggia et al., 2005). Those associated with small caliber axons (<1µm) will typically encapsulate up to 30 or 40 axons (Taveggia et al., 2005) and defasciculate these axons into distinct Schwann cell domains, or Schwann cell "pockets", characterized by distinct Schwann cell cytoplasm ensheathing each axon. These non-myelinating Schwann cell/multiple axon units are also referred to as "Remak bundles". Mature mSCs and nmSCs begin to appear embryonic day 17 (E17) until birth and lose their proliferative capacity. There is no adult stem cell population in the adult peripheral nerve, but differentiated mSCs and nmSCs have the ability to de-differentiate into immature Schwann cells in response to nerve damage and acquire either mature cell fate (Stewart et al., 1993). A battery of cellular markers has been developed to identify the differentiation status of developing Schwann cells (Table 2) (Jessen and Mirsky, 2005).

Table 2 - Cellular markers used to identify Schwann cell differentiation status

	Neural Crest Cell	Schwann cell Precursor	Immature Schwann Cell	Nonmyelinating Schwann Cell	Myelinating Schwann Cell
P75^{NGFR}	+	+	+	+	–
Sox10	+	+	+	–	+
BLBP	–	+	+	–	–
GAP43	–	+	+	–	–
GFAP	–	–	+	+	–
S100	–	–	+	Low	+

A Temporal Requirement for Loss of *NF1* in Peripheral Nerve Sheath Tumorigenesis

I performed systematic histopathological analysis on nerves isolated from 6 *Nf1*^{Kx}CKO1 [*Krox20*-Cre+; Nf1$^{flox/ko}$] mice. As previously documented (Zhu et al., 2002), the brachial plexus (containing cervical dorsal root ganglia) and trigeminal nerves (cranial nerve V) gave rise to robust pNFs. The sciatic and cutaneous nerves developed hyperplasia but not pNFs (Figure 3).

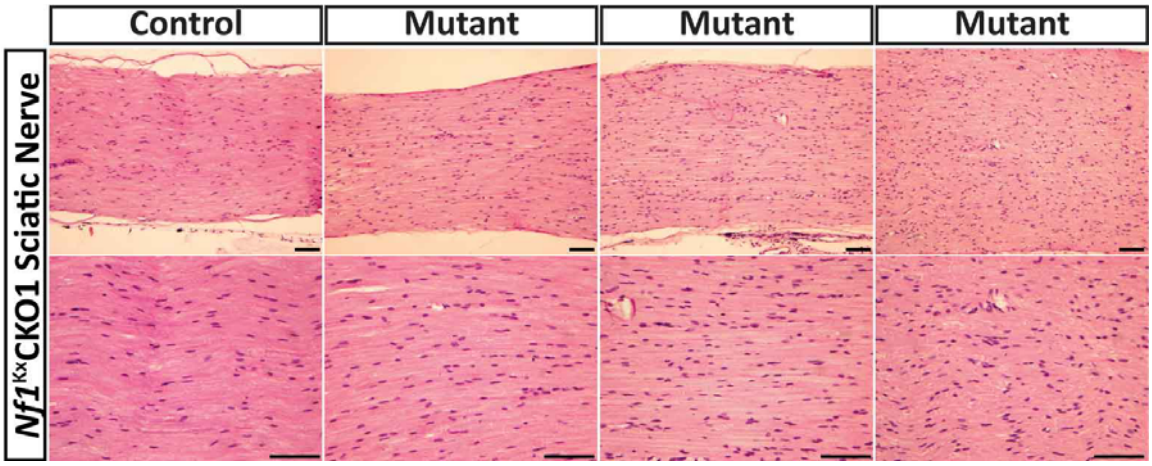

Figure 3 – *Nf1*^{Kx}CKO1 Sciatic Nerves Do Not Develop Neurofibromas. Representative images of hematoxylin and eosin (H&E) stained sciatic nerves dissected from 10-14 month old *Nf1*^{Kx}CKO1 mice. There is a noticeable increase in cellularity in mutant nerves, but the organization of the axons and Schwann cells remains intact and is diagnosed as hyperplasia. Scale bars, 100 µm.

The expression pattern of *Krox20*-Cre was first characterized in Voiculescu et al., 2000 and was further verified by Yuan Zhu by crossing mice carrying *Krox20*-Cre to GEM carrying the Rosa26R-LacZ reporter allele and performing whole-mount X-gal stains on E12.5 embryos (Figure 4). From these X-gal stains, robust staining can be appreciated in the dorsal roots, but not in the rest of the peripheral nervous system. Robust *Krox20*-Cre expression can be late observed at E18.5 in the rest of the PNS (Voiculescu et al., 2000). The sites where tumors develop correspond to locations where *Krox20*-Cre is expressed during SCP stage of Schwann cell development (Figure 2). This leads to the hypothesis that ***Nf1*-deficiency must be acquired during the SCP developmental stage for neurofibromas to form.**

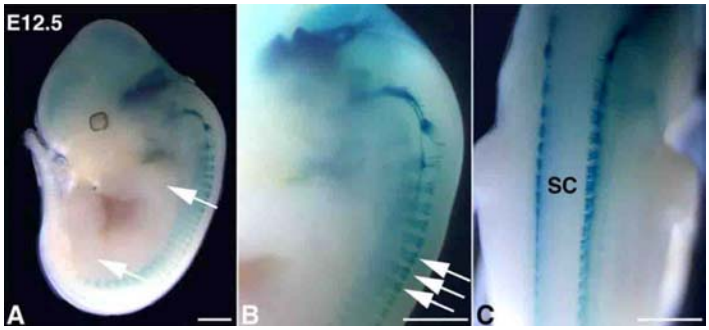

Figure 4 - Whole-mount X-gal stain of *Krox20*-Cre Rosa26R-LacZ reporter. Arrows in (A) demonstrate lack of staining in nerves innervating limbs, while (B) highlight robust staining along peripheral nerves. SC – spinal cord; Scale bars, 1mm

The test of this hypothesis necessitates a Cre-recombinase transgene that is expressed throughout the peripheral nerve at E12.5 while avoiding embryonic lethality. An attempt was made using *Mpz*-Cre, *Pax3*-Cre and *Wnt1*-Cre to generate pan-neural crest *Nf1*-deficient mice (Gitler et al., 2003). These mice all had extensive recombination in the neural crest lineage, and managed to avoid the embryonic lethality associated with loss of *Nf1* in cardiac development. The authors found the presence of abnormalities throughout the sympathetic nervous system with histopathologies reminiscent of ganglioneuromas and pheochromocytomas. Unfortunately, these mice died shortly after birth, precluding subsequent PNST analysis. This suggests that Neurofibromin activity in the neural crest may be necessary for viability after birth, and that subsequent attempts should focus on transgenic Cre-recombinases with more limited expression in the PNS.

The *P0*-Cre transgene was generated and successfully used by Dr. Marco Giovannini to create a murine model for Neurofibromatosis type II (Giovannini et al., 2000). He graciously provided the use of mice carrying *P0*-Cre Recombinase for use in my research. With the collaboration of Dr. Huarui Zheng, we set upon characterization of the *P0*-Cre expression pattern in developing nerves. Dr. Zheng crossed mice carrying *P0*-Cre to GEM carrying the Rosa26R-LacZ reporter allele and collected at least three embryos that carried both *P0*-Cre and Rosa26R-LacZ genes from E9.5, E10.5, E11.5 and E12.5. I performed whole-mount X-gal stains on these embryos to detect the Rosa26R-LacZ reporter. No staining was observed in the developing PNS at E9.5 or E10.5 (Figure 5A, 5B). X-gal staining of the LacZ reporter was first evident at E11.5 (Figure 5C) and became more robust at E12.5 (Figure 5D). Dr. Zheng further demonstrated that Cre-recombination occurred in SCPs by sectioning and double-staining these embryos for $p75^{NGFR}$, BLBP, GAP43 or S100 with X-gal (Figure 6). X-gal positive cells co-label for p75NGFR (Figure 6A-C,M-O), BLBP (Figure 6D-F,P-R), GAP43 (Figure 6G-I,S-U) but not S100 (Figure 6J-L,V-X), uniquely corresponding to the expression pattern expected from SCPs (Table 2). Its embryonic expression pattern is more robust than *Krox20*-Cre, but less extensive compared to *Wnt1*-Cre. The level of Cre-mediated recombination that occurs in adult P0-Cre and Kx-Cre sciatic nerve was compared by Dr. Zhu through X-gal staining of mice carrying both Cre and Rosa26R-LacZ genes, and no significant difference was found (Figure 7). These findings demonstrate that *P0*-Cre is expressed throughout the entire peripheral nervous system at E11.5 and E12.5 in cells that are presumably SCPs (Figure 2), but ultimately results in similar levels of recombination compared to *Krox20*-Cre in the adult.

Figure 5 - Whole-mount X-gal profiling of *P0*-Cre expression during development. E9.5 (A) and E10.5 (B) embryos displayed no significant X-gal staining in the developing peripheral nervous system. The notochord was positive at these time points and arrows in A and B point to positive cranial-facial staining. At E11.5 (C) and E12.5 (D), positive X-gal staining was evident. The recombination was more robust in the lumbar regions (arrows, Cc and Dc) than in the thoracic regions (Ca and Da). Dashed lines in Ca and Da denote border between thoracic and lumbar regions. Arrows in Cb, Cd, Db and Dd point to recombined peripheral nerves innervating forelimbs (Cb and Db) and hindlimbs (Cd and Dd). Scale bar, 1mm.

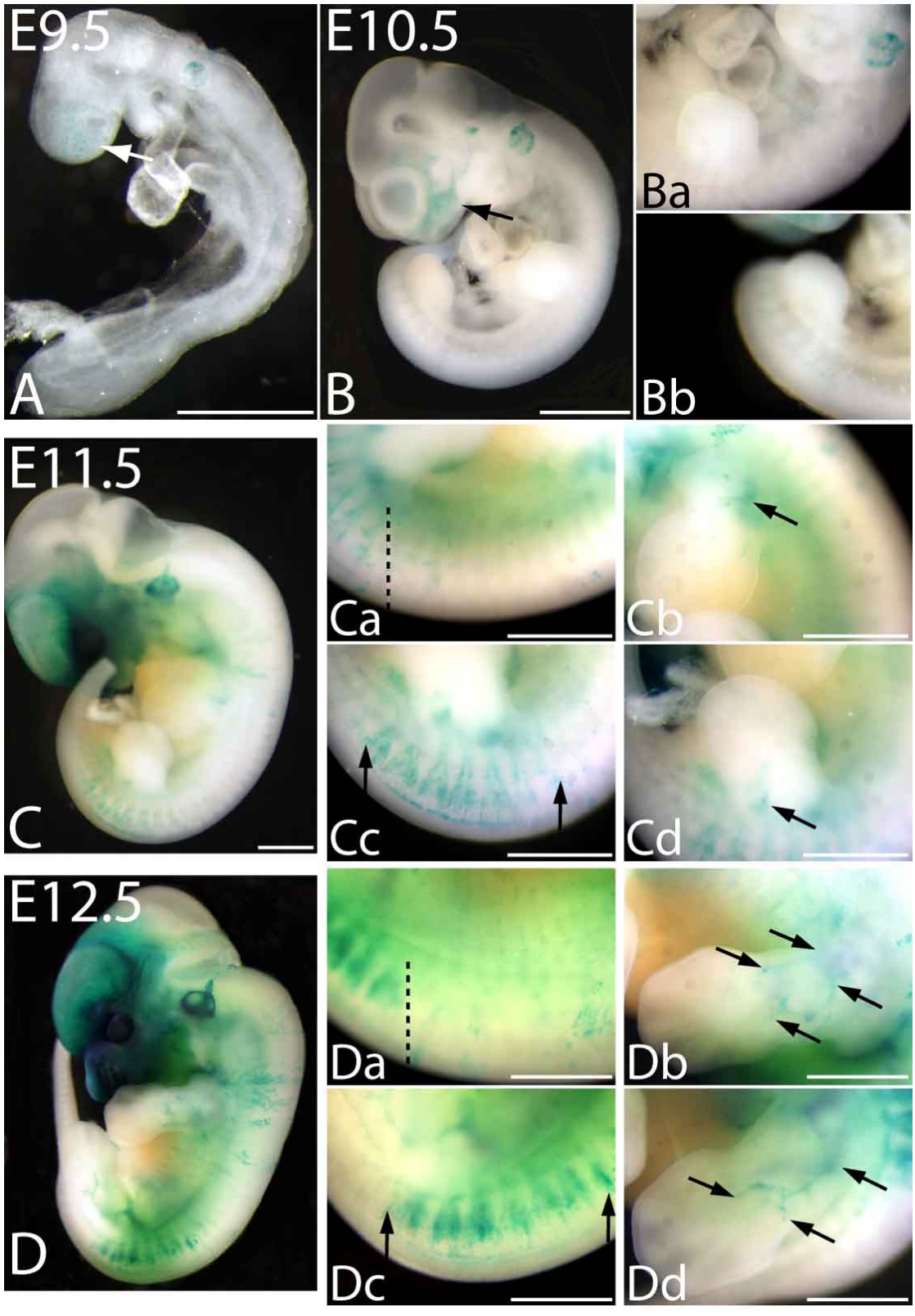
E9.5
A
E10.5
B
Ba
Bb
E11.5
C
Ca
Cb
Cc
Cd
E12.5
D
Da
Db
Dc
Dd

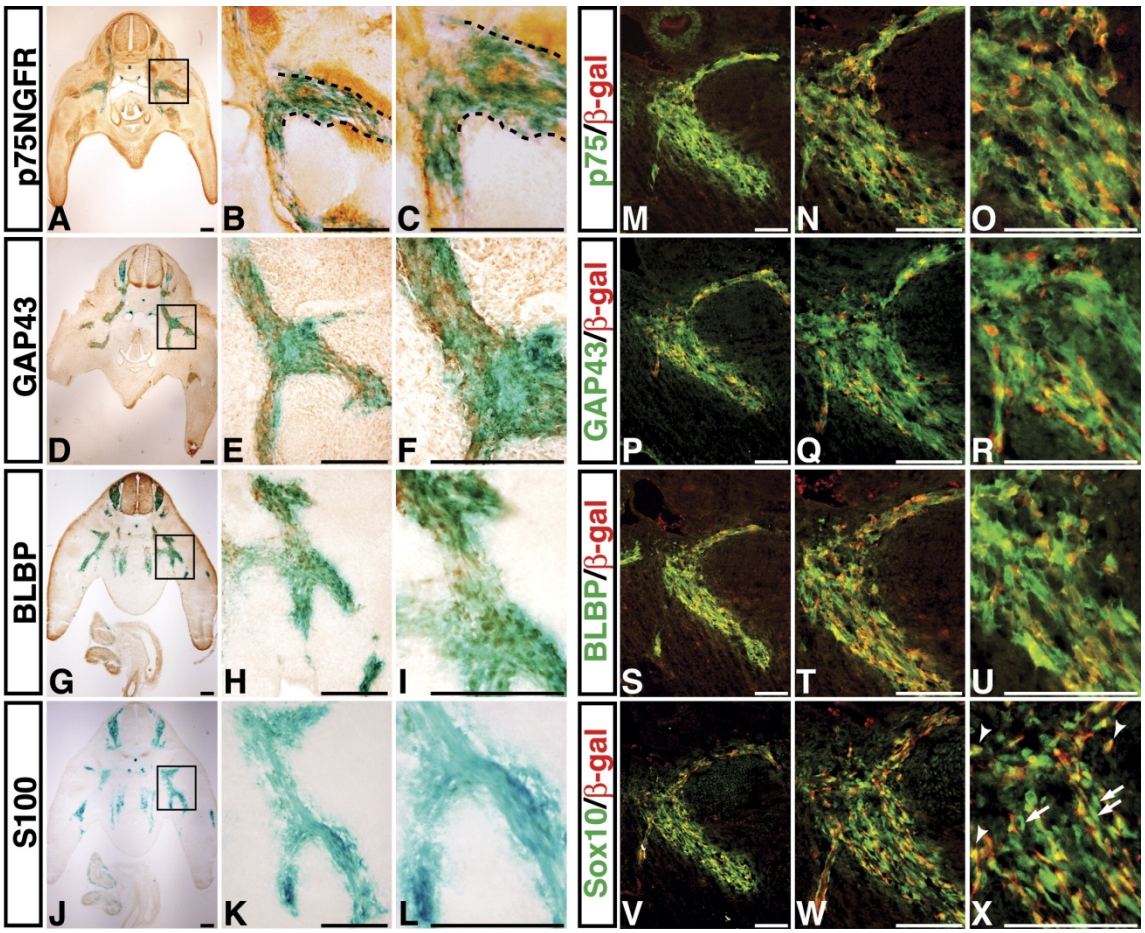

Figure 6 - *P0*-Cre-Mediated Recombination in SCP/NCSCs. Transverse sections from the lumbar region of X-gal-stained E12.5 P0A-cre/R26R-LacZ double transgenic embryos were stained with anti-p75NGFR (A–C), GAP43 (D–F), BLBP (G–I), and S100 (J–L) antibodies. The dashed lines (B and C) mark the p75NGFR and β-gal double-positive developing peripheral nerves. The expression of p75NGFR (M–O), GAP43 (P–R), BLBP (S–U), or Sox10 (V–X) in β-gal positive cells was further confirmed by double immuofluorescence. Arrowheads and arrows in X point to Sox10/β-gal double-positive cells and Sox10-positive/β-gal-negative cells, respectively. Scale bars: (A)–(L), 50 µm; (M)–(X), 25 µm.

To test whether loss of *Nf1* in the SCP stage is sufficient for neurofibroma formation, I crossed *P0*-cre transgenic mice to *Nf1*$^{flox/ko}$ mice and subsequently generated 14 *Nf1* mutant mice with genotypes of [P0-Cre+;*Nf1*$^{flox/ko}$] (*Nf1*^{P0}CKO1). It should be noted that these mice possess a germline knockout allele, providing an *Nf1* heterozygous environment for *Nf1*-deficient cells to interact with. The *Nf1*^{P0}CKO1 mutant mice were viable, fertile, and indistinguishable from their control littermates. However, in the second year of life, all the mutant mice developed signs of sickness including lethargy, ruffled hair, skin lesions, or hindlimb paralysis. My histopathological analysis revealed that all of the sick mutant mice exhibited neurofibroma formation throughout the PNS. Of particular interest, 10 of 14 (71%) mutant mice developed frank pNFs in the sciatic nerve (Figure 8). To summarize, only nerves that undergo *Nf1* inactivation during early Schwann cell develop neurofibromas in both *Nf1*^{Kx}CKO1 and *Nf1*^{P0}CKO1 mice (Figure 2). Conversely, differentiated Schwann cells that undergo *Nf1* inactivation have very limited tumorigenic potential. From these observations I conclude that **there exists a critical temporal window during Schwann cell development in which *NF1* must become inactivated to permit subsequent tumorigenesis**. This temporal requirement for *NF1* inactivation in benign peripheral nerve sheath tumorigenesis would explain the congenital nature of pNFs and provide contributing factor for why Nf1 patients are so exclusively susceptible to developing pNFs.

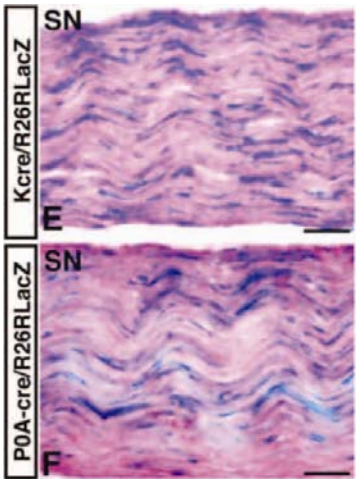

Figure 7 - No difference between *Krox20*-Cre and *P0*-Cre mediated recombination in the adult nerve.

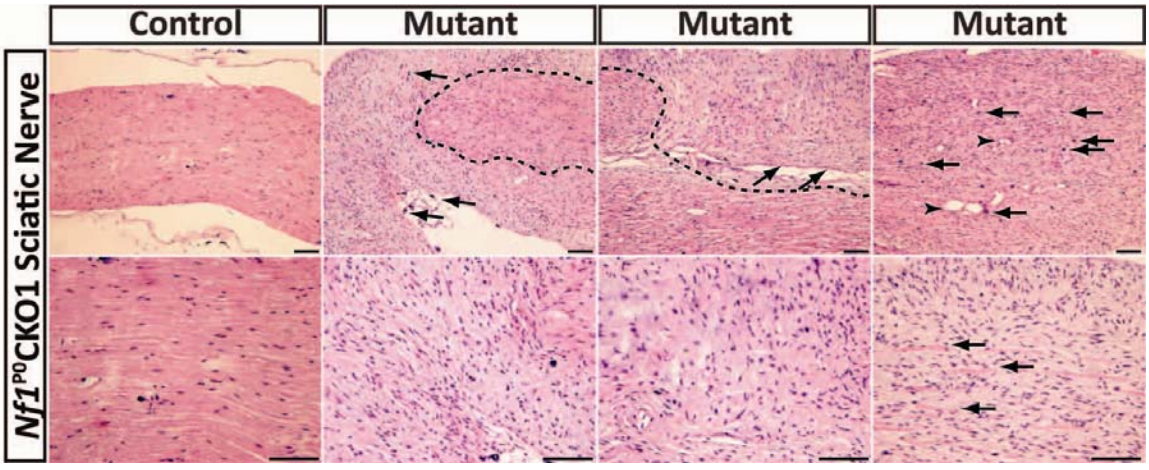

Figure 8 - *Nf1*^{P0}CKO1 Sciatic Nerves Develop Robust Neurofibromas. Representative images of hematoxylin and eosin (H&E) stained sciatic nerves dissected from 10 to 14 month old *Nf1*^{P0}CKO1 mice. The dashed lines mark the border of neurofibromas and hyperplasia in mutant nerves. Arrows in point to infiltrating mast cells and arrowheads point to blood vessels. Scale bars, 100 µm.

The Etiology of Neurofibromas: The Role of *NF1* in Schwann cell development

The genetic studies described above raise the question of what function *NF1* plays during Schwann cell development. The most tantalizing hypothesis to explain this window for neurofibroma tumorigenesis is that *NF1* plays a critical role in regulating neural crest stem cells. In the PNS, stem cells only exist during development and do not persist into adulthood. If loss of *Nf1* allowed these stem cells to persist into adulthood, they may be then become the cell-of-origin for neurofibromas. Our collaborators in the Morrison lab took an *in vitro* approach investigate whether loss of *Nf1* in SCPs leads to tumorigenesis by altering normal stem cell function (Joseph et al., 2008). To test this hypothesis, they used media conditions that support NCSC sphere formation to culture E13 and adult, wildtype and *Nf1*-deficient sciatic nerves and neurofibromas. Of these cell types, they were only able to culture self-renewing neural crest spheres from the E13 wildtype and *Nf1*-deficient nerves. This observation rules out neural crest stem cell persistence as mechanism for neurofibroma initiation. E13 *Nf1*-deficient cells isolated from the sciatic nerve generated increased numbers of neurospheres with improved self-renewal capacities compared with cells derived from wildtype mice. However, these cells were incapable of forming tumors upon transplantation. Together these observations suggest that while loss of *Nf1* in SCPs may impact some of their self-renewal and proliferative characteristics, these alterations are ultimately inconsequential in terms of the tumorigenic potential of neural crest stem cells (Joseph et al., 2008).

Dr. Zheng and I opted to take an *in vivo* approach to uncover the function of *Nf1* in the developing PNS. Taking into consideration that at 10-14 months of age, 70% of $Nf1^{P0}$CKO1 mice develop neurofibromas in their sciatic nerve and that *Nf1*-deficient E13 neural crest stem cells are hyperproliferative *in vitro*, postnatal day 22 (P22) sciatic nerves of $Nf1^{P0}$CKO1 mice were chosen to be analyzed. P22 is a time point when Schwann cell development is nearly complete. Dr. Zheng performed light microscopy based histological analysis while I performed transmission electron microscopy (TEM) based morphological analysis of 4 *Nf1*-deficient P22 nerves. Surprisingly, no significant difference in cell density or $p75^{NGFR}$ expression was detected between sciatic nerves of control and mutant mice based on light microscopy (Figure 9A-E). This observation provides further support against the notion that *Nf1* has any direct effect on peripheral nerve stem cells, as the hyperproliferative phenotype found *in vitro* either was either not recapitulated *in vivo* or of no consequence after birth.

My TEM analysis revealed a subtle but significant change in the morphology of non-myelinating Schwann cells (nmSCs) (Figure 9F-L). A normal part of nmSC development is the defasciculation of multiple axons sharing a single Schwann cell domain into their own individual domains, or Schwann cell "pocket". In *Nf1*-deficient mice, this process appears to be partially compromised (Figure 9H-I,K), where I found a greater proportion of Schwann cell pockets that contain multiple axons, some with even more than 10 axons per pocket (Figure 9L). I performed a Chi-Squared goodness-of-fit test and found that the mutant and control nerves had significantly different ($P<0.0001$) profiles for rates of axons defasciculation into pockets (Figure 9L). To address whether this alteration was due to a defect in immature Schwann cells

ensheathing too many axons or in differentiated nmSC ability to defasciculate axons into distinct pockets, Dr. Neha Patel categorized and quantified the number of axons ensheathed by non-myelinating Schwann cells and found no difference from control (Figure 9F). **Thus, my TEM-based morphological analysis found a developmental defect associated with *Nf1*-deficiency: non-myelinating Schwann cells defasciculate axons into their own distinct Schwann cell pockets with reduced efficiency.**

To investigate the consequence of this nmSC pocket defect identified at P22, Dr. Zheng and I collected sciatic nerves from 2 control and 3 $Nf1^{P0}$CKO1 mice at postnatal day 90 (P90). Employing the same methodology for studying P22 nerves, abnormalities in P90 mutant nerves were found using both light and electron microscopy. The light microscopy analysis performed by Dr. Zheng found that P90 mutant nerves were significantly ($P<0.01$) more hyperplastic compared to wildtype nerves (Figure 9C). My TEM analysis found a distinct difference between myelinating Schwann cell (mSC) and nmSC response to *Nf1*-deficiency. mSCs from mutant nerves appeared to be unaltered, with comparable cellularity and morphology compared to control nerves (Figure 10A-B). In contrast, the nmSC population underwent striking morphological changes over the course of two months. Most of the abnormally differentiated Remak bundles with unseparated or poorly segregated axons observed in P22 mutant sciatic nerves were no longer detected. In their place, an entirely new spectrum of non-myelinating Schwann cell phenotypes appeared. Abnormal nonmyelinating Schwann cells (anmSCs) were characterized by an association of morphologically abnormal axons (e.g., dilated or naked axons), many of which had myelin-like fragments (Figure 10G–10H). Dissociating Schwann cells (dSCs) were characterized by the presence of free Schwann cell processes (arrowheads, Figures 10J and 10K), which progressively dissociated from axons leading to the degeneration of unmyelinated axons (arrows, Figures 10K and 10L). Unassociated Schwann cells (uSCs) completely lost axonal contact in spite of the presence of a continuous basal lamina that sometimes encircled collagen fibers (Figures 10M and 10N). The uSCs are morphologically identical to the tumor cells observed in both human and mouse neurofibromas (Cichowski et al., 1999; Lassmann et al., 1977; Zhu et al., 2002). When combined with these aberrant nmSC cell types, the entire nmSCs population was found to have expanded 61% compared to the controls (10C). The notable lack of nmSCs containing >10 axons in either the normal or aberrant P90 nmSC populations prompts a potential mechanism that may account for this absence as well as the myriad of nmSC defects.

Figure 9 - Abnormal Remak Bundles in *Nf1* Mutant Sciatic Nerves. Sections of sciatic nerves from P22 control and *Nf1*^{P0}CKO mice were stained with H&E (A and B) and anti-p75NGFR antibody (C and D). (E) Quantification of the number of cells per surface area (mm^2) in P22 and P90 control and mutant sciatic nerves. For P22 analysis, 8 control and 3 mutant mice were used, and for P90 analysis, 3 control and 7 mutant mice were used. Cell density for the P22 and P90 is plotted as mean ± SEM. (F) The numbers of Remak bundles per surface area (1,000 μm^2) in control and mutant P22 sciatic nerves were categorized into five groups based upon the number of axons that they ensheathed. N values represent Remak bundles quantified for each genotype. Data in (F) represent mean ± SEM from 2 control and 4 mutant nerves. Transmission electron microscopy (TEM) analysis of Remak bundles in sciatic nerves of P22 control (G and J) and mutant (H, I, and K) mice show abnormal axonal segregation in the mutant mice. Arrowheads in [G] indicate Schwann cell cytoplasm between different axons, which isolates each individual axon into a dedicated Schwann cell pocket in the Remak bundle. Mutant Remak bundles contain unsegregated axons, which remain directly apposed to each other (arrowheads, [H], [I], and [K]). (J and K) The number of myelinated Schwann cells ensheathing multiple axons (arrows) is significantly increased in mutants compared to controls (p = 0.0036). (L) The percentage distribution of axons per Schwann cell pocket in control and mutant nerves. N values indicate the number of Schwann cell pockets counted for each genotype (mean ± SEM). The majority of axons in control nerves were segregated into individual pockets, while the number of axons properly segregated was dramatically reduced in mutant nerves (Chi-square goodness-of-fit test, p < 0.0001). A, myelinated axons; a, unmyelinated axons; a*, dilated axons. Scale bars: (A)–(D), 100 μm; (G)–(K), 1 μm.

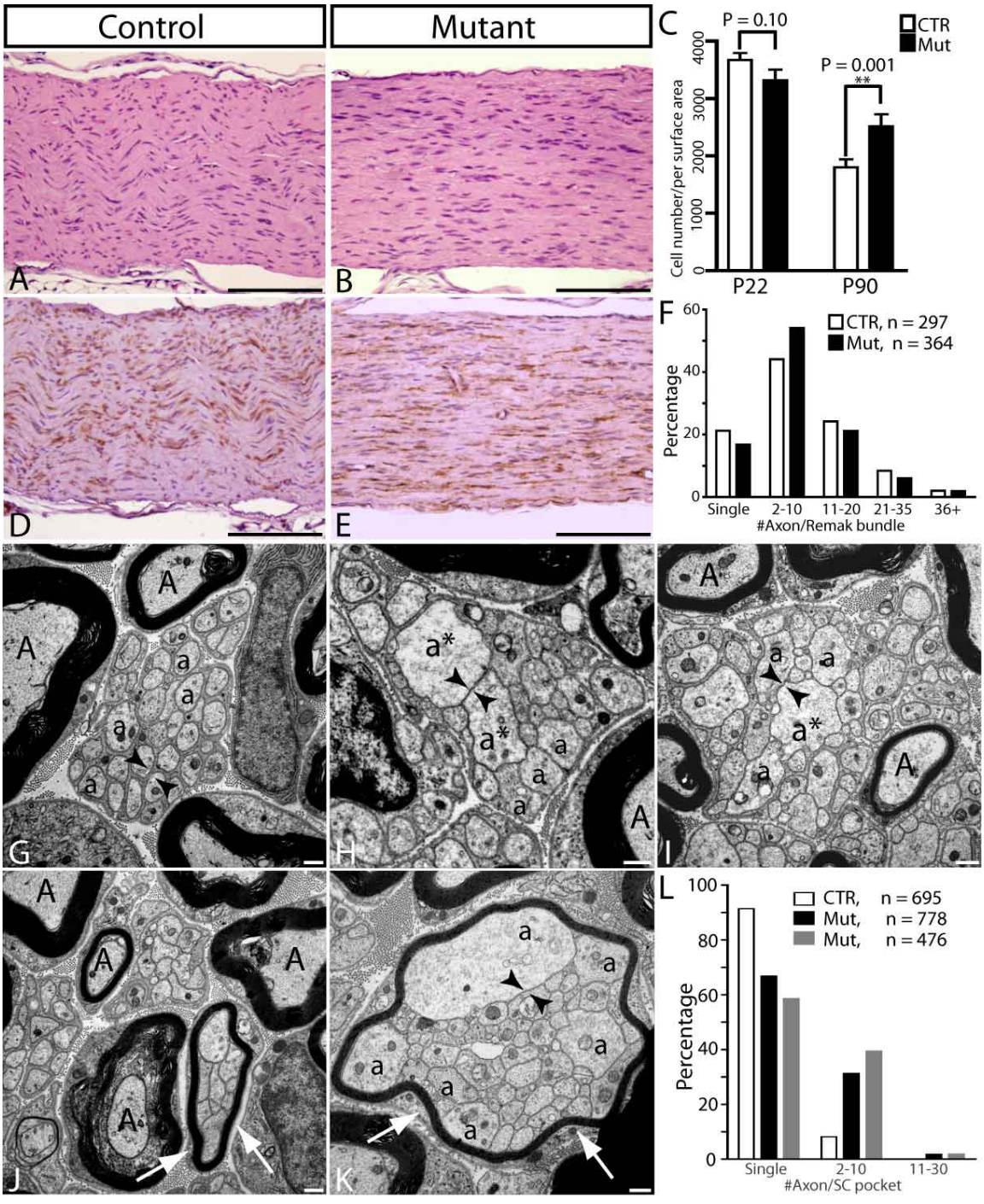
Control
Mutant
A
B
C
D
E
F
G
H
I
J
K
L
P = 0.10
P = 0.001
**
CTR
Mut
Cell number/per surface area
0
1000
2000
3000
4000
P22
P90
CTR, n = 297
Mut, n = 364
Percentage
0
20
40
60
Single
2-10
11-20
21-35
36+
#Axon/Remak bundle
CTR, n = 695
Mut, n = 778
Mut, n = 476
0
20
40
60
80
100
Single
2-10
11-30
#Axon/SC pocket

Figure 10 - Degeneration of *Nf1* Mutant Remak Bundles at P90. Electron micrographs show cross-sections of P90 control (A and D) and mutant (B, E, and F) sciatic nerves. (C) The number of myelinating (mSC) and nonmyelinating (nmSC) Schwann cells in P90 control and mutant sciatic nerves was presented by the cell number per surface area (mean ± SEM). a, abnormal nmSCs; d, dissociating SCs; nm, normal nmSCs. Arrows in (D) point to a typical Remak bundle in control nerves containing multiple unmyelinated axons (*). (E) and (F) show two examples of abnormally differentiated Remak bundles with "broken pockets" that have dissociating axons. Arrows in (E) and (F) point to unsegregated axons (*) dissociating from each other. (G) and (H) show two representative anmSCs containing "naked" axons and myelin-like fragments (arrows). M, normal myelin. (I) and (J) show the morphological similarity between a pair of anmSC and dSC. Arrows in (I) point to "naked" axons in an anmSC whose degeneration likely generates free Schwann cell processes seen in a dSC (arrowheads, [J]). (K and L) Two examples of dSCs with free Schwann cell processes (arrowheads, [K]) and degenerating unmyelinated axons (arrows). (M and N) Two examples of unassociated Schwann cells (uSCs) with continuous basal lamina and no axon contact. Arrowheads in (M) point to collagen fibers ensheathed by uSCs, which were also shown in Insets (M) with higher magnification. Arrows in the Insets of (M) and (N) (top) point to continuous basal lamina in uSCs as compared to a fibroblast process (arrows, bottom inset in [N]). (O) The numbers of Remak bundles per surface area (1,000 μm2) in control and mutant sciatic nerves were categorized into five groups based upon the number of axons that they ensheathed. Data in [O] represent mean ± SEM from 2 control and 3 mutant nerves. Top panel, abnormal nonmyelinating Schwann cells (anmSCs); middle panel, dissociating Schwann cells (dSCs); bottom panel, normal nonmyelinating Schwann cells (nmSCs). *p < 0.05, ***p < 0.001. Scale bar, 1 μm.

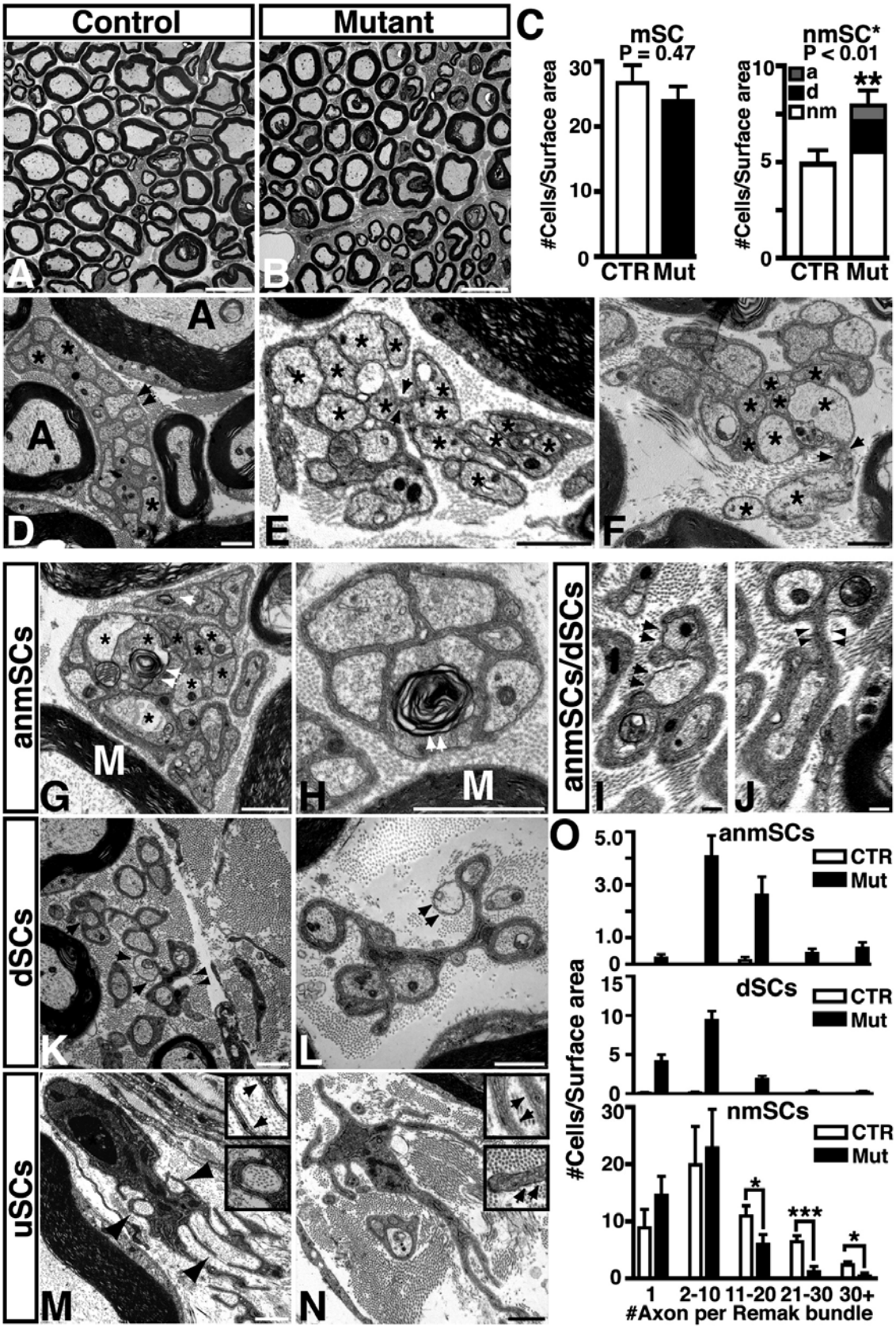
Control
Mutant
A
B
C
mSC
P = 0.47
#Cells/Surface area
30
20
10
0
CTR Mut
nmSC*
P < 0.01
a
d
nm
**
10
5
0
CTR Mut
D
E
F
anmSCs
G
M
H
M
anmSCs/dSCs
I
J
dSCs
K
L
uSCs
M
N
O
anmSCs
5.0
3.0
1.0
0
CTR
Mut
dSCs
15
10
5
0
nmSCs
30
20
10
0
*
***
*
#Cells/Surface area
1
2-10
11-20
21-30
30+
#Axon per Remak bundle

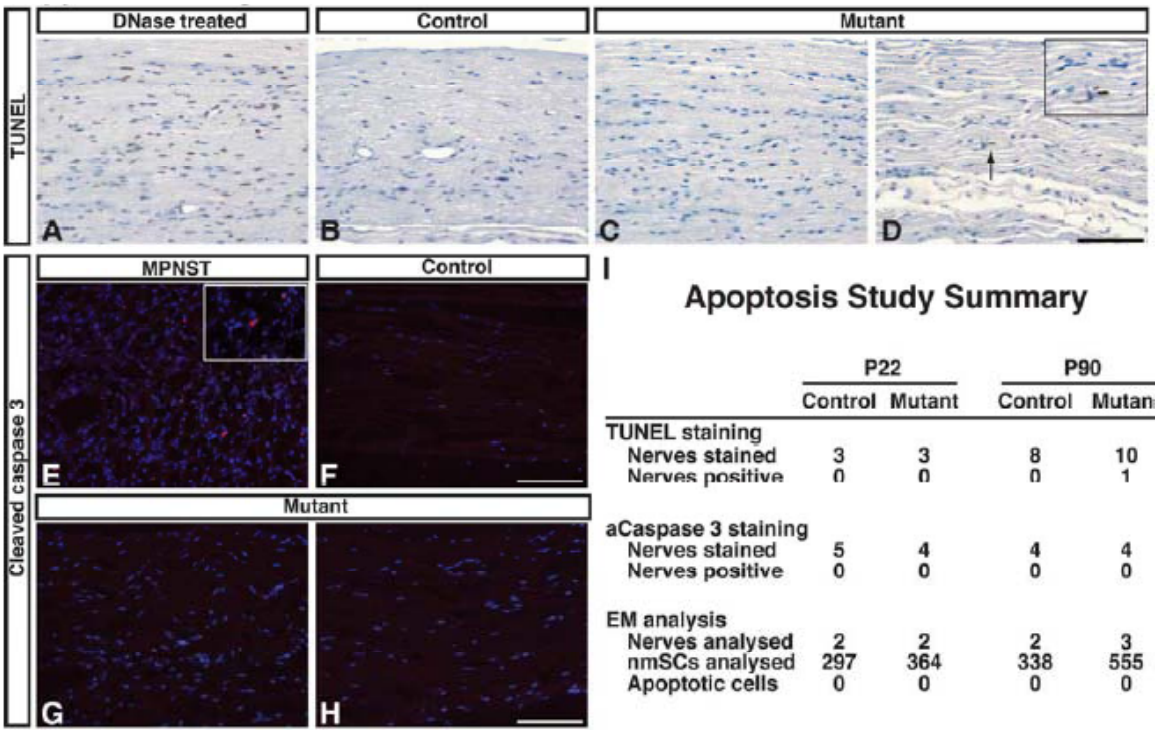

Figure 11 - Little evidence of apoptosis in P22 and P90 sciatic nerves. TUNEL was performed on sections of DNase I treated (A), control (B) and mutant sciatic nerves (C, D) from P90 mice. DNase I treated sections served as a positive control. A cluster of positive cells was detected in only one of ten mutant nerves analyzed (D, arrow). Immunofluorescence was performed with antibodies against cleaved caspase 3 on sectioned MPNST (E) and P90 control (F) and mutant sciatic nerves (G, H). Sections from MPNSTs served as a positive control. (I) Summary of three independent methods to detect apoptotic cells. Apoptosis via TUNEL staining was below detection limit for P22 and P90 control nerves, while only a single cluster of positive cells was detected in one P90 mutant nerve. Cleaved caspase-3 immunofluorescence was not detected in either control or mutant nerves. No Schwann cells that displayed apoptotic morphology were detected via electron microscopy in either control or mutant nerves. Together, this data suggests that no excess apoptosis was observed in P22 or P90 *NF1* mutant nerves. Scale bar: 50 µm.

There are three potential mechanisms by which the loss of poorly defasciculated Schwann cells can be accounted: (1) they undergo apoptosis, (2) they defasciculate over time and repair the damage or (3) they are unstable and degenerate into the anmSCs, dSCs and uSCs found in P90. To rule out apoptosis, I performed TUNEL and cleaved Caspase3 staining on P22 and P90 mutant nerves (Figure 11). TEM images from these nerves were also analysed to identify cells with characteristic apoptotic morphology (Figure 11). From these cases, a single instance of apoptosis was detected using TUNEL staining (Figure 11D), suggesting that the rate of apoptosis is extremely low in these nerves. If Schwann cells are degenerating and losing the axons they ensheath, then it would be expected that the remaining Schwann cells in *Nf1*-deficient nerves would ensheath fewer axons than their wildtype counterparts. Indeed, this is what I found when I compared the quantification of axons per Remak bundle in mutant and wildtype nerve (Figure 12). There was a significant decrease in the distribution of Remak

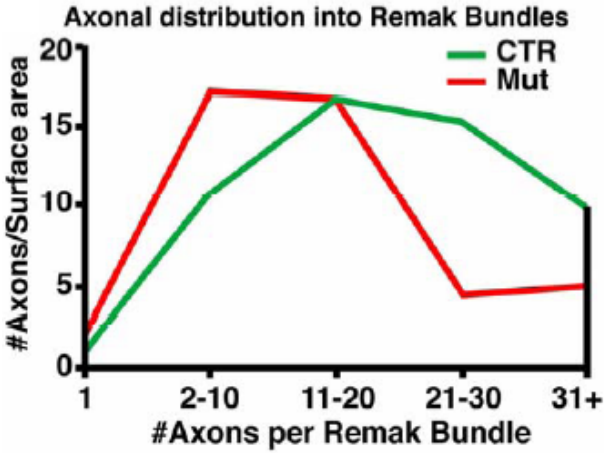

Figure 12 - Axonal distribution into Remak bundles. The numbers of axons per surface area (1,000 μm^2) in P90 control (green) and mutant (red) sciatic nerves were categorized into five groups based upon the number of axons within each Remak bundle. For mutant nerves, the axon number was pooled from all three non-myelinating Schwann cell populations (nmSCs, anmSCs and dSCs).

bundles with >20 axons, and an increase in Schwann cells with <10 axons. Although the defasciculation over time mechanism cannot be ruled out definitively based on my current methodologies, the observation that the aberrant Schwann cells display a spectrum of nmSCs progressively dissociating from their axons lends credence that this is the eventual fate of poorly defasciculated Schwann cells. Such a model would explain both the fate of Schwann cells with pocket defects and a pre-existing unstable Schwann cell/axon interaction would provide an explanation for why aberrant Schwann cells progressively dissociate from the axons they ensheath.

Expansion of Aberrant nmSC Population Results in Neurofibromas

I have termed the aberrant nmSCs as such based off their morphological resemblance to normal nmSCs. They have a basal lamina, Schwann-cell like processes and often ensheath small caliber axons. To further this claim, Dr. Zheng performed immunohistochemistry and found that P90 nerves have increased p75^{NGFR} and GFAP staining, but not BLBP, GAP43 or Sox10 (data not presented). This pattern of expression uniquely matches that of differentiated non-myelinating Schwann cells (Table 2). As there are no other cell types at this stage that express p75^{NGFR}, it can be utilized to specifically label nmSCs and aberrant nmSCs. To provide quantitative analysis of this increased p75^{NGFR} population, I performed FACS analysis on 2 P90 wildtype and 4 *Nf1*-deficient sciatic nerves using markers for p75^{NGFR} and BrdU with the assistance of Dr. Nancy Joseph from the Morrison lab. In wildtype mice, 6.27%

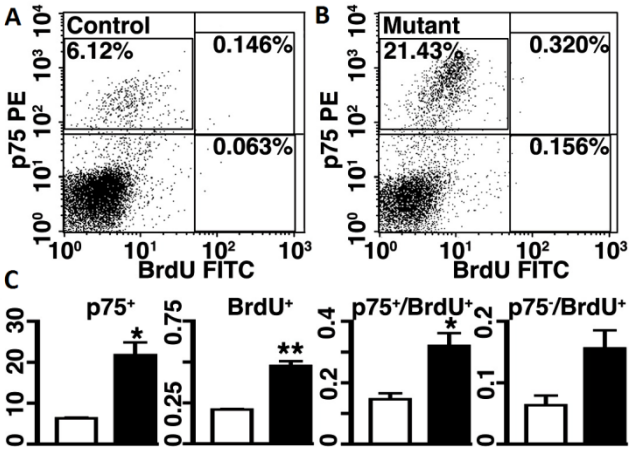

Figure 13 - Representative flow-cytometry plots demonstrate approximately a 2.5-fold increase in frequency of p75^{NGFR}-positive cells in mutant nerves. Data in (C) represent mean ± SEM from two independent experiments using age-matched control (n = 2) and mutant (n = 4) mice. $^{*}p < 0.05$, $^{**}p < 0.01$.

of the dissociated peripheral nerve cells were positive for $p75^{NGFR}$ (Figure 13A), while in mutants this population jumped to 21.75% (Figure 13B). This translates into an approximately 2.5 fold increase in the percentage of $p75^{NGFR}$ positive cells. Similarly, I found a 1.3 fold increase in the percentage of BrdU positive cells, from 0.209% in controls to 0.476% in mutants (Figure 12C). Together, these findings underscore aberrant nmSCs as an expansive population during the first stages of neurofibroma development.

To determine the role of these early-stage tumor cells during tumor progression, I analyzed 6 healthy *Nf1* mutant mice at 6 to 12 months of age, in which I identified the preneoplastic lesions in sciatic nerves similar to those seen in end-stage mutant nerves as described above. These observations suggest that hyperplasia and hyperplasia/NF are the precursors for neurofibroma. However, unlike the hyperplastic lesions observed in sciatic nerves of younger P90 mutant mice, similar lesions in aged mutant nerves exhibited focal loss of myelinated axons, revealed by loss of S100 staining (arrows, Figure 14B) as compared to age-matched controls (Figure 14A). Significantly increased $p75^{NGFR}$ expression also occurred in these mutant nerves (arrows, Figure 14F) compared to controls (Figure 14E), indicating further expansion of these $p75^{NGFR}$-expressing cell populations (compare Figures 14F and 14J to Figures 14E and 14I). In semithin sections, control nerves were tightly packed with myelinated axons with only a small intervening interstitial space (Figures 14M and 14Q). Aged hyperplastic mutant nerves, in contrast, were significantly enlarged by an expanded interstitial compartment (Figures 14N and 14R). The expression pattern of S100 and $p75^{NGFR}$ revealed that hyperplasia/NF (Figures 14C, 14G, and 14K) and neurofibromas (Figures 14D, 14H, and 14L) had continuous expansion of the $p75^{NGFR}$-expressing cells similar to that observed in hyperplasia, leading to further increased interstitial cellularity and depletion of myelinated axons (Figures 14O and 14S, 14P and 14T, Figure 15). Together, these results suggest that **neurofibroma progression is driven by continuous expansion of the *Nf1*-deficient cells with molecular characteristics of nonmyelinating Schwann cells (BLBP−/Sox10−/GFAP+/p75+) similar to the early-stage tumor cells that were identified in sciatic nerves of younger P90 mutant mice.**

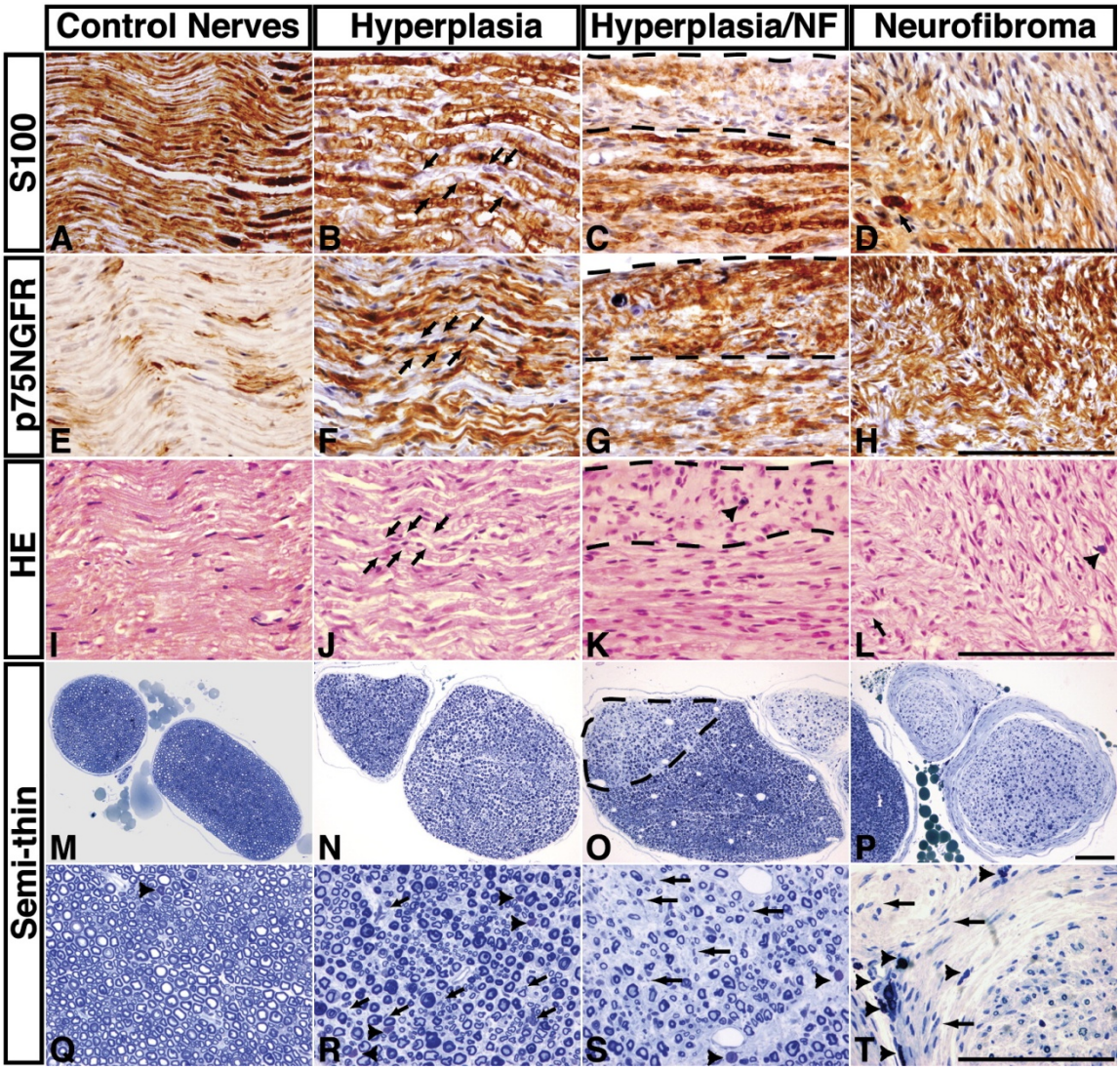

Figure 14 - Progression Stages of Neurofibroma Formation. Sciatic nerves from control (A, E, and I) and *Nf1*^{P0}CKO mutant mice harboring hyperplasia (B, F, and J), hyperplasia with focal neurofibroma (C, G, and K), and neurofibroma (D, H, and L) were sectioned and stained with anti-S100, anti-p75^{NGFR}, and H&E. Arrows in (B), (F) and (J) point to focal loss of S100-positive myelin sheath that was accompanied by increased numbers of p75^{NGFR}-expressing cells. The dashed lines in (C, G, and K) mark the border of hyperplasia and neurofibroma tissues. Arrows in (D) and (L) point to residual S100-positive myelin sheath in a neurofibroma. Arrowheads in (K) and (L) point to infiltrating mast cells in neurofibroma tissues. Semithin sections of sciatic nerves from control (M and Q) and mutant mice harboring hyperplasia (N and R), hyperplasia with focal NF (O and S), and neurofibroma (P and T) were stained with toluidine blue. The dashed lines in (O) mark the areas undergoing transition from hyperplasia to neurofibroma, which is characterized by significant loss of myelinated axons at ultrastructural levels. Arrows in (R), (S), and (T) point to increased numbers of cells between myelinated axons in mutant nerves compared to controls. Arrowheads (Q–T) point to infiltrating mast cells, staining metachromatically in this preparation. Scale bars, 100 μm.

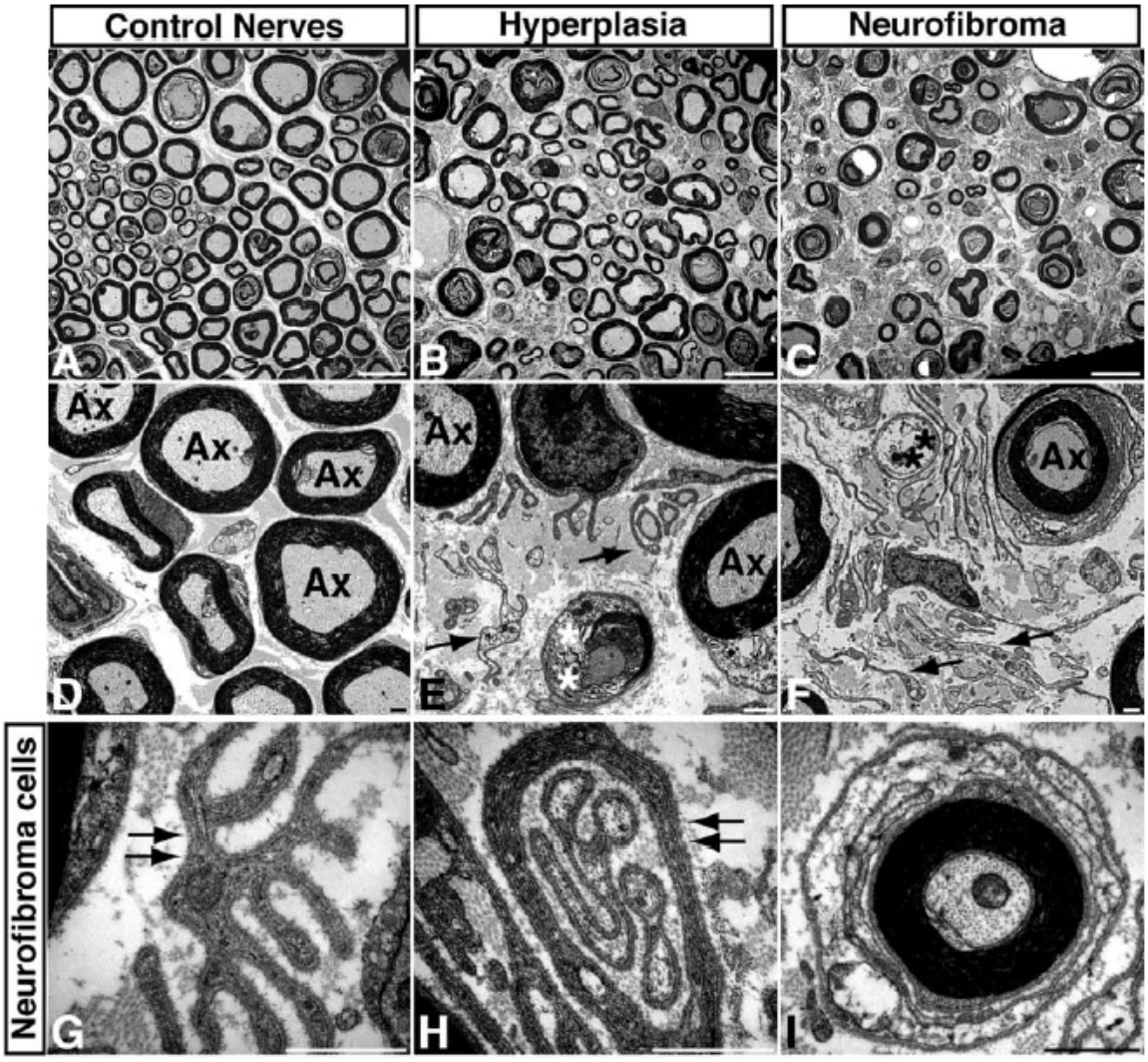

Figure 15 - Ultrastructural analysis of neurofibroma. Electron micrographs show control nerves (A, D), hyperplastic lesions (B, E), and neurofibromas (C, F) of mutant sciatic nerves. Arrows in E, F point to abnormal cells completely unassociated with axons (Ax). *, denoting degenerating axons. Very few normal non-myelinating Schwann cells were observed in neurofibromas, which is consistent with the observation that degeneration of this cell lineage was detected at the initiation stage of neurofibroma formation. (G, H) Two examples of unassociated Schwann cells (uSCs) with continuous basal lamina (arrows). (I) A perineurial-like cell lacking a continuous basal lamina and surrounds axons in a concentric fashion. Scale bar: 1 µm.

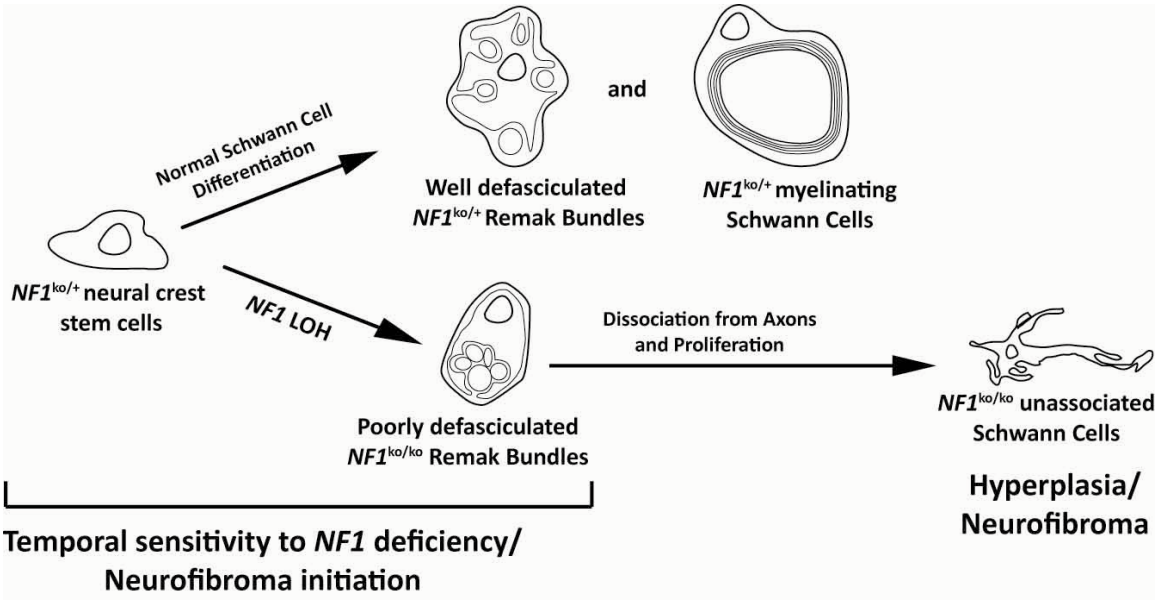

Figure 16 - Schematic Model of the Etiology of plexiform neurofibromas. *NF1*-deficiency during Schwann cell development leads to neurofibromas by causing abnormal non-myelinating Schwann cell development, loss of Schwann cell/axon interaction, dissociation and unassociated Schwann cell proliferation. Highlighted is the temporally sensitive period for *NF1* loss, which may also constitute the ideal therapeutic window for prophylactic intervention.

To summarize, the major conclusions in this chapter are: (1) *Nf1* inactivation must occur in Schwann cell precursors for plexiform neurofibromas to form and (2) *Nf1* loss causes abnormal differentiation of non-myelinating Schwann cells that will ultimately give rise to neurofibromas in supportive microenvironments. This process is mediated through poor defasciculation of axons into their own unique Schwann cell pockets, leading to loss of Schwann cell/axon interactions, dissociation and proliferation, and ultimately resulting in plexiform neurofibromas (Figure 16). These morphological changes are the earliest abnormalities observed over the course of peripheral nerve sheath tumorigenesis, and thus I posit they characterize neurofibroma initiation.

The data presented in this chapter was published in Volume 13, Issue 2 of Cancer cell in 2008 (Zheng et al., 2008).

One of the most exciting findings from a therapeutic perspective is that all of these subsequent transformations of the Schwann cells depend on the inactivation of *Nf1* during Schwann cell development. If therapies can be developed to somehow stabilize the Schwann cell-axon interaction during development and prevent dissociation, it may be possible to preclude peripheral nerve sheath tumorigenesis from NF1 patients altogether. Investigation of therapeutic approaches that exploit this window will be a focus of the following chapter.

CHAPTER III

Appropriate Therapeutic Windows for the Treatment of Peripheral Nerve Sheath Tumors

The *NF1* Heterozygous Microenvironment as a Potential Therapeutic Target

A great deal of attention has been recently paid to *NF1* heterozygous cells, which compose the tumor microenvironment, in NF1 patients as a potential therapeutic target (Reilly and Van Dyke, 2008). This approach is championed by the Clapp laboratory at the Indiana University School of Medicine, who have already reported on a successful case of managing pNFs using imatinib mesylate (Yang et al., 2008) and are currently conducting phase 2 clinical trials using imatinib on patients with pNFs. Imatinib mesylate is a small molecule inhibitor of tyrosine kinases, including c-abl, PDGFR and c-kit and has been widely deployed to treat chronic myelogenous leukemia (Savage and Antman, 2002). As c-kit activity is critical to mast cell development (Galli et al., 1993), it is assumed that imatinib's anti-neurofibroma effects are due to loss of mast cells in the tumor microenvironment (Yang et al., 2008). It should be noted, however, that imatinib may also have a direct effect on *Nf1*-deficient cells, as the molecular basis for its pharmacological activity on neurofibromas is poorly understood.

There exists some controversy over the contribution of *Nf1* heterozygosity in the PNST microenvironment. The strongest objection is in the form of a GEM that forms pNFs in the absence of a heterozygous environment. These mice were constructed using a genetic strategy similar to $Nf1^{Kx}$CKO2 mice; the primary difference is that *Krox20*-Cre is replaced with *Dhh*-Cre (Wu et al., 2008) Therefore I shall refer to these mice as $Nf1^{Dhh}$CKO2. *Dhh*-Cre is expressed in the SCP population during peripheral nerve development beginning at E12.5, similar to *P0*-Cre (Joseph et al., 2004). In $Nf1^{Dhh}$CKO2 mice, *Nf1* is specifically ablated in the SCP lineage, leaving unrecombined tissue wildtype for *Nf1*. The finding that $Nf1^{Dhh}$CKO2 mice develop neurofibromas is starkly at odds with previously published $Nf1^{Kx}$CKO2 mice, challenging the validity of the impact of the *Nf1* heterozygous microenvironment in tumorigenesis. A *Krox20*-based GEM was used to demonstrate that an *Nf1* heterozygous hematopoietic cell type is critical to providing a permissive tumor microenvironment (Yang et al., 2008), thus also calling into question whether their result may be mouse model specific.

My objectives in this chapter are to (1) determine if *Nf1* heterozygosity in the microenvironment is permissive or promotive to neurofibroma development and if so, (2) to define which stages of tumor development are susceptible to the influence of the microenvironment. By addressing these outstanding issues, I can define the appropriate therapeutic windows for microenvironment targeted therapies. Finally, based off our findings in the previous chapter, (3) to identify a therapeutic strategy that may stabilize the Schwann cell/axon interaction during development and potentially prevent tumors from arising in NF1 patients completely.

I have categorized PNST development in mice into three distinct stages: (1) initiation, (2) progression and (3) malignant transformation. Initiation, as described in the previous chapter, can be characterized by Schwann cell pocket defects at P22 and the appearance of anmSCs, dSCs and uSCs at P90. Progression is characterized by nerve hyperplasia, degeneration of myelinated axons, mast cell infiltration and the appearance of pNFs, which can be diagnosed histopathologically. Finally, malignant transformation is characterized by the appearance of palpable masses that grow rapidly and invade into adjacent tissues. MPNSTs are histologically distinct from benign neurofibromas, and can be diagnosed histopathologically.

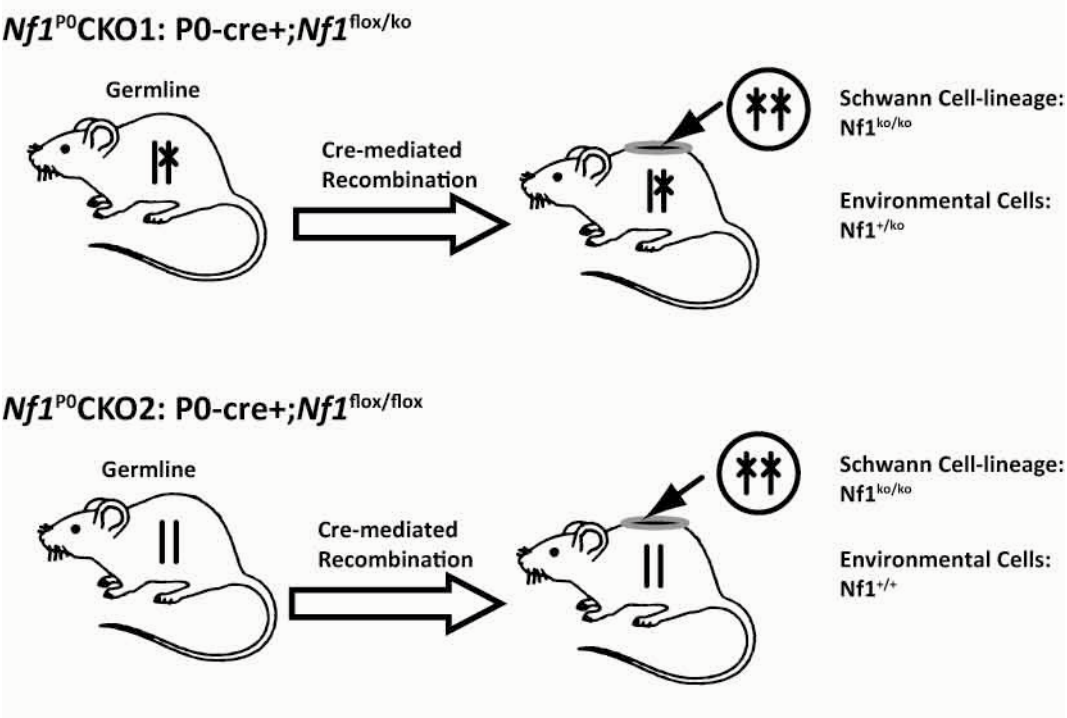

Figure 17 - Experimental approach to assessing the contribution of an *Nf1* heterozygous environment in neurofibroma initiation and progression.

Nf1 heterozygosity in the microenvironment is dispensable for neurofibroma initiation

To assess whether *Nf1* heterozygosity in the microenvironment will impact initiation and progression, I used mice with the genotypes [*P0*-Cre+; $Nf1^{flox/ko}$] ($Nf1^{P0}$CKO1) and [*P0*-Cre+;$Nf1^{flox/flox}$] ($Nf1^{P0}$CKO2) (Figure 17). Notably, this is the same genetic comparisons used in the original *Nf1* microenvironment study (Zhu et al., 2002) but with *P0*-Cre, a Cre recombinase that has a similar expression pattern to *Dhh*-Cre (Joseph et al., 2008; Joseph et al., 2004). $Nf1^{P0}$CKO2 mice allow me to determine whether extensive *Nf1* ablation during Schwann cell development throughout the PNS is sufficient to generate pNFs in a wildtype microenvironment. It would also allow me to make a comparison which was not performed by Wu et al., 2008, namely to determine whether *Nf1* heterozygosity in unrecombined cells ($Nf1^{P0}$CKO1) enhanced the pre-neoplastic or pNF phenotypes.

Figure 18 - Axon defasciculation defects in *Nf1* deficient non-myelinating Schwann cells does not depend on an *Nf1* heterozygous microenvironment. The cellular density of P22 sciatic nerve was unchanged between wildtype (A), $Nf1^{P0}$CKO1 nerves (C) and $Nf1^{P0}$CKO2 (B). (D) Cellular density for the nerve is plotted as mean ± SEM, and no significant difference exists between wildtype and mutant nerves (Student's T-test). Ultrastructural analysis of axon defasciculation in non-myelinating Schwann cells in P22 sciatic nerve demonstrates that the majority of wildtype Schwann cells (A', A'') segregate axons into either a distinct Schwann cell pocket or a pocket containing between two and ten axons. In contrast, both CKO1 (C', C'') and CKO2 (B', B'') sciatic nerves have increased rates of defasciculation defects in Schwann cells, with some pockets enveloping more than ten axons. A'', B'' and C'' are schematized representations of A', B' and C' TEM images, respectively. Schwann cell pockets in A'', B'', and C'' are color-coded in accordance with axons enveloped: a single axon (green), between two and ten axons (yellow), or more than 10 axons (red). (E) Quantification and chi-squared analysis reveal that while CKO1 and CKO2 have significantly higher rates of defasciculation defects than wildtype mice, the defect rates are not significantly different between mutant mice. N numbers represent number of axons quantified for each mutant. Scale bars: (A-C) 50 µm. (A'-C'') 1 µm.

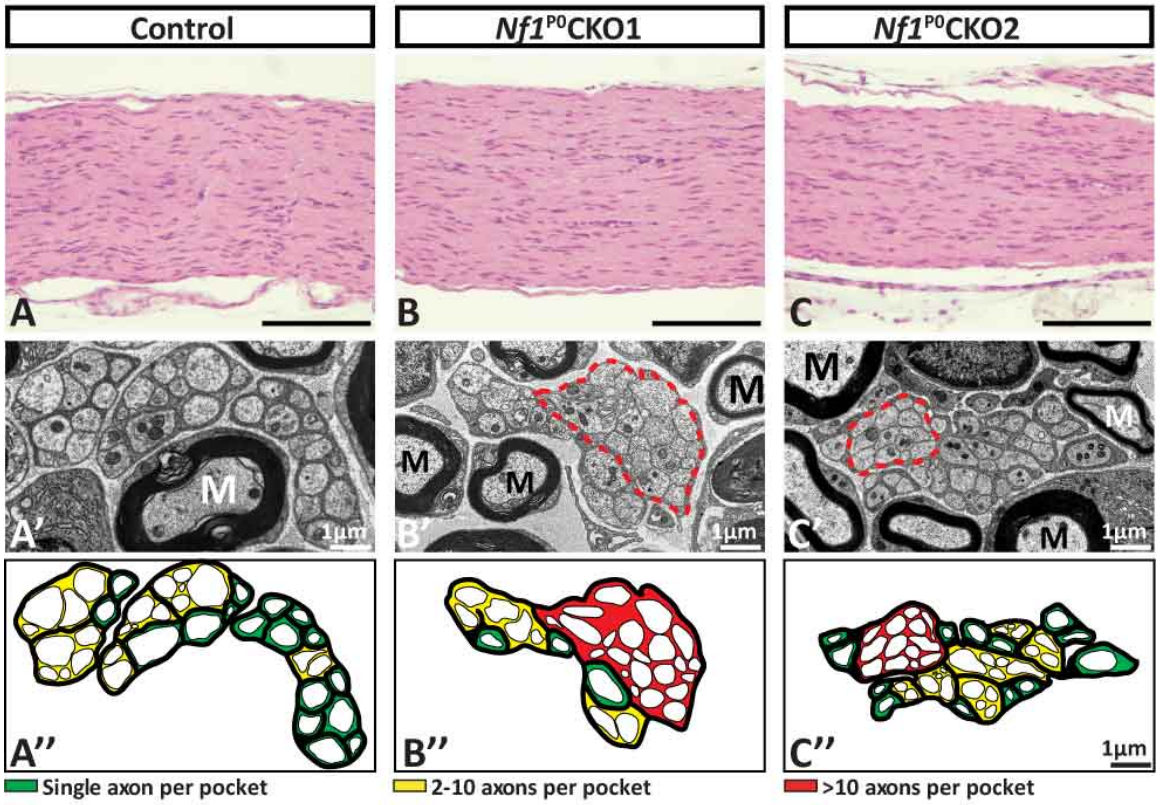
Control
Nf1P0CKO1
Nf1P0CKO2
A
B
C
A'
B'
C'
M
1µm
A''
B''
C''
Single axon per pocket
2-10 axons per pocket
>10 axons per pocket

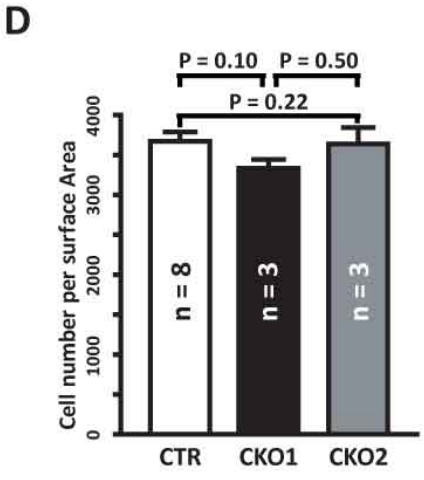
D
P = 0.10
P = 0.50
P = 0.22
Cell number per surface Area
0
1000
2000
3000
4000
n = 8
n = 3
n = 3
CTR
CKO1
CKO2

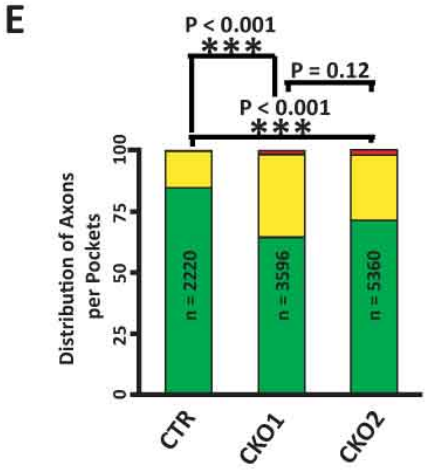
E
P < 0.001
***
P = 0.12
P < 0.001
***
Distribution of Axons per Pockets
0
25
50
75
100
n = 2220
n = 3596
n = 5360
CTR
CKO1
CKO2

Neurofibroma initiation was analyzed by collecting sciatic nerves from littermate wildtype, *Nf1*^{P0}CKO1 and *Nf1*^{P0}CKO2 mice at P22. Sciatic nerves from these mice were subjected to light and electron microscopy, as described in Chapter II. 8 wildtype, 3 *Nf1*^{P0}CKO1 and 3 *Nf1*^{P0}CKO2 P22 mice was collected by Dr. Zheng for light microscopy and I collected 5 wildtype, 4 *Nf1*^{P0}CKO1 and 2 *Nf1*^{P0}CKO2 P22 mice for electron microscopy. As expected, there were no detectable differences between control and either mutant sciatic nerve histology (Figure 18A-C). Performing ANOVA, I found no significant difference in the cellularity of the sciatic nerve, based on light microscopy (Figure 18D). Ultrastructurally, I could detect Schwann cell pocket defects in far greater frequency in both *Nf1*^{P0}CKO1 and *Nf1*^{P0}CKO2 derived sciatic nerves (Figure 18A'-C'). With the assistance of Dr. Zheng and Dr. Patel, the incidence of 1, 2-10 or >10 axons per Schwann cell pocket was quantified. Notably, more than 10 axons occupying a single Schwann cell pocket could be observed in both mutant nerves with regularity, but was extremely rare for control nerves. Using chi-squared goodness-of-fit test, I discovered that while both *Nf1*^{P0}CKO1 and *Nf1*^{P0}CKO2 nerves had significantly greater incidence of Schwann cell pocket defects than in control nerves, they were not significantly different from each other (Figure 18E). From this, I conclude that there is no difference between *Nf1*^{P0}CKO1 and *Nf1*^{P0}CKO2 mice in terms of abnormal Schwann cell differentiation, and *Nf1*-deficiency alone in SCPs is sufficient to produce this pre-neoplastic phenotype.

I next investigated the propensity of *Nf1*-deficient cells to generate pre-neoplastic abnormal non-myelinating Schwann cells in a wildtype and heterozygous environment. Sciatic nerves from littermate wildtype, *Nf1*^{P0}CKO1 and *Nf1*^{P0}CKO2 mice at P90 were subjected to light and electron microscopy, as previously described. 3 wildtype, 6 *Nf1*^{P0}CKO1 and 7 *Nf1*^{P0}CKO2 P90 mice were collected by Dr. Zheng for light microscopy and I collected 2 wildtype, 3 *Nf1*^{P0}CKO1 and 3 *Nf1*^{P0}CKO2 P22 mice for electron microscopy. In nerves from both *Nf1*^{P0}CKO1 and *Nf1*^{P0}CKO2 mice, I could identify a range of abnormal Schwann cells (Figure 19B), dissociating Schwann cells (Figure 19C) and unassociated Schwann cells. Quantification of light microscopy-based cellular density by Dr. Zheng revealed significantly increased cellularity in the mutant peripheral nerves compared to control but not to each other (Figure 19D). The myelinating Schwann cell population was decreased by approximately 10% in both mutants, but due to large sample variation, this was not significant (Figure 19E). I quantified the number of abnormal, dissociating and normal non-myelinating Schwann cells in the wildtype, *Nf1*^{P0}CKO1 and *Nf1*^{P0}CKO2 sciatic nerve to determine if *Nf1* environmental heterozygosity impacted the efficacy of generating pre-neoplastic cell types. Both *Nf1*^{P0}CKO1 and *Nf1*^{P0}CKO2 mice had significantly greater cellularity than littermate controls, and a significant presence of abnormal or dissociating Schwann cells (Figure 19F). Although a trend was observed where *Nf1*^{P0}CKO1 had slightly more non-myelinating Schwann cells than *Nf1*^{P0}CKO2, this difference was not statistically significant. Finally, Dr. Patel noted that mast cells were not observed in P22 nerves, but were significantly increased in mutant nerves at P90 compared to control nerves (Figure 19G). Together, this data demonstrates that ***Nf1* heterozygosity in the microenvironment and mast cells have little, if any, effect on neurofibroma initiation**. Consequently, **targeting the microenvironment likely will not successfully prevent peripheral nerve sheath tumorigenesis.**

Figure 19 - Neurofibroma initiation and the spectrum of aberrant non-myelinating Schwann cells is not modulated by *Nf1* environmental heterozygosity. Neurofibroma initiation can be documented at P90 in the sciatic nerves. (A) Typical non-myelinating Schwann cell ensheath multiple axons without myelination. It is globular in form, with all Schwann cell processes engaged in ensheathing axons. Each axon is fully defasciculated and only one axon occupies each axon pocket. (B) A similar spectrum of Abnormal Schwann cells (aSCs) could be identified in both *Nf1*^{P0}CKO1 and *Nf1*^{P0}CKO2 sciatic nerves. These aSCs are characterized by degenerating axons (a, a'), identified by the presence of bloated axons with sparse neurofilaments, focal dissociation (b, b', arrowhead), identified by Schwann cell processes that are not engaged in ensheathing axons, crevassing (c, c', red dotted line) and axons with focal loss of ensheathment (c, c', inset). (C) A similar spectrum of Dissociating Schwann cells (dSCs) could also be identified in both *Nf1*^{P0}CKO1 and *Nf1*^{P0}CKO2 sciatic nerves. Initial stages of dSCs are characterized by subcompartments of Schwann cells that are only attached to the main structure with only a thin Schwann cell process (a, a', red dotted line) in conjunction with a free Schwann cell process (a, a', arrowhead) while maintaining a globular form. Progressive stages of dSCs are characterized by progressive loss of globularity, with increased incidences of tenuous attachment (b, b', red dotted line) and free Schwann cell processes (b, b', arrow heads). Advanced stages of dSCs are characterized by complete loss of globular form, a decrease in total number of ensheathed axons, and a large proportion of Schwann cell processes that do not ensheath axons (c, c'). Finally, unassociated Schwann cells (uSCs) that ensheath no axons but still possess Schwann cells structures can also be identified at similar levels in both *Nf1*^{P0}CKO1 and *Nf1*^{P0}CKO2 sciatic nerves (d, d'). These uSCs can be distinguished from fibroblasts and perineural cells from the presence of a continuous basal lamina. (D) P90 sciatic nerve cellularity reveals a similar pattern, where both *Nf1*^{P0}CKO1 (n=6) and *Nf1*^{P0}CKO2 (n=7) are significantly higher in cellularity than controls (n=3) but are similar to each other. (E) Ultrastructural analysis of P90 sciatic nerve reveals no significant difference in cellular density of myelinating Schwann cells any mutant nerves. (F) In contrast, ultrastructural analysis of non-myelinating Schwann cells in P90 sciatic nerves reveal the difference in cellularity between mutant and control nerves is caused by increased number of non-myelinating Schwann cells, retaining the pattern where both mutants are significantly higher in cellularity than the control, but are not significantly different from each other. (F) Furthermore, there is a similar distribution of normal non-myelinating Schwann cells, abnormal non-myelinating Schwann cells and dissociating Schwann cells between *Nf1*^{P0}CKO1 and *Nf1*^{P0}CKO2 nerves, but not to control nerves. (G) Mast cell infiltration into peripheral nerves was analyzed based on light microscopy. No mast cells were present in P20 either control (n=6), *Nf1*^{P0}CKO1 (n=3) or *Nf1*^{P0}CKO2 (n=3) sciatic nerves. At P90, *Nf1*^{P0}CKO1 (n=7) and *Nf1*^{P0}CKO2 (n=7) mice had significantly increased mast cell infiltration in sciatic nerves compared to controls (n=3). 19 fields from 2 control nerves, 28 fields from 3 CKO1 and 25 fields from 3 CKO2 nerves were analyzed for the ultra structural study; linear mix modeling was used to calculate statistical significance. Scale bars: 1 μm.

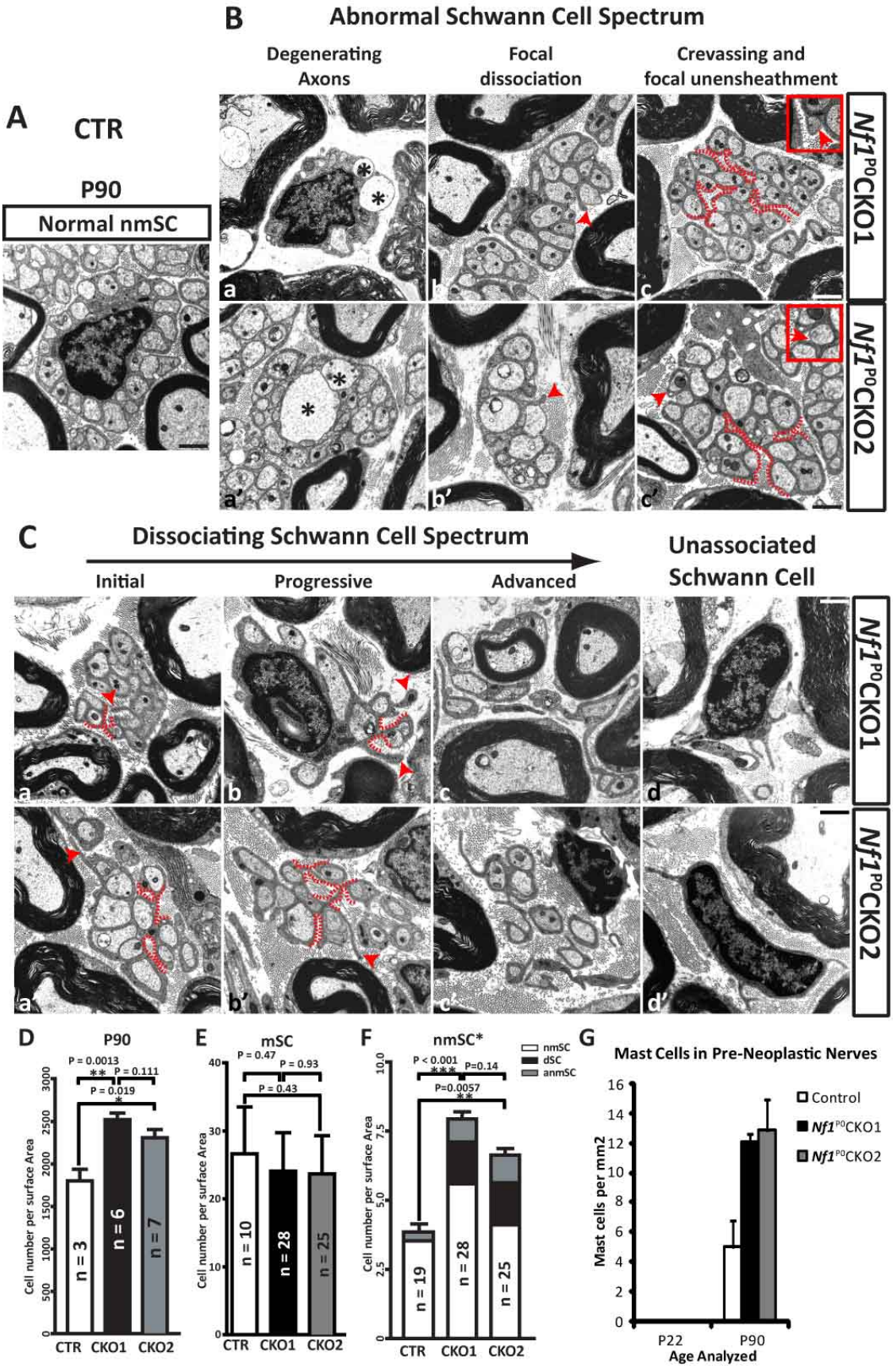
A
CTR
P90
Normal nmSC
B
Abnormal Schwann Cell Spectrum
Degenerating Axons
Focal dissociation
Crevassing and focal unensheathment
Nf1P0CKO1
Nf1P0CKO2
C
Dissociating Schwann Cell Spectrum
Initial
Progressive
Advanced
Unassociated Schwann Cell
Nf1P0CKO1
Nf1P0CKO2
D
P90
Cell number per surface Area
P = 0.0013
P = 0.111
P = 0.019
n = 3
n = 6
n = 7
CTR CKO1 CKO2
E
mSC
Cell number per surface Area
P = 0.47
P = 0.93
P = 0.43
n = 10
n = 28
n = 25
CTR CKO1 CKO2
F
nmSC*
nmSC
dSC
anmSC
Cell number per surface Area
P < 0.001
P=0.14
P=0.0057
n = 19
n = 28
n = 25
CTR CKO1 CKO2
G
Mast Cells in Pre-Neoplastic Nerves
Mast cells per mm2
Control
Nf1P0CKO1
Nf1P0CKO2
P22
P90
Age Analyzed

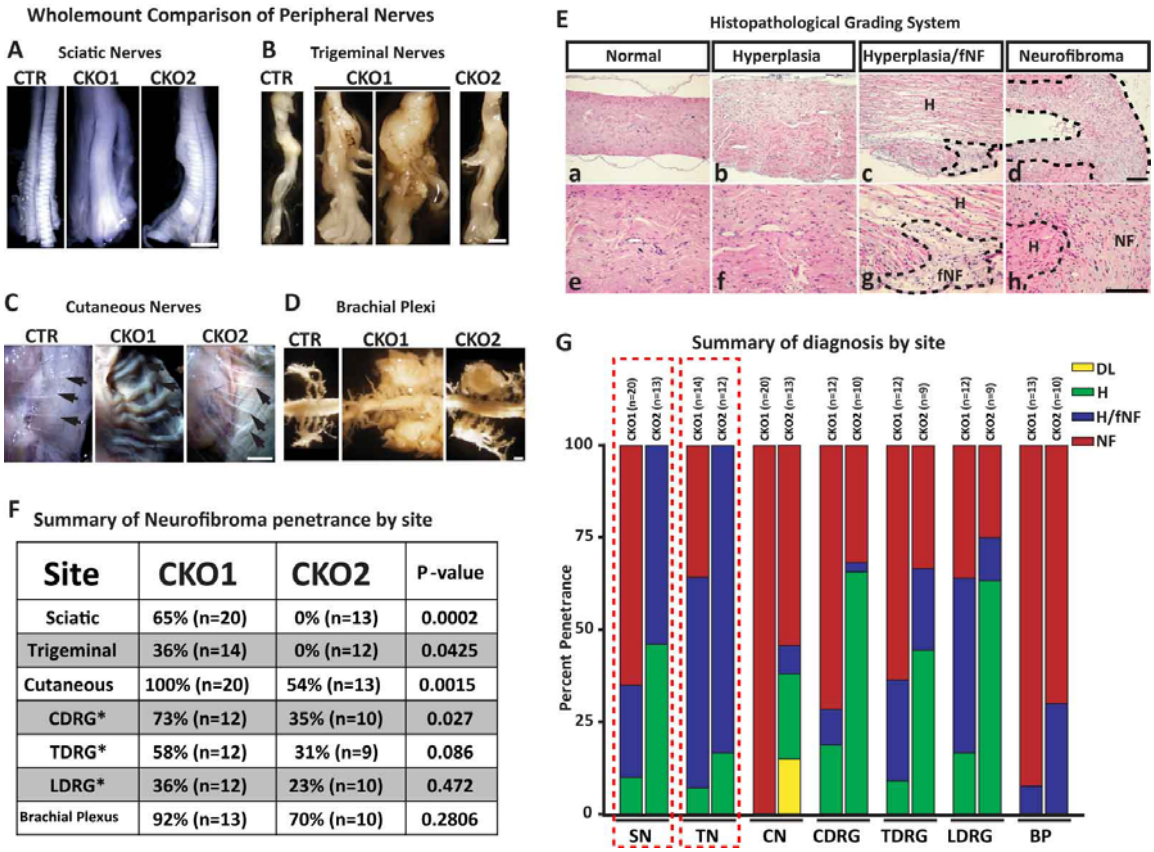

F Summary of Neurofibroma penetrance by site

Site	CKO1	CKO2	P-value
Sciatic	65% (n=20)	0% (n=13)	0.0002
Trigeminal	36% (n=14)	0% (n=12)	0.0425
Cutaneous	100% (n=20)	54% (n=13)	0.0015
CDRG*	73% (n=12)	35% (n=10)	0.027
TDRG*	58% (n=12)	31% (n=9)	0.086
LDRG*	36% (n=12)	23% (n=10)	0.472
Brachial Plexus	92% (n=13)	70% (n=10)	0.2806

Figure 20 - *Nf1* heterozygosity in the environment promotes neurofibroma development. Representative whole-mount comparison of sciatic nerves (A), trigeminal nerves (B), cutaneous/subcutaneous nerves (C), and brachial plexus (D) from control, CKO1 and CKO2 littermate mice demonstrate that the enlarged nerve size of mutant mice is sensitive to genotype of environmental cells. Despite both mutant nerves being enlarged compared to controls, CKO1 nerves are markedly larger in size than those from age-matched CKO2 mice. The largest CKO1 trigeminal nerve (B, right panel) is also presented to demonstrate the range of trigeminal nerve sizes, while CKO2 trigeminal nerves have lower variation. (E) Histological grading criteria for peripheral nerve sheath tumors. (F) Summary of the penetrance of neurofibroma for sciatic nerves, cutaneous/subcuteneous nerves, trigeminal nerves, brachial plexus, cervical dorsal root ganglia (C-DRG), thoracic DRG (T-DRG) and lumbar DRG (L-DRG). (G) The summary of our diagnostics for all nerves examined, based on genotype, is presented. Frank neurofibromas (NF) are labeled by red, hyperplasia (H) by green, focal neurofibromas (H/fNF) by blue, and non-neurofibroma, degenerative lesions (DF) by yellow. Bars representing CKO1 nerves are on the left while CKO2 are on the right. A pattern emerges across the board, where the *Nf1* heterozygosity in the environment enhances the neurofibroma phenotypes of *Nf1* deficiency. Scale bars: (A-D) 1 mm. (E) 50 µm.

Nf1 heterozygosity in the microenvironment promotes neurofibroma progression

The impact of the *Nf1* heterozygous microenvironment was assessed by analyzing 20 *Nf1*^{P0}CKO1 and 13 *Nf1*^{P0}CKO2 mice between 10 and 14 month of age. As documented in Chapter II, at this time point, *Nf1*^{P0}CKO1 mice develop pNFs in the sciatic nerve. Whenever possible, comparisons were made between littermates to decrease potential influences resulting from different genetic backgrounds. I performed a systematic analysis of seven distinct sites across the peripheral nervous system: sciatic nerves (SN), trigeminal nerves (TN), cutaneous nerves (CN), cervical dorsal root ganglia (CDRG), thoracic dorsal root ganglia (TDRG), lumbar dorsal root ganglia (LDRG) and brachial plexus. These nerves were histopathologically diagnosed based on their H&E staining patterns. This comparison would allow me to resolve whether (1) mice with sufficient burden of *Nf1*-deficient cells in the developing PNS could generate tumors and (2) the *Nf1* heterozygous microenvironment plays a significant role in peripheral nerve sheath tumorigenesis in a *Krox20*-Cre independent GEM.

One of the most salient observations I found upon dissecting the peripheral nerves was that while both *Nf1*^{P0}CKO1 and *Nf1*^{P0}CKO2 nerves were enlarged throughout the peripheral nervous system, *Nf1*^{P0}CKO1 nerves consistently had a more severe phenotype (Figure 20A-D). The degree to which nerves were enlarged varied between sites, where the sciatic and trigeminal nerves had a mild but appreciable enlargement (Figure 20A-B), while cutaneous nerves and brachial plexi were often grossly enlarged (Figure 20C-D). Based upon previously established histological grading criteria (Zheng et al., 2008), each nerve was diagnosed into one of four categories based primarily on H&E staining. Normal nerves (Figure 20Ea, e) have low cellularity. Hyperplastic nerves (Figure 20Eb, f) exhibit higher cellularity, while maintaining tissue organization and often accompanied by increased blood vessels and mast cells. Hyperplastic nerves with focal neurofibromas (Figure 20E, fNF, inside dotted line) resemble hyperplastic nerves (Figure 20E, H outside dotted line), however, contain focal areas of increased cellularity and loss of organization (Figure 20Ec, g). Finally, frank neurofibromas (Figure 20Ed, h; NF region) resemble human neurofibromas with high levels of collagen deposition, disruption of tissue organization and greatly increased cellularity (compare H with NF).

From these histological criteria, the penetrance of neurofibroma (Figure 20F) was determined for the seven sites described above. For sciatic nerve, cutaneous/subcutaneous nerves, trigeminal nerves and brachial plexus, one nerve was examined for each mouse. For DRGs, from 1-6 DRGs were examined for each site in each mouse, and used to generate an average penetrance of all DRGs per mouse. Specifically, 46 C-DRG from 12 CKO1 , 45 C-DRG from 10 CKO2 ; 23 T-DRG from 12 CKO1 , 16 T-DRG from 9 CKO2; 29 L-DRG from 12 CKO1 and 20 L-DRG from CKO2 mice were analyzed. A Z-test was used to determine whether a difference in neurofibroma penetrance exists based on the environmental genotype for sciatic nerves, cutaneous/subcuteneous nerves, trigeminal nerves and the brachial plexus. Linear mixed modeling was used to determine whether the penetrance in DRGs was different based on *Nf1* heterozygosity in the environment. A more detailed breakdown consisting of the diagnosis I made for each nerve is summarized in Figure 20G.

It is evident from the summaries provided (Figure 20F, G) that there exists a significant difference in terms of tumor burden between *Nf1*^{P0}CKO1 and *Nf1*^{P0}CKO2 mice. This leads me to conclude that *Nf1* heterozygosity in the microenvironment does indeed promote peripheral nerve sheath tumorigenesis. This is especially true for the sciatic and trigeminal nerves, where neurofibromas were never diagnosed in *Nf1*^{P0}CKO2 mice and were relatively common in *Nf1*^{P0}CKO1 mice (Figure 20G). However, our *Nf1*^{P0}CKO2 mice also formed pNFs with high penetrance at certain sites such as cutaneous nerves, DRGs and brachial plexi. This would suggest that an *Nf1* heterozygous microenvironment is not necessary to permit pNF formation provided sufficient quantities of *Nf1*-deficient cells are present in the peripheral nerves. In fact, approximately 35% of the peripheral nerves show recombination in mice carrying *P0*-Cre and 60% in *Dhh*-Cre across all SCP-derived lineages (Joseph et al., 2008; Joseph et al., 2004). This large number of *Nf1*-deficient cells may be the reason why an *Nf1* heterozygous microenvironment is unnecessary to support tumor growth in *Nf1*^{P0}CKO2 and *Nf1*^{Dhh}CKO2 mice. *Nf1*^{Kx}CKO2 mice may instead reflect a case where only a small number of cells undergo recombination in SCPs, making this GEM far more reliant on environmental *Nf1* heterozygosity. I would posit that the *Nf1*^{Kx}CKO mice better represent what is occurring in NF1 patient populations, but technical limitations prevent this line of investigation in humans. Taking into consideration that *Nf1*-deficient sciatic nerves had identical phenotypes at three months regardless of *Nf1* heterozygousity and the robust difference observed nine month later, it becomes apparent a difference in Cre-mediated recombination efficiency due to the number of *Nf1* flox alleles is not a viable explanation for the phenotypic differences in CKO1 and CKO2 mice. Instead, I conclude that **the *Nf1* heterozygous microenvironment promotes neurofibroma progression, and thus makes an ideal therapeutic window for microenvironment targeted therapies.**

Nf1 heterozygosity and Benign tumor burden does not impact Malignant Transformation

To assess the role of an *Nf1* heterozygous microenvironment in the malignant transformation of PNSTs, I had to use mouse models that satisfied two criteria: (1) they must form MPSNTs and (2) they must allow me to directly compare how *Nf1* wildtype and *Nf1* heterozygous microenvironments contribute to MPNST formation. *Nf1*^{P0}CKO1 and *Nf1*^{P0}CKO2 mice rarely, if ever, developed malignant peripheral nerve sheath tumors. NPcis mice developed MPNSTs, but required the germline *Nf1* knockout allele to be linked to the *p53* knockout allele, precluding analysis of tumorigenesis in a wildtype microenvironment (Cichowski et al., 1999; Vogel et al., 1999). To address this question, I needed to generate a novel mouse model.

The NPcis mice provided the inspiration for the development of these novel GEMs. These mice demonstrate that cells that are double deficient for *Nf1* and *p53* can give rise to MPNSTs. Thus, I focused my attempt on generating *Nf1*/*p53* double deficient cells in either a wildtype or *Nf1* heterozygous environment. This was accomplished by generating mice that carry a chromosome with an *Nf1* flox allele and a *p53* knockout allele in cis. When these mice were crossed to P0-Cre positive mice carrying *Nf1* knockout, *Nf1* flox or *Nf1* wildtype alleles, three useful genetic configurations would be produced. NP^{P0}CKO1 [P0-Cre+; *Nf1*$^{flox/ko}$; *p53*$^{ko/+}$] mice possessed a germline *Nf1* knockout allele, providing an *Nf1* heterozygous microenvironment, and would be *Nf1*-deficient after Cre-mediated recombination. These mice should presumably develop a high burden of benign neurofibromas due to the presence of *Nf1*-deficient cells in a heterozygous microenvironment. A LOH event at the *p53* locus after Cre-mediate recombination would produce *Nf1*/*p53* double deficient cells (Figure 21A). NP^{P0}CKO2 [P0-Cre+; *Nf1*$^{flox/flox}$; *p53*$^{ko/+}$] mice possessed two *Nf1* flox alleles and thus have an *Nf1* wildtype microenvironment. Similar to NP^{P0}CKO1 mice, NP^{P0}CKO2 mice become *Nf1*-deficient after Cre-mediated recombination and an LOH event at the *p53* locus after Cre-mediate recombination would produce *Nf1*/*p53* double deficient cells (Figure 21A). These mice should presumably develop a medium burden of benign neurofibromas due to the presence of *Nf1*-deficient cells in a wildtype microenvironment. A comparison of the rate of malignant transformation and tumor burden between NP^{P0}CKO1 and NP^{P0}CKO2 mice would determine whether *Nf1* heterozygosity affects malignant transformation. Finally as a control, NP^{P0}Cis [P0-Cre+; *Nf1*$^{flox/+}$; *p53*$^{ko/+}$] mice would only generate the *Nf1*/*p53* cis mutant chromosome upon Cre-mediated recombination (Figure 21A). These mice will rarely have *Nf1*-deficient cells alone as a co-LOH event that also inactivates *p53* is the most common mode of LOH in mice (Luongo et al., 1994). Thus NP^{P0}Cis nerves should not have any inflammatory response associated with the presence of *Nf1*-deficient cells (Figure 19G, 20E). Thus these three *p53* based models provide *Nf1*/*p53* double deficient cells with three distinct cellular microenvironments to develop in: nerves with high benign tumor burden in *Nf1* heterozygous microenvironment with NP^{P0}CKO1, nerves with medium benign tumor burden in *Nf1* wildtype environment with NP^{P0}CKO2 and nerves with no tumor burden in *Nf1* wildtype environment with NP^{P0}Cis.

Benign tumor burden was assessed for NP^{P0}CKO1, NP^{P0}CKO2 and NP^{P0}Cis mice through the systematic diagnosis of four sites from the PNS of these mice: sciatic nerves (SN), cutaneous

nerves (CN), trigeminal nerves (TN) and brachial plexi (BP). Histological slides of these nerves were prepared with the assistance of Jessica Lee, and I diagnosed these nerves based on my previously described grading criteria (Figure 20E). The benign tumors in these mice are not as robust as previously documented, likely due to the different genetic background on which these mice were generated. Nevertheless, mice with a heterozygous *Nf1* microenvironment had a more robust benign tumor phenotype than mice with a wildtype environment (Figure 21B). As expected, nerves from NP^{P0}Cis mice were histologically normal.

Despite the increased benign tumor phenotype and *Nf1* heterozygous environment in NP^{P0}CKO1 mice, they developed MPNSTs with the same rate and penetrance as NP^{P0}CKO2 and NP^{P0}Cis mice (Figure 21C-E). **This result suggests that neither *Nf1* environmental heterozygosity nor benign tumor burden impacts the propensity for cells to undergo malignant transformation, provided the cell is already *Nf1*/*p53* double deficient.** I performed molecular characterization of the MPNST cells to verify that the genetics of MPNSTs is as I described (Figure 21A). I found that recombination of the *Nf1* flox allele was detected in all tumors (Figure 21F), but curiously the *Nf1* ko allele was retained in NP^{P0}CKO1mice. Finally, LOH of the *p53* allele could be detected in the majority of NP^{P0}CKO1, NP^{P0}CKO2 and NP^{P0}Cis tumors, as verified by Daniel Treisman using qPCR (Figure 21G). To verify that P53 function was lost in tumors that do not display LOH, I extracted cDNA and performed rtPCR for *p53* transcripts. These tumors indeed only expressed the *p53* ko allele, suggesting loss of P53 function (Figure 21H).

Figure 21 - Progressive mouse models of neurofibroma and MPNSTs. (A) Schematic of the genetic configurations of $NP^{P0}CKO1$, $NP^{P0}CKO2$ and $NP^{P0}Cis$ mice. The green color is used to label functional alleles, including the wild-type allele (+) and the flox allele (x1); the red color is used to label non-functional alleles, including the recombined flox allele (Δ) and the knockout allele (–). Genotypes for each cell type are indicated in parentheses. While both $NP^{P0}CKO$ configurations generate the same cell type after Cre-mediated recombination, the unrecombined cells in $NP^{P0}CKO1$ are Nf1 heterozygous while the unrecombined cells in $NP^{P0}CKO2$ are Nf1 wildtype. $NP^{P0}CKO$ mutant mice require an LOH event at the P53 locus after recombination, while the $NP^{P0}Cis$ mice require a co-LOH event after recombination, to generate a cell deficient for both Nf1 and p53 activity. (B) Nerves from $NP^{P0}CKO1$ and $NP^{P0}CKO2$ mice develop benign peripheral nerve sheath tumors, but with greater severity when the environment is heterozygous. No abnormalities were detected in $NP^{P0}Cis$ nerves. (C) The survival curve and (D) MPNST-free curve for $NP^{P0}CKO1$, $NP^{P0}CKO2$ and $NP^{P0}Cis$ mice were nearly identical, with the majority of the mice euthanized due to presence of body tumor or abdominal mass. The rates at which our three mouse models developed MPNSTs were indistinguishable (P>0.5). (E) The tumor spectrum of $NP^{P0}CKO1$ (n=18 tumors), $NP^{P0}CKO2$ (n=34 tumors) and $NP^{P0}Cis$ (n=34) mice are relatively similar, with MPNSTs comprising the predominant tumors generated (60%, 78% and 68%, respectively). Malignant pheochromocytoma accounted for 20% of tumors in $NP^{P0}CKO1$ mice, and 6% in both $NP^{P0}CKO2$ and $NP^{P0}Cis$ mice. In some instances (10%, 11% or 18% for $NP^{P0}CKO1$, $NP^{P0}CKO2$ and $NP^{P0}Cis$ respectively), tumors that arose from tissue that had not undergone Cre-mediated recombination. (F) PCR analysis of MPNST tissue confirms our schematic model of MPNST generation in these mice. All MPNSTs from these mice demonstrate recombination of the Nf1 allele, and commonly demonstrate LOH of the P53 allele. However, there is significant contamination with unrecombined tissue, resulting in a fainter band, as opposed to complete absence of band. (G) Scatter plot of residual wildtype p53 allele, as measured by qPCR of genomic DNA with primers against exons 6 and 7 of p53. (H) rtPCR of p53 and GAPDH transcripts from tumor cDNA. WT control tissue was isolated from irradiated gut and spleen, The brain tumor controls are from $p53^{\Delta 2\text{-}11/\Delta 2\text{-}11}$, $p53^{\Delta 5\text{-}6/\Delta 5\text{-}6}$ and $p53^{point/\Delta 2\text{-}11}$, from left to right. S stands for sarcoma and M stands for MPNSTs.

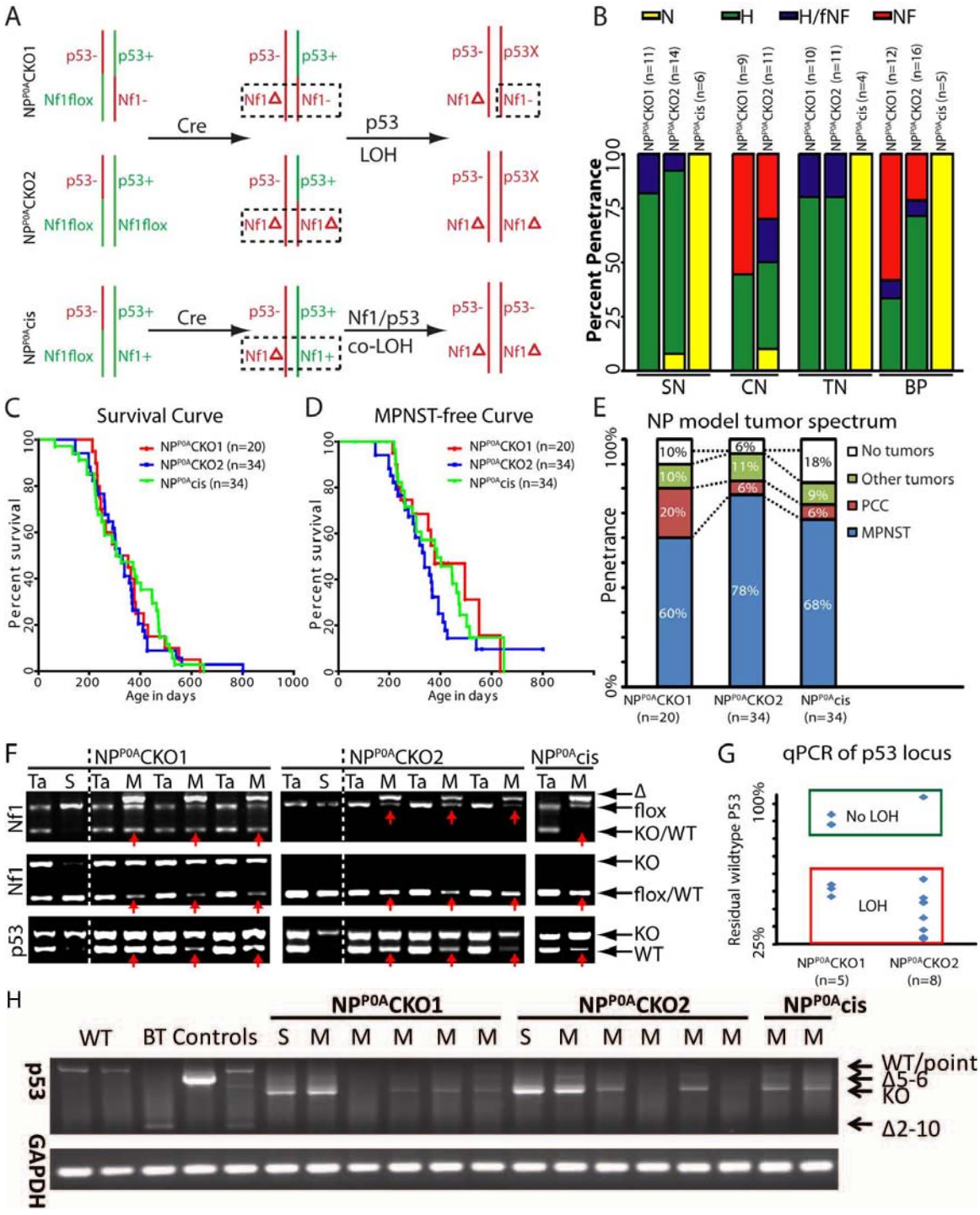
A
NP^P0ACKO1
p53-
p53+
Nf1flox
Nf1-
Cre
Nf1Δ
p53
LOH
p53X
NP^P0ACKO2
Nf1flox
NP^P0Acis
Nf1+
Nf1/p53
co-LOH
B
N
H
H/fNF
NF
Percent Penetrance
SN
CN
TN
BP
C
Survival Curve
Percent survival
Age in days
D
MPNST-free Curve
E
NP model tumor spectrum
Penetrance
No tumors
Other tumors
PCC
MPNST
F
Nf1
p53
Δ
flox
KO/WT
KO
flox/WT
WT
G
qPCR of p53 locus
Residual wildtype P53
No LOH
LOH
H
WT
BT Controls
WT/point
Δ5-6
KO
Δ2-10
GAPDH

To verify that the *Nf1* heterozygous microenvironment did not play a role in malignant transformation, I generated a MPNST model that was independent from P53. Mutations in the CDKN2A loci are more commonly found in MPNSTs from NF1 patients than *p53* (Upadhyaya et al., 2008). As *Ink4a/Arf/Nf1* compound mutant mice were previously demonstrated to generate MPNSTs (Joseph et al., 2008) and the *Ink4a/Arf* flox allele was available for my use (Krimpenfort et al., 2001), I attempted to generate compound conditional knockouts of *Ink4a/Arf* and *Nf1*. To examine the role of *Nf1* heterozygous microenvironment in *Nf1/Ink4a/Arf* tumorigenesis, I used a similar strategy as previous described for *p53*. I generated NI^{P0}CKO1 [P0-Cre+; *Nf1*$^{flox/ko}$; *Ink4a/Arf*$^{flox/flox}$] and NI^{P0}CKO2 [P0-Cre+; *Nf1*$^{flox/flox}$; *Ink4a/Arf*$^{flox/flox}$] mice, where upon Cre-mediated recombination, NI^{P0}CKO1 would have *Nf1/Ink4a/Arf* deficient cells in an *Nf1* heterozygous microenvironment while NI^{P0}CKO2 mice will have those cells in a wildtype environment. NI^{P0}CKO1 and NI^{P0}CKO2 mice developed MPNSTs very rapidly, between four and five months, precluding a robust neurofibroma phenotype (Figure 22A). As seen with the previously described *p53*-based mouse models, neither the rate of tumor formation (Figure 22B-C) nor the tumor spectrum (Figure 22D) was influenced by the presence of *Nf1* heterozygosity in unrecombined cells. Indeed, mast cells are uncommon in MPNSTs from all mouse models (Figure 23A), further supporting the notion that mast cells This once again demonstrates that malignant transformation does not depend on the status of *Nf1* in the tumor microenvironment.

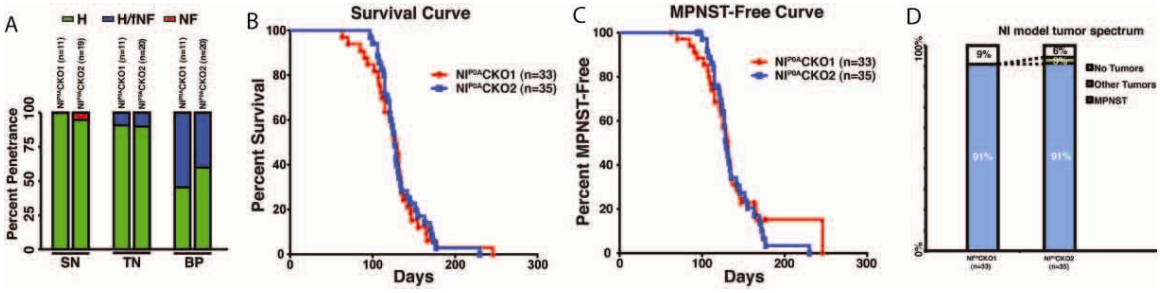

Figure 22 - Benign and malignant tumors in *Nf1/Ink4a/Arf* mutant mice. (A) Diagnostic breakdown of benign tumors found in NIP0CKO1 and NI^{P0}CKO2 mice. (B) The survival curve and (C) MPNST-free curve for NI^{P0}CKO1 and NI^{P0}CKO2 mice were nearly identical, with the majority of the mice euthanized due to presence of body tumors. The rates at which these mouse models developed MPNSTs were indistinguishable (P>0.5). (D) The tumor spectrum of NI^{P0}CKO1 (n=33 tumors) and NI^{P0}CKO2 (n=35 tumors) mice are nearly identical, with MPNSTs comprising the predominant tumors generated (91% in both cases).

By using five novel GEM models of MPNST, I have demonstrated that malignant transformation of peripheral nerve sheath tumors does not depend on *Nf1* heterozygosity, or even an inflammatory nerve environment. Instead it appears that the largest contributory factor to malignant transformation is the presence of additional oncogenic somatic mutations in tumor suppressors such as *p53* and *Ink4/Arf*. Thus, therapies being developed for MPNSTs must target the cells carrying these mutations directly, as attempts to target the microenvironment will most likely be met with failure.

Figure 23 - Mouse model recapitulates human peripheral nerve sheath features and MPNSTs display immature neural crest features. (A) Tumors collected from MPNST mice models recapitulate common histopathological features of human MPNSTs. Commonly found features in mice are malignant spindle cells arranged in intertwining fascicles, with ill-defined cytoplasms and a high mitotic rate (a, a'). Occasionally, geographic necrosis can be found, sometimes accompanied by peripheral palisading malignant spindle cells (b, b'). Another manifestation of MPNSTs seen are unoriented malignant cells dispersed in sheets (c, c'). In some tumors, nuclear pleomorphism can be found, with marked variation in size and shape of cells (d, d'). (B) MPNSTs collected from these mouse models often express $p75^{NGFR}$ (a, a') and BLBP (b, b') throughout the tumor tissues. Less frequently, MPNSTs express S100 (c, c'), GFAP (d, d'), and/or Sox10 (e, e') in approximately 50% of tumors analyzed, without correlations in expression patterns. While immunohistological markers varied highly between MPNSTs, staining patterns were indistinguishable between the NPP0ACKO mice. (C) Ultrastructural analysis of murine benign (a, b) and malignant (c, d) peripheral nerve sheath tumors reveal a high degree of similarity with their human counterparts (a'-d'). Benign tumor cells retain differentiated phenotype: continuous basal lamina (inset, arrows), extended Schwann cell processes, sheet-like organization, low rates of proliferation. MPNST have immature and tumor phenotypes: loss of basal lamina (inset, arrows), prominent nuclei, ovoid shape, crowded and highly proliferative. Scale bars: (A, B) 50 μm, (C) 10 μm.

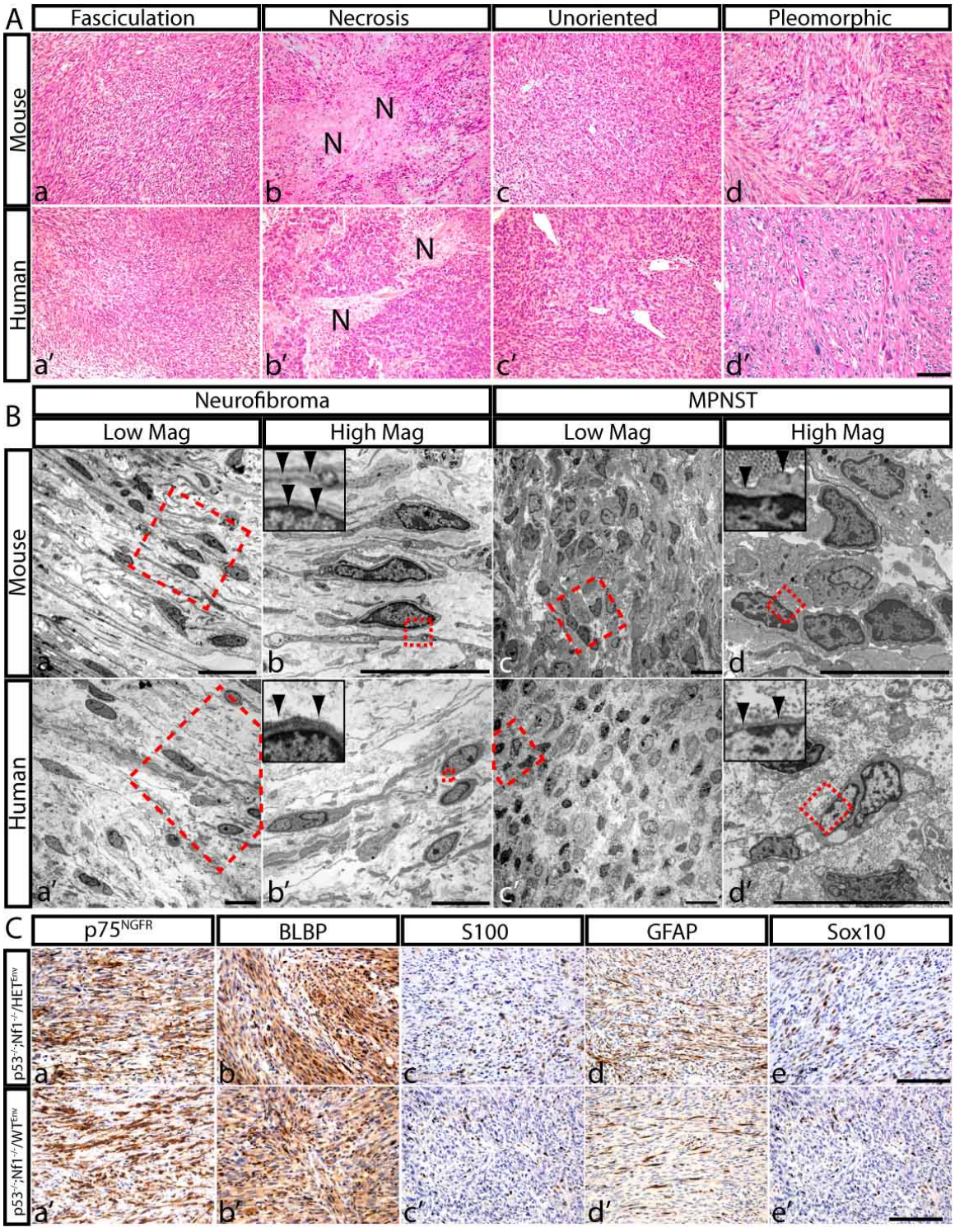
A
Fasciculation
Necrosis
Unoriented
Pleomorphic
Mouse
Human
N
N
N
N
a
b
c
d
a′
b′
c′
d′
B
Neurofibroma
MPNST
Low Mag
High Mag
Low Mag
High Mag
Mouse
Human
a
b
c
d
a′
b′
c′
d′
C
p75NGFR
BLBP
S100
GFAP
Sox10
p53-/-;Nf1-/-/HETEnv
p53-/-;Nf1-/-/WTEnv
a
b
c
d
e
a′
b′
c′
d′
e′

Contribution of Novel Mouse Models to NF1 Community

The mouse models that I have developed not only address the role of environmental *Nf1* haploinsufficiency in malignant transformation, but are improvements over currently existing GEM models of MPNSTs. Tumors collected from all five MPNST mouse models have a nearly identical spectrum of histopathology to their human counterparts (Figure 23A). This similarity is also reflected at the ultrastructural level in terms of benign neurofibromas (for NP^{P0}CKO1 and NP^{P0}CKO2 mice) and MPNSTs (Figure 23B). As all of these mouse models utilize Cre-mediated recombination to generate the *Nf1*/p*53*-deficient cis chromosome, tumors from these mice are typically derived from the neural crest lineage. This lineage can be verified through genotyping for recombined *Nf1* alleles. As a result, these mice produce relatively pure populations of MPNSTs (Figure 20E, 22D). One advantage to having a pure population of MPNSTs is that it becomes possible to determine which markers consistently label tumors and thus are candidates for biomarkers to help differentially diagnose MPNSTs from benign neurofibromas or other sarcomas. I have performed a preliminary battery of neural crest lineage markers and found that MPNSTs express many of the proteins commonly found in cells from the immature Schwann cell lineage (Figure 23C, Table2). These GEM are ideal for pre-clinical trials, as $Nf1^{P0}$CKO1 mice carry both benign and malignant tumor, allowing simultaneous assessment of both tumor's response to potential therapies. NI^{P0}CKO1 and NI^{P0}CKO2 develop tumors extremely rapidly, permitting rapid assessment of therapeutic outcomes within 5 months. Together, the mouse models that I have generated provide a valuable contribution to the NF1 community and should replace previously developed mouse models of MPNSTs.

Overview of Peripheral Nerve Sheath Tumor Development and Therapeutic Windows

From the data presented in these chapters, neurofibroma development can broadly be defined as three distinct stages (Figure 24). Step 1, initiation: LOH of *NF1* in Schwann cell precursors during development results in abnormal non-myelinating Schwann cell differentiation. Poor defasciculation of axons ensheathed by non-myelinating Schwann cells leads to unstable Schwann cell/axon interactions, followed by progressive dissociation and proliferation of unassociated Schwann cells. Step 2, progression: the presence of unassociated Schwann cells cause inflammation and the recruitment of heterozygous mast cells to the tumor microenvironment. The interaction between *Nf1*-deficient unassociated Schwann cells, *Nf1* heterozygous cells in the tumor microenvironment then cause progression of tumors resulting in demyelination, a more severe inflammatory response and proliferation of all peripheral nerve sheath cells. Thus a tumor mass is composed of both *Nf1*-deficient unassociated nonmyelinating Schwann cells and *Nf1* heterozygous stromal cells. Step 3, malignant transformation: *Nf1*-deficient cells that acquire additional oncogenic mutations such as *p53* or *Ink4a/Arf* will eventually undergo malignant transformation and ultimately form MPNSTs. From a microenvironmental therapeutic perspective, the primary cell types to target are the *Nf1* heterozygous cells during Step 2, tumor progression. To treat Step 1 and Step 3, we will need to turn to other therapeutic avenues.

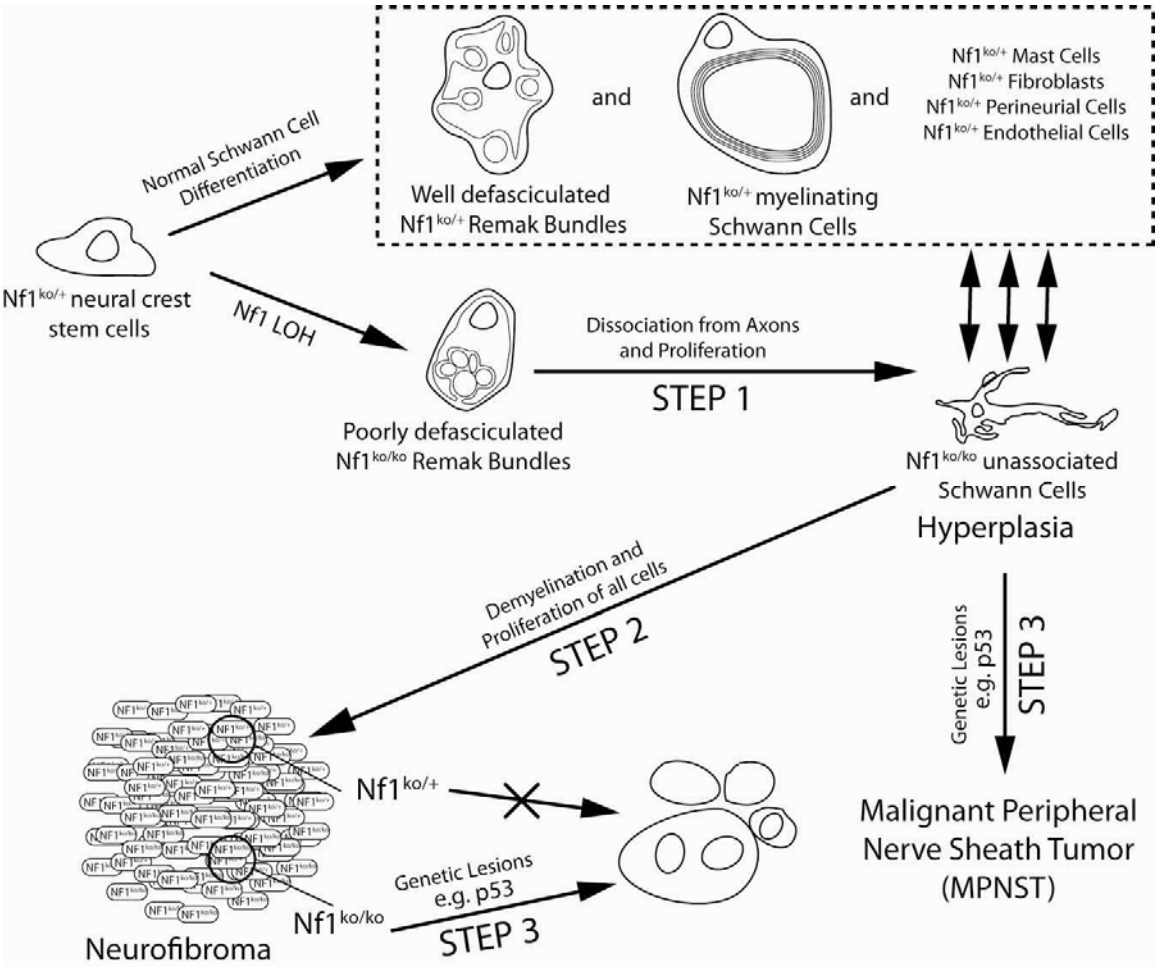

Figure 24 - Schematic Model for the Development of Peripheral Nerve Sheath Tumors. Appropriate microenvironment targets for therapy are highlighted, and only appropriate for Step 2.

Rapamycin treatment can stabilize early Schwann cell/axon interaction in *Nf1*-deficient mice

Targeting the *Nf1* heterozygous microenvironment does not appear to be a viable strategy to prevent neurofibroma initiation. To find potential alternative therapeutic approaches to treating pre-neoplastic nerves, Dr. Zheng performed signal transduction analysis on *Nf1*^{P0}CKO1 and *Nf1*^{P0}CKO2 sciatic nerve at the P22 and P90 time points. No abnormal signal transduction activity was detected at P22 (Figure 25A). In contrast, the mutant P90 *Nf1* nerves consistently increased phospho-Erk and phospho-S6 (Figure 25B). This suggests that the MAPK/ERK and mTORC1 two signal transduction pathways may be dysregulated during neurofibroma initiation. Phospho-S6 is not upregulated in neurofibromas (data not shown).

Dr. Zheng and I opted to pursue the mTORC1 pathway, as its inhibitor, rapamycin and its analogs, have been approved and used as immunosuppressive medication for organ transplant patients and because there have been reports of rapamycin acting as a temporary cytostatic agent for MPNSTs (Johannessen et al., 2008). If the mTORC1 pathway is critical to neurofibroma

initiation, it may be possible to revert the phenotype observed at P22 and stabilize the Schwann cell/axon interaction (Figure 26A), preventing subsequent dissociation and tumor formation.

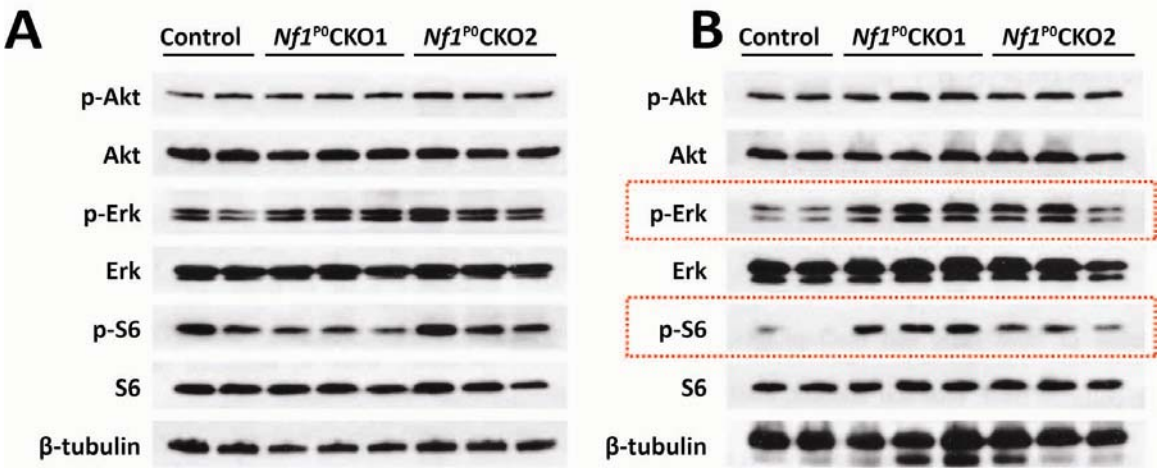

Figure 25 - Western blot analysis of MAPK/ERK, PI3K/AKT and mTORC1 signal transduction pathways in *Nf1*^{P0}CKO1 and *Nf1*^{P0}CKO2 nerves at P22 (A) and P90 (B).

To test the therapeutic efficacy of rapamycin in preventing early neurofibroma initiation phenotypes, two preliminary trials were conducted by Dr. Zheng. Five *Nf1*^{P0}CKO1 mice were treated with rapamycin at a dose of 5 mg/kg every other day via intra-peritoneal injection every other day starting P30 until P90. A second batch comprised of 7 *Nf1*^{P0}CKO1 mice with the same regiment was treated starting at P21 until P90. Wildtype mice treated with rapamycin and *Nf1*^{P0}CKO1 mice treated with vehicle were also included as negative and positive controls for neurofibroma initiation, respectively. At P90, nerves were collected for light and electron microscopic analysis. My efforts were focused on ultrastructural and statistical analysis of the sciatic nerves isolated from these preliminary trials. My ultrastructural analysis revealed that rapamycin treatment was indeed capable of stabilizing the Schwann cell/axon interaction in a subset of mice when administered during the neurofibroma initiation period. Despite the presence of abnormally differentiated Remak bundles with pocket defects at P22, when treated with rapamycin, 40% of mice with treatment starting at P30 and over 70% of mice with treatment starting at P21 had a dramatically less severe ultrastructural phenotype, with fewer aberrant non-myelinating Schwann Cells (Figure 26B). Rapamycin treated control mice had no abnormal Schwann cell phenotype (Figure 26Ca, e), while vehicle treated mutant mice had aberrant non-myelinating Schwann cell phenotypes: the presence of dissociating and unassociated Schwann cells (Figure 26Cb, f). I categorized rapamycin treated mutant mice as either “unrescued” (Figure 26Cd, h) or “rescued” (Figure 26Cc, g) based on the presence or absence of more than one unassociated Schwann cells per low magnification (1450X) field, respectively. At least one unassociated Schwann cell could be found in each “rescued” nerve, suggesting that these mice were indeed mutants and that there may be a minority of *Nf1*-deficient cells that are unresponsive to rapamycin treatment. Ultrastructural quantification of sciatic nerve cellularity is correlated to the light microscopy findings of cellular density by Dr. Zheng, suggesting that the ultrastructural cross-section is representative of the entire length of

the nerve. I quantified the cell types found in the vehicle treated mutants, rapamycin treated controls, rescued and unrescued mice and found a striking alteration in the number of dissociating cells in the rescued nerves (Figure 26 D, E, top chart). The numbers of dissociating and unassociated Schwann cells have been reduced to rapamycin treated control levels, and are significantly different from the untreated and the unrescued mutants (Figure 26 D, E, top charts). However, the total number of non-myelinating Schwann cells was not reduced to wildtype levels (Figure 26D, E, bottom charts). This suggests that rapamycin can stabilize Schwann cell/axon interaction but only after some Schwann cells have undergone proliferation. Nevertheless, **this represents the first successful attempt at targeting the pre-neoplastic population of neurofibroma initiation.**

Appropriate therapeutic windows for treatment of PNSTs

The primary objective of determining the role of *Nf1* heterozygousity in peripheral nerve sheath tumor development for identifying appropriate therapeutic windows has been accomplished. I have found that *Nf1* heterozygousity promotes neurofibroma progression, likely by eliciting an inflammatory response involving mast cells. However, *Nf1* heterozygousity appears to be dispensable for neurofibroma initiation and malignant transformation. From these observations, I predict that therapies that target the heterozygous environment will be met with success in limiting plexiform neurofibroma growth. Unfortunately, these therapies will likely be unable in reducing the number of incipient tumor cells, which may still undergo malignant transformation if they acquire additional oncogenic mutations. Furthermore, mast cell based therapies will unlikely be effective in treating MPNSTs, as my data suggests that mast cells do not participate in malignant transformation or maintenance of malignant tumors. The data presented in this chapter resolves the conflict in the literature regarding the role of Nf1 heterozygosity. The observation that having greater number of cells deficient for Nf1 may alleviate the requirement for an Nf1 heterozygous environment, provides an explanation that reconciles the discordant data in the NF1 field. Nevertheless, Nf1 heterozygosity plays a role in promoting robust peripheral nerve sheath tumor formation.

The secondary objective of identifying a therapeutic strategy that may stabilize the Schwann cell/axon interaction during development and prevent tumors from arising has partially been accomplished. Preliminary data using rapamycin treatment in post-natal *Nf1*-deficient nerves demonstrates that in a subset of mutants, the number of dissociating and unassociated Schwann cells was dramatically reduced by P90. The long-term consequence of this reduction of incipient tumor cells is unknown, but taking into consideration the temporal requirement for *Nf1* loss documented in Chapter II, prevention of later peripheral nerve sheath tumor development is within the realm of possibility.

The contents of this chapter are currently being prepared for publication.

Figure 26 - Treatment with Rapamycin Reverses Neurofibroma Initiation in a Subset of *Nf1* Deficient Nerves. (A) Schematic diagram of proposed rapamycin function in *Nf1* deficient cells. (B) Results from preliminary treatment of *Nf1*^{P0}CKO1 mice treated starting P21 or P30. (C) Representative TEM morphology of normal (a, e), vehicle treated mutants (b, d), successfully rescued mutants (c, f) and unsuccessfully rescued mutants (d, g). Quantification of the aberrant nonmyelinating Schwann cell population from *Nf1*^{P0}CKO1 mice treated starting P21 (D) or P30 (E), reveals a distinct loss of the dissociating Schwann cell population in successfully rescued mice. P-values were calculated using linear mixed modeling; * represent significance level <0.05.

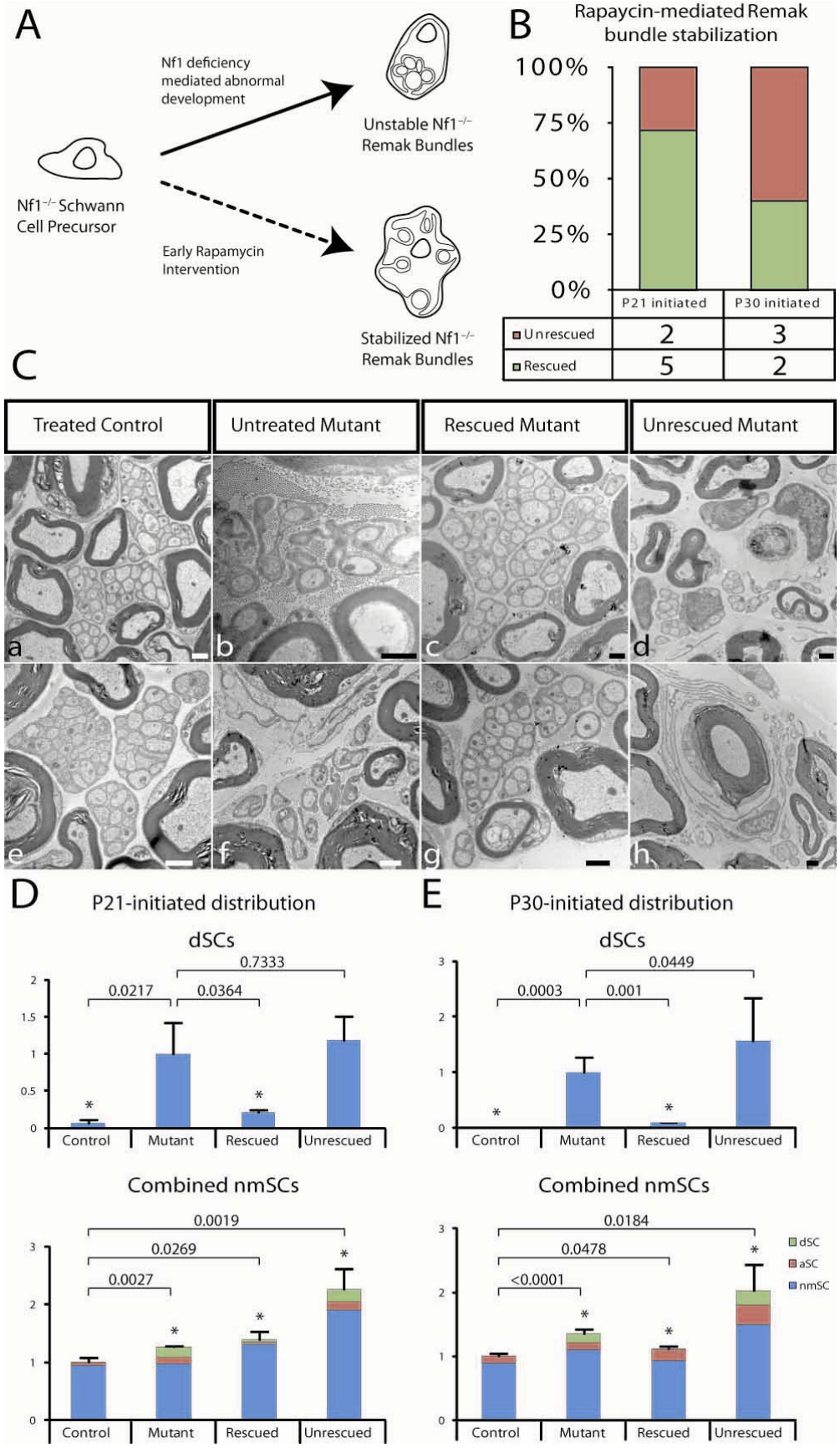
A
Nf1 deficiency mediated abnormal development
Unstable Nf1−/− Remak Bundles
Nf1−/− Schwann Cell Precursor
Early Rapamycin Intervention
Stabilized Nf1−/− Remak Bundles
B
Rapaycin-mediated Remak bundle stabilization
100%
75%
50%
25%
0%
P21 initiated
P30 initiated
Unrescued 2 3
Rescued 5 2
C
Treated Control
Untreated Mutant
Rescued Mutant
Unrescued Mutant
a
b
c
d
e
f
g
h
D
P21-initiated distribution
dSCs
0.0217
0.0364
0.7333
Control
Mutant
Rescued
Unrescued
Combined nmSCs
0.0027
0.0269
0.0019
E
P30-initiated distribution
dSCs
0.0003
0.001
0.0449
Combined nmSCs
<0.0001
0.0478
0.0184
dSC
aSC
nmSC

CHAPTER IV

Discussion and Future Directions

Clinical and basic science contribution of Murine Models of NF1

The major motivation for biomedical research is the generation of data and reagents that can be used to provide insight into the etiology of human disease for the purpose of improving therapeutic outcomes. The major deficit in the field of NF1 is the lack of effective therapies for both benign plexiform neurofibromas and MPNSTs, leaving surgical resection the only modality available to clinicians. By taking a basic science approach to understanding how *Nf1*-deficient Schwann cells give rise to plexiform neurofibromas and careful documentation of the stages of peripheral nerve sheath tumor development, I have attempted to discover therapeutic windows in tumorigenesis and develop potential therapies for NF1 patients. Thus, it is worthwhile to evaluate how the data and reagents generated in this thesis contributes to the field of NF1 and how it can be applied clinically.

The generation of murine models of NF1 that recapitulate the most important features of human PNSTs provides an ideal platform by which future pre-clinical trials can be performed. In this thesis, I have generated and characterized four models of pNFs and five models of malignant peripheral nerve sheath tumors. Of these models, *Nf1*^{P0}CKO1 mice represent a model in which robust pNFs develop throughout the peripheral nerve, including the sciatic nerves. As peripheral nerve development is best documented in the sciatic nerves (Jessen and Mirsky, 2005), *Nf1*^{P0}CKO1 mice allows for the documentation of how *Nf1*-deficiency impacts on Schwann cell development, as demonstrated in Chapter II. Thus, *Nf1*^{P0}CKO1 mice are ideal for pre-clinical trials that assay the efficacy of therapies due to their robust neurofibroma development throughout the peripheral nerves and the investigation of how therapeutics can interact with *Nf1*-deficient Schwann cell development, as demonstrated in Chapter III. In contrast, while *Nf1*^{Kx}CKO1 mice has less robust pNFs, the limited recombination during the temporal requirement for *Nf1* loss results in a model that is more sensitive to *Nf1* heterozygousity than *Nf1*^{P0}CKO1, as documented in Chapter III and previous publications (Zhu et al., 2002). Thus, *Nf1*^{Kx}CKO1 mice, and their counterparts *Nf1*^{Kx}CKO2 mice, provide ideal models to study the effects of *Nf1* heterozygousity in the microenvironment, as previously documented (Yang et al., 2008; Zhu et al., 2002). NI^{P0}CKO1 and NI^{P0}CKO2 mice rapidly generate MPNSTs with high penetrance, and are indistinguishable with respect to the histopathology of these MPNSTs. These mice thus permit rapid assessment of potential therapeutic interventions for MPNSTs. NP^{P0}CKO1 mice develop neurofibromas and MPNSTs simultaneous, recapitulating the development of human MPNSTs in a degenerative and inflamed peripheral nerve environment. These mice thus allows for the simultaneous assessment of how potential therapeutic interventions impacts both benign and malignant PNSTs within the same animal. All of the murine MPNST models I have developed have higher penetrance than previously documented

NPCis mice due to Schwann cell lineage specific Cre-mediated recombination. This provide greater confidence that results from pre-clinical trials are applicable to MPNSTs. Together, these new murine models of PNSTs in NF1 patients introduced in this thesis contribute valuable new reagents to the NF1 field.

The short term clinical contribution of this thesis is in directing pre-clinical trials. Based on the results presented in Chapter III, it becomes apparent that attempts to target *NF1* heterozygous cells should be directed towards NF1 patients that need to manage their pNF tumor burden. *Nf1* heterozygousity appears to only promote neurofibroma growth once *Nf1*-deficient Schwann cells have dissociated from the axons they ensheath, and does not appear to play any role in mediating malignant transformation. These efforts may also be met with greater success during early stages of pNFs, as a tumor with sufficient number of *NF1*-deficient Schwann cells may escape the requirement for a heterozygous environment, as demonstrated by *Nf1*^{Dhh}CKO2 (Wu et al., 2008) and *Nf1*^{P0}CKO2 mice. Another result presented in Chapter III that can impact pre-clinical trials is the observation that phospho-S6 levels are elevated at P90 in *Nf1*-deficient nerves but drop in later pNFs. This suggests that while mTORC1 activity may be required for neurofibroma initiation, it is no longer required, or potentially even detrimental, for later pNFs. This suggests that rapamycin and its analogs will unlikely be effective in treating patients with pre-existing pNFs. These observations from murine models of NF1 can help clinicians direct their efforts in developing effective therapies for NF1 patients.

The long term clinical contribution of this thesis is the identification of a therapeutic window that may prevent peripheral nerve sheath tumor entirely. With the data presented in Chapter II that pNFs have a critical period for LOH, there is hope that early intervention may help susceptible cells to escape a tumor fate by passing this critical time period. In chapter III, I demonstrated that rapamycin can, in some cases, alleviate the developmental defect generated by *Nf1*-deficiency, this therapeutic approach has the potential to preclude pNFs development in later life of NF1 patients completely. Since pNFs are thought to be the precursor tumors to MPNSTs, it may be possible to alleviate all peripheral nerve sheath tumors from NF1 patients by targeting neurofibroma initiating cells. Additional experiments must be performed on mice to determine the long-term consequence of stabilized *Nf1*-deficient Schwann cell-axon interactions. While rapamycin is a teratogen during early gestation in mice (Hentges et al., 2001), lethality can be avoided if administered after E13.5 with few abnormalities (Liu et al., 2007). Further investigation into equivalent stages in human peripheral nerve development and rapamycin sensitivity must be performed in order to translate this approach into an effective therapy for NF1 patients.

From a basic science perspective, I have implicated Neurofibromin as critical to early Schwann cell development. While *Nf1* does not appear to impact stem cells or differentiation in any consequential manner, it does appear to facilitate the defasciculation of individual axons into unique Schwann cell pockets. The cellular mechanism by which Neurofibromin mediates this defasciculation is currently unknown, but recent evidence that reduced Semaphorin 4F in

response to elevated Ras/ERK signaling results in proliferative Schwann cells despite axonal contact provides a potential explanatory mechanism (Parrinello et al., 2008).

It should be noted that many of the basic science and clinical insights into Neurofibromatosis Type I disease presented in this thesis would have been impossible without the use of genetically engineered mouse models. The identification of the dissociating Schwann cell as the cell-of-origin for pNFs necessitates the examination of pre-neoplastic nerve, an experiment that no NF1 patient would consent to. The impact of the *Nf1* heterozygousity on PNSTs can only be determined with well controlled genetic experiments by which *Nf1*-deficient cells are introduced to a wildtype or *Nf1* heterozygous environment. These results from these experiments clearly demonstrate the value and utility of murine models to the understanding of human diseases.

Future Directions

The body of work in this thesis has answered some of the questions I initially sought to address, but in turn has also opened up many follow up inquiries. The most promising result for clinical application is the observation that plexiform neurofibromas requires NF1 loss during development and that rapamycin treatment during this therapeutic window can reverse the earliest identifiable phenotype associated with neurofibromas. The implications of these observations will be the focus of the majority of my future directions.

The most pressing inquiry is to determine the long-term effect of transient early rapamycin intervention on *Nf1*-deficient Schwann cells, and their interactions with axons. The observation that there is a critical temporal window for *Nf1*-inactivation for PNSTs to form opens the possibility that transient rapamycin treatment during this critical window may prevent future PNSTs from arising. The experiment to test this is relatively straightforward: Administer rapamycin treatment every other day from P21 until P90 on $Nf1^{P0}$CKO1 mice and then perform histopathological analysis on the peripheral nerves at 12 months. If the early intervention is indeed capable of alleviating tumor burder later in life, I would predict that between 40% and 70% of these mice would have no tumors, in accordance with the success rate when evaluated at P90. Since peripheral nerve regeneration involves limited dedifferentiation and redifferentiation, it is possible that injuries may represent another window by which *Nf1*-deficient cells can initiate neurofibromas. Thus, it is possible that isolated pNFs may arise in treated mice at injury sites. Nonetheless, if this series of experiments demonstrates that transient early intervention with rapamycin can grant long-term PNST protection with minimal side effects, it would provide the impetus to move this therapeutic approach onto human patients.

A corollary to the last experiment is to investigate the long-term effects of transient early rapamycin on MPNSTs. The experiment to test this is also relatively straightforward: Administer rapamycin treatment every other day from P21 until P90 on NI^{P0}CKO1 and NI^{P0}CKO2 mice and determine if they develop MPNSTs at the same rate as their untreated counterparts.

My preliminary data for this experiment found that rapamycin had no significant effect on MPNST growth rates. I still need to perform follow-up experiments to determine if the sciatic nerves of these mice had stabilized Schwann cell/axon interactions. One potential rationale for the failure of this study is that these cells become *Ink/Arf/Nf1* triple deficient upon Cre-mediated recombination, which may drive the cells to malignancy regardless of rapamycin. Since MPNSTs are thought to arise from *NF1*-deficient cells that acquire additional somatic mutations, it is still possible that our approach can prevent MPNSTs in humans by limiting the pool of *NF1*-deficient cells to undergo malignant transformation. A more appropriate test may be to inactivate *Nf1* and *Ink/Arf* or *p53* in the Schwann cells after differentiation has finished to determine whether fully mature cells possess the potential to undergo malignant transformation and become MPNSTs. This experiment would necessitate a Schwann cell specific Cre-recombinase transgene that only expresses after development is complete or can be induced. If these differentiated cells indeed lose their potential to form MPNSTs, it would lend credence to the idea that transient early therapeutic intervention with rapamycin provides protection against both pNFs and MPNSTs.

Much of this preclinical research is focused on using small-molecule inhibitors to prevent neurofibromas from arising. Stromal-based therapies may prove useful in managing pNF tumor burden, but no effective therapy besides surgery exists for MPNSTs. To address pre-existing MPNSTs, I propose a personalized medicine approach which relies on the identification of the somatic mutations that facilitate malignant transformation. My malignant murine models can serve this purpose well since *p53* and *INK4a/Arf* are the two most frequently mutations associated with MPNST progression in humans. For mutant *p53* dependent MPNSTs, I have acquired a reactivatable *p53* allele (Christophorou et al., 2005) to test the effects of reactivating p53 in MPNSTs. While this may not provide a direct therapeutic approach for future clinical translations as it is currently impossible to restore p53 function in humans, it will test whether p53 is required for maintenance of MPNSTs once they have formed. For mutant *INK4a/Arf* dependent MPNSTs, I propose to investigate the integrity of the p53 pathway, especially the radiation induced apoptosis pathway. It is possible that these tumors have an intact p53 pathway, which may be activated to cause tumor cells to undergo apoptosis by ionizing radiation or small molecule inhibitors of MDM2/p53 interaction (Shangary and Wang, 2009). Through these approaches, it is possible to develop MPNST therapeutics from a basic science perspective.

An underlying theme of this thesis is the emphasis on understanding the biological underpinnings of disease processes before attempts are made to develop therapies. Despite the clamor for rapid generation of new therapies, therapies that are developed based on well understood biological processes consistently achieve greater success rates. I hope that with this thesis, I have demonstrated a positive example by which basic scientific approaches through murine modeling of human disease can lead to translatable and clinically relevant results.

References

Ballester, R., Marchuk, D., Boguski, M., Saulino, A., Letcher, R., Wigler, M., and Collins, F. (1990). The NF1 locus encodes a protein functionally related to mammalian GAP and yeast IRA proteins. Cell *63*, 851-859.

Basu, T.N., Gutmann, D.H., Fletcher, J.A., Glover, T.W., Collins, F.S., and Downward, J. (1992). Aberrant regulation of ras proteins in malignant tumour cells from type 1 neurofibromatosis patients [see comments]. Nature *356*, 713-715.

Bhaskar, P.T., and Hay, N. (2007). The two TORCs and Akt. Dev Cell *12*, 487-502.

Brannan, C.I., Perkins, A.S., Vogel, K.S., Ratner, N., Nordlund, M.L., Reid, S.W., Buchberg, A.M., Jenkins, N.A., Parada, L.F., and Copeland, N.G. (1994). Targeted disruption of the neurofibromatosis type-1 gene leads to developmental abnormalities in heart and various neural crest-derived tissues [published erratum appears in Genes Dev 1994 Nov 15;8(22):2792]. Genes & Development *8*, 1019-1029.

Brems, H., Beert, E., de Ravel, T., and Legius, E. (2009). Mechanisms in the pathogenesis of malignant tumours in neurofibromatosis type 1. Lancet Oncol *10*, 508-515.

Buchberg, A.M., Cleveland, L.S., Jenkins, N.A., and Copeland, N.G. (1990). Sequence homology shared by neurofibromatosis type-1 gene and IRA-1 and IRA-2 negative regulators of the RAS cyclic AMP pathway [see comments]. Nature *347*, 291-294.

Carey, D.J., Eldridge, C.F., Cornbrooks, C.J., Timpl, R., and Bunge, R.P. (1983). Biosynthesis of type IV collagen by cultured rat Schwann cells. J Cell Biol *97*, 473-479.

Carroll, S.L., and Ratner, N. (2008). How does the Schwann cell lineage form tumors in NF1? Glia *56*, 1590-1605.

Cawthon, R.M., Weiss, R., Xu, G.F., Viskochil, D., Culver, M., Stevens, J., Robertson, M., Dunn, D., Gesteland, R., O'Connell, P*., et al.* (1990). A major segment of the neurofibromatosis type 1 gene: cDNA sequence, genomic structure, and point mutations. Cell *62*, 193-201.

Chen, Z.L., Yu, W.M., and Strickland, S. (2007). Peripheral regeneration. Annu Rev Neurosci *30*, 209-233.

Christophorou, M.A., Martin-Zanca, D., Soucek, L., Lawlor, E.R., Brown-Swigart, L., Verschuren, E.W., and Evan, G.I. (2005). Temporal dissection of p53 function in vitro and in vivo. Nat Genet *37*, 718-726.

Cichowski, K., and Jacks, T. (2001). NF1 tumor suppressor gene function: narrowing the GAP. Cell *104*, 593-604.

Cichowski, K., Shih, T.S., Schmitt, E., Santiago, S., Reilly, K., McLaughlin, M.E., Bronson, R.T., and Jacks, T. (1999). Mouse models of tumor development in neurofibromatosis type 1. Science *286*, 2172-2176.

Colman, S.D., Williams, C.A., and Wallace, M.R. (1995). Benign neurofibromas in type 1 neurofibromatosis (NF1) show somatic deletions of the NF1 gene. Nat Genet *11*, 90-92.

De Schepper, S., Maertens, O., Callens, T., Naeyaert, J.M., Lambert, J., and Messiaen, L. (2008). Somatic mutation analysis in NF1 cafe au lait spots reveals two NF1 hits in the melanocytes. J Invest Dermatol *128*, 1050-1053.

DeBella, K., Szudek, J., and Friedman, J.M. (2000). Use of the national institutes of health criteria for diagnosis of neurofibromatosis 1 in children. Pediatrics *105*, 608-614.

DeClue, J.E., Papageorge, A.G., Fletcher, J.A., Diehl, S.R., Ratner, N., Vass, W.C., and Lowy, D.R. (1992). Abnormal regulation of mammalian p21ras contributes to malignant tumor growth in von Recklinghausen (type 1) neurofibromatosis. Cell *69*, 265-273.

Dombi, E., Solomon, J., Gillespie, A.J., Fox, E., Balis, F.M., Patronas, N., Korf, B.R., Babovic-Vuksanovic, D., Packer, R.J., Belasco, J.*, et al.* (2007). NF1 plexiform neurofibroma growth rate by volumetric MRI: relationship to age and body weight. Neurology *68*, 643-647.
Dong, Z., Sinanan, A., Parkinson, D., Parmantier, E., Mirsky, R., and Jessen, K.R. (1999). Schwann cell development in embryonic mouse nerves. J Neurosci Res *56*, 334-348.
Ducatman, B.S., Scheithauer, B.W., Piepgras, D.G., Reiman, H.M., and Ilstrup, D.M. (1986). Malignant peripheral nerve sheath tumors. A clinicopathologic study of 120 cases. Cancer *57*, 2006-2021.
Easton, D.F., Ponder, M.A., Huson, S.M., and Ponder, B.A. (1993). An analysis of variation in expression of neurofibromatosis (NF) type 1 (NF1): evidence for modifying genes. Am J Hum Genet *53*, 305-313.
Evans, D.G., Baser, M.E., McGaughran, J., Sharif, S., Howard, E., and Moran, A. (2002). Malignant peripheral nerve sheath tumours in neurofibromatosis 1. J Med Genet *39*, 311-314.
Fisher, D.A., Chu, P., and McCalmont, T. (1997). Solitary plexiform neurofibroma is not pathognomonic of von Recklinghausen's neurofibromatosis: a report of a case. Int J Dermatol *36*, 439-442.
Friedman, J.M., Arbiser, J., Epstein, J.A., Gutmann, D.H., Huot, S.J., Lin, A.E., McManus, B., and Korf, B.R. (2002). Cardiovascular disease in neurofibromatosis 1: report of the NF1 Cardiovascular Task Force. Genet Med *4*, 105-111.
Friedman, J.M., and Birch, P.H. (1997). Type 1 neurofibromatosis: a descriptive analysis of the disorder in 1,728 patients. Am J Med Genet *70*, 138-143.
Friedman, J.M., Gutmann, D.H, MacCollins, M., Riccardi, V.M. (1999). Neurofibromatosis: Phenotype, Natural History, and Pathogenesis, Third Edition edn (Baltimore and London, Johns Hopkins University Press).
Galli, S.J., Tsai, M., and Wershil, B.K. (1993). The c-kit receptor, stem cell factor, and mast cells. What each is teaching us about the others. Am J Pathol *142*, 965-974.
Giovannini, M., Robanus-Maandag, E., van der Valk, M., Niwa-Kawakita, M., Abramowski, V., Goutebroze, L., Woodruff, J.M., Berns, A., and Thomas, G. (2000). Conditional biallelic Nf2 mutation in the mouse promotes manifestations of human neurofibromatosis type 2. Genes Dev *14*, 1617-1630.
Gitler, A.D., Zhu, Y., Ismat, F.A., Lu, M.M., Yamauchi, Y., Parada, L.F., and Epstein, J.A. (2003). Nf1 has an essential role in endothelial cells. Nat Genet *33*, 75-79.
Gutmann, D.H., Aylsworth, A., Carey, J.C., Korf, B., Marks, J., Pyeritz, R.E., Rubenstein, A., and Viskochil, D. (1997). The diagnostic evaluation and multidisciplinary management of neurofibromatosis 1 and neurofibromatosis 2. JAMA *278*, 51-57.
Gutmann, D.H., Wood, D.L., and Collins, F.S. (1991). Identification of the neurofibromatosis type 1 gene product. Proc Natl Acad Sci U S A *88*, 9658-9662.
Hagel, C., Zils, U., Peiper, M., Kluwe, L., Gotthard, S., Friedrich, R.E., Zurakowski, D., von Deimling, A., and Mautner, V.F. (2007). Histopathology and clinical outcome of NF1-associated vs. sporadic malignant peripheral nerve sheath tumors. J Neurooncol *82*, 187-192.
Hentges, K.E., Sirry, B., Gingeras, A.C., Sarbassov, D., Sonenberg, N., Sabatini, D., and Peterson, A.S. (2001). FRAP/mTOR is required for proliferation and patterning during embryonic development in the mouse. Proc Natl Acad Sci U S A *98*, 13796-13801.
Huson, S.M., Harper, P.S., and Compston, D.A. (1988). Von Recklinghausen neurofibromatosis. A clinical and population study in south-east Wales. Brain *111 (Pt 6)*, 1355-1381.
Jacks, T., Shih, T.S., Schmitt, E.M., Bronson, R.T., Bernards, A., and Weinberg, R.A. (1994). Tumour predisposition in mice heterozygous for a targeted mutation in Nf1. Nat Genet *7*, 353-361.

Jessen, K.R., Brennan, A., Morgan, L., Mirsky, R., Kent, A., Hashimoto, Y., and Gavrilovic, J. (1994). The Schwann cell precursor and its fate: a study of cell death and differentiation during gliogenesis in rat embryonic nerves. Neuron *12*, 509-527.
Jessen, K.R., and Mirsky, R. (2005). The origin and development of glial cells in peripheral nerves. Nat Rev Neurosci *6*, 671-682.
Johannessen, C.M., Johnson, B.W., Williams, S.M., Chan, A.W., Reczek, E.E., Lynch, R.C., Rioth, M.J., McClatchey, A., Ryeom, S., and Cichowski, K. (2008). TORC1 is essential for NF1-associated malignancies. Curr Biol *18*, 56-62.
Johannessen, C.M., Reczek, E.E., James, M.F., Brems, H., Legius, E., and Cichowski, K. (2005). The NF1 tumor suppressor critically regulates TSC2 and mTOR. Proc Natl Acad Sci U S A *102*, 8573-8578.
Joseph, N.M., Mosher, J.T., Buchstaller, J., Snider, P., McKeever, P.E., Lim, M., Conway, S.J., Parada, L.F., Zhu, Y., and Morrison, S.J. (2008). The loss of Nf1 transiently promotes self-renewal but not tumorigenesis by neural crest stem cells. Cancer Cell *13*, 129-140.
Joseph, N.M., Mukouyama, Y.S., Mosher, J.T., Jaegle, M., Crone, S.A., Dormand, E.L., Lee, K.F., Meijer, D., Anderson, D.J., and Morrison, S.J. (2004). Neural crest stem cells undergo multilineage differentiation in developing peripheral nerves to generate endoneurial fibroblasts in addition to Schwann cells. Development *131*, 5599-5612.
Kenny, P.A., Lee, G.Y., and Bissell, M.J. (2007). Targeting the tumor microenvironment. Front Biosci *12*, 3468-3474.
King, A.A., Debaun, M.R., Riccardi, V.M., and Gutmann, D.H. (2000). Malignant peripheral nerve sheath tumors in neurofibromatosis 1. Am J Med Genet *93*, 388-392.
Kinzler, K.W., and Vogelstein, B. (1996). Lessons from hereditary colorectal cancer. Cell *87*, 159-170.
Korf, B.R. (1999). Plexiform neurofibromas. Am J Med Genet *89*, 31-37.
Kourea, H.P., Cordon-Cardo, C., Dudas, M., Leung, D., and Woodruff, J.M. (1999a). Expression of p27(kip) and other cell cycle regulators in malignant peripheral nerve sheath tumors and neurofibromas: the emerging role of p27(kip) in malignant transformation of neurofibromas. Am J Pathol *155*, 1885-1891.
Kourea, H.P., Orlow, I., Scheithauer, B.W., Cordon-Cardo, C., and Woodruff, J.M. (1999b). Deletions of the INK4A gene occur in malignant peripheral nerve sheath tumors but not in neurofibromas. Am J Pathol *155*, 1855-1860.
Krimpenfort, P., Quon, K.C., Mooi, W.J., Loonstra, A., and Berns, A. (2001). Loss of p16Ink4a confers susceptibility to metastatic melanoma in mice. Nature *413*, 83-86.
Lassmann, H., Jurecka, W., Lassmann, G., Gebhart, W., Matras, H., and Watzek, G. (1977). Different types of benign nerve sheath tumors. Light microscopy, electron microscopy and autoradiography. Virchows Arch A Pathol Anat Histol *375*, 197-210.
Legius, E., Dierick, H., Wu, R., Hall, B.K., Marynen, P., Cassiman, J.J., and Glover, T.W. (1994). TP53 mutations are frequent in malignant NF1 tumors. Genes Chromosomes Cancer *10*, 250-255.
Levine, A.J., Feng, Z., Mak, T.W., You, H., and Jin, S. (2006). Coordination and communication between the p53 and IGF-1-AKT-TOR signal transduction pathways. Genes Dev *20*, 267-275.
Lin, V., Daniel, S., and Forte, V. (2004). Is a plexiform neurofibroma pathognomonic of neurofibromatosis type I? Laryngoscope *114*, 1410-1414.
Liu, K.J., Arron, J.R., Stankunas, K., Crabtree, G.R., and Longaker, M.T. (2007). Chemical rescue of cleft palate and midline defects in conditional GSK-3beta mice. Nature *446*, 79-82.
Luongo, C., Moser, A.R., Gledhill, S., and Dove, W.F. (1994). Loss of Apc+ in intestinal adenomas from Min mice. Cancer Res *54*, 5947-5952.

Mantripragada, K.K., de Stahl, T.D., Patridge, C., Menzel, U., Andersson, R., Chuzhanova, N., Kluwe, L., Guha, A., Mautner, V., Dumanski, J.P*., et al.* (2009). Genome-wide high-resolution analysis of DNA copy number alterations in NF1-associated malignant peripheral nerve sheath tumors using 32K BAC array. Genes Chromosomes Cancer *48*, 897-907.
Martin, G.A., Viskochil, D., Bollag, G., McCabe, P.C., Crosier, W.J., Haubruck, H., Conroy, L., Clark, R., O'Connell, P., Cawthon, R.M*., et al.* (1990). The GAP-related domain of the neurofibromatosis type 1 gene product interacts with ras p21. Cell *63*, 843-849.
Mautner, V.F., Asuagbor, F.A., Dombi, E., Funsterer, C., Kluwe, L., Wenzel, R., Widemann, B.C., and Friedman, J.M. (2008). Assessment of benign tumor burden by whole-body MRI in patients with neurofibromatosis 1. Neuro Oncol *10*, 593-598.
McCaughan, J.A., Holloway, S.M., Davidson, R., and Lam, W.W. (2007). Further evidence of the increased risk for malignant peripheral nerve sheath tumour from a Scottish cohort of patients with neurofibromatosis type 1. J Med Genet *44*, 463-466.
McClatchey, A.I. (2007). Neurofibromatosis. Annu Rev Pathol *2*, 191-216.
Menon, A.G., Anderson, K.M., Riccardi, V.M., Chung, R.Y., Whaley, J.M., Yandell, D.W., Farmer, G.E., Freiman, R.N., Lee, J.K., Li, F.P*., et al.* (1990). Chromosome 17p deletions and p53 gene mutations associated with the formation of malignant neurofibrosarcomas in von Recklinghausen neurofibromatosis. Proc Natl Acad Sci U S A *87*, 5435-5439.
Messiaen, L.M., Callens, T., Mortier, G., Beysen, D., Vandenbroucke, I., Van Roy, N., Speleman, F., and Paepe, A.D. (2000). Exhaustive mutation analysis of the NF1 gene allows identification of 95% of mutations and reveals a high frequency of unusual splicing defects. Hum Mutat *15*, 541-555.
Morrison, S.J., White, P.M., Zock, C., and Anderson, D.J. (1999). Prospective identification, isolation by flow cytometry, and in vivo self-renewal of multipotent mammalian neural crest stem cells. Cell *96*, 737-749.
Nave, K.A., Sereda, M.W., and Ehrenreich, H. (2007). Mechanisms of disease: inherited demyelinating neuropathies--from basic to clinical research. Nat Clin Pract Neurol *3*, 453-464.
Nave, K.A., and Trapp, B.D. (2008). Axon-glial signaling and the glial support of axon function. Annu Rev Neurosci *31*, 535-561.
Nielsen, G.P., Stemmer-Rachamimov, A.O., Ino, Y., Moller, M.B., Rosenberg, A.E., and Louis, D.N. (1999). Malignant transformation of neurofibromas in neurofibromatosis 1 is associated with CDKN2A/p16 inactivation. Am J Pathol *155*, 1879-1884.
Parrinello, S., Noon, L.A., Harrisingh, M.C., Digby, P.W., Rosenberg, L.H., Cremona, C.A., Echave, P., Flanagan, A.M., Parada, L.F., and Lloyd, A.C. (2008). NF1 loss disrupts Schwann cell-axonal interactions: a novel role for semaphorin 4F. Genes Dev *22*, 3335-3348.
Pasmant, E., Masliah-Planchon, J., Levy, P., Laurendeau, I., Ortonne, N., Parfait, B., Valeyrie-Allanore, L., Leroy, K., Wolkenstein, P., Vidaud, M*., et al.* (2010). Identification of genes potentially involved in the increased risk of malignancy in NF1-microdeleted patients. Mol Med.
Peltonen, J., Jaakkola, S., Lebwohl, M., Renvall, S., Risteli, L., Virtanen, I., and Uitto, J. (1988). Cellular differentiation and expression of matrix genes in type 1 neurofibromatosis. Lab Invest *59*, 760-771.
Rangarajan, A., and Weinberg, R.A. (2003). Opinion: Comparative biology of mouse versus human cells: modelling human cancer in mice. Nat Rev Cancer *3*, 952-959.
Rasmussen, S.A., Yang, Q., and Friedman, J.M. (2001). Mortality in neurofibromatosis 1: an analysis using U.S. death certificates. Am J Hum Genet *68*, 1110-1118.
Reilly, K.M., and Van Dyke, T. (2008). It takes a (dysfunctional) village to raise a tumor. Cell *135*, 408-410.

Rutkowski, J.L., Wu, K., Gutmann, D.H., Boyer, P.J., and Legius, E. (2000). Genetic and cellular defects contributing to benign tumor formation in neurofibromatosis type 1. Hum Mol Genet *9*, 1059-1066.
Sabatini, D.M. (2006). mTOR and cancer: insights into a complex relationship. Nat Rev Cancer *6*, 729-734.
Sarbassov, D.D., Ali, S.M., and Sabatini, D.M. (2005). Growing roles for the mTOR pathway. Curr Opin Cell Biol *17*, 596-603.
Savage, D.G., and Antman, K.H. (2002). Imatinib mesylate--a new oral targeted therapy. N Engl J Med *346*, 683-693.
Serra, E., Rosenbaum, T., Winner, U., Aledo, R., Ars, E., Estivill, X., Lenard, H.G., and Lazaro, C. (2000). Schwann cells harbor the somatic NF1 mutation in neurofibromas: evidence of two different Schwann cell subpopulations. Hum Mol Genet *9*, 3055-3064.
Shangary, S., and Wang, S. (2009). Small-molecule inhibitors of the MDM2-p53 protein-protein interaction to reactivate p53 function: a novel approach for cancer therapy. Annu Rev Pharmacol Toxicol *49*, 223-241.
Shaw, R.J., and Cantley, L.C. (2006). Ras, PI(3)K and mTOR signalling controls tumour cell growth. Nature *441*, 424-430.
Sheela, S., Riccardi, V.M., and Ratner, N. (1990). Angiogenic and invasive properties of neurofibroma Schwann cells. J Cell Biol *111*, 645-653.
Sherr, C.J. (2001). The INK4a/ARF network in tumour suppression. Nat Rev Mol Cell Biol *2*, 731-737.
Staser, K., Yang, F.C., and Clapp, D.W. (2010). Mast cells and the neurofibroma microenvironment. Blood *116*, 157-164.
Stewart, H.J., Morgan, L., Jessen, K.R., and Mirsky, R. (1993). Changes in DNA synthesis rate in the Schwann cell lineage in vivo are correlated with the precursor--Schwann cell transition and myelination. Eur J Neurosci *5*, 1136-1144.
Taveggia, C., Zanazzi, G., Petrylak, A., Yano, H., Rosenbluth, J., Einheber, S., Xu, X., Esper, R.M., Loeb, J.A., Shrager, P*., et al.* (2005). Neuregulin-1 type III determines the ensheathment fate of axons. Neuron *47*, 681-694.
Theos, A., and Korf, B.R. (2006). Pathophysiology of neurofibromatosis type 1. Ann Intern Med *144*, 842-849.
Tidyman, W.E., and Rauen, K.A. (2009). The RASopathies: developmental syndromes of Ras/MAPK pathway dysregulation. Curr Opin Genet Dev *19*, 230-236.
Tonsgard, J.H., Yelavarthi, K.K., Cushner, S., Short, M.P., and Lindgren, V. (1997). Do NF1 gene deletions result in a characteristic phenotype? Am J Med Genet *73*, 80-86.
Trahey, M., Wong, G., Halenbeck, R., Rubinfeld, B., Martin, G.A., Ladner, M., Long, C.M., Crosier, W.J., Watt, K., Koths, K*., et al.* (1988). Molecular cloning of two types of GAP complementary DNA from human placenta. Science *242*, 1697-1700.
Tucker, T., Wolkenstein, P., Revuz, J., Zeller, J., and Friedman, J.M. (2005). Association between benign and malignant peripheral nerve sheath tumors in NF1. Neurology *65*, 205-211.
Upadhyaya, M., Kluwe, L., Spurlock, G., Monem, B., Majounie, E., Mantripragada, K., Ruggieri, M., Chuzhanova, N., Evans, D.G., Ferner, R*., et al.* (2008). Germline and somatic NF1 gene mutation spectrum in NF1-associated malignant peripheral nerve sheath tumors (MPNSTs). Hum Mutat *29*, 74-82.
Van Dyke, T., and Jacks, T. (2002). Cancer modeling in the modern era: progress and challenges. Cell *108*, 135-144.
Vigil, D., Cherfils, J., Rossman, K.L., and Der, C.J. (2010). Ras superfamily GEFs and GAPs: validated and tractable targets for cancer therapy? Nat Rev Cancer *10*, 842-857.

Viskochil, D., Buchberg, A.M., Xu, G., Cawthon, R.M., Stevens, J., Wolff, R.K., Culver, M., Carey, J.C., Copeland, N.G., Jenkins, N.A*., et al.* (1990). Deletions and a translocation interrupt a cloned gene at the neurofibromatosis type 1 locus. Cell *62*, 187-192.
Vogel, K.S., Klesse, L.J., Velasco-Miguel, S., Meyers, K., Rushing, E.J., and Parada, L.F. (1999). Mouse tumor model for neurofibromatosis type 1. Science *286*, 2176-2179.
Voiculescu, O., Charnay, P., and Schneider-Maunoury, S. (2000). Expression pattern of a Krox-20/Cre knock-in allele in the developing hindbrain, bones, and peripheral nervous system. Genesis *26*, 123-126.
Waggoner, D.J., Towbin, J., Gottesman, G., and Gutmann, D.H. (2000). Clinic-based study of plexiform neurofibromas in neurofibromatosis 1. Am J Med Genet *92*, 132-135.
Wallace, M.R., Marchuk, D.A., Andersen, L.B., Letcher, R., Odeh, H.M., Saulino, A.M., Fountain, J.W., Brereton, A., Nicholson, J., Mitchell, A.L*., et al.* (1990). Type 1 neurofibromatosis gene: identification of a large transcript disrupted in three NF1 patients. Science *249*, 181-186.
Waterston, R.H., Lindblad-Toh, K., Birney, E., Rogers, J., Abril, J.F., Agarwal, P., Agarwala, R., Ainscough, R., Alexandersson, M., An, P*., et al.* (2002). Initial sequencing and comparative analysis of the mouse genome. Nature *420*, 520-562.
Windebank, A.J., Wood, P., Bunge, R.P., and Dyck, P.J. (1985). Myelination determines the caliber of dorsal root ganglion neurons in culture. J Neurosci *5*, 1563-1569.
Woodruff, J.M. (1999). Pathology of tumors of the peripheral nerve sheath in type 1 neurofibromatosis. Am J Med Genet *89*, 23-30.
Wu, J., Williams, J.P., Rizvi, T.A., Kordich, J.J., Witte, D., Meijer, D., Stemmer-Rachamimov, A.O., Cancelas, J.A., and Ratner, N. (2008). Plexiform and dermal neurofibromas and pigmentation are caused by Nf1 loss in desert hedgehog-expressing cells. Cancer Cell *13*, 105-116.
Xu, G.F., Lin, B., Tanaka, K., Dunn, D., Wood, D., Gesteland, R., White, R., Weiss, R., and Tamanoi, F. (1990). The catalytic domain of the neurofibromatosis type 1 gene product stimulates ras GTPase and complements ira mutants of S. cerevisiae. Cell *63*, 835-841.
Yang, F.C., Chen, S., Clegg, T., Li, X., Morgan, T., Estwick, S.A., Yuan, J., Khalaf, W., Burgin, S., Travers, J*., et al.* (2006). Nf1+/- mast cells induce neurofibroma like phenotypes through secreted TGF-beta signaling. Hum Mol Genet *15*, 2421-2437.
Yang, F.C., Ingram, D.A., Chen, S., Zhu, Y., Yuan, J., Li, X., Yang, X., Knowles, S., Horn, W., Li, Y*., et al.* (2008). Nf1-dependent tumors require a microenvironment containing Nf1+/-- and c-kit-dependent bone marrow. Cell *135*, 437-448.
Zheng, H., Chang, L., Patel, N., Yang, J., Lowe, L., Burns, D.K., and Zhu, Y. (2008). Induction of abnormal proliferation by nonmyelinating schwann cells triggers neurofibroma formation. Cancer Cell *13*, 117-128.
Zhu, Y., Ghosh, P., Charnay, P., Burns, D.K., and Parada, L.F. (2002). Neurofibromas in NF1: Schwann cell origin and role of tumor environment. Science *296*, 920-922.
Zhu, Y., and Parada, L.F. (2002). The molecular and genetic basis of neurological tumours. Nat Rev Cancer *2*, 616-626.
Zhu, Y., Romero, M.I., Ghosh, P., Ye, Z., Charnay, P., Rushing, E.J., Marth, J.D., and Parada, L.F. (2001). Ablation of NF1 function in neurons induces abnormal development of cerebral cortex and reactive gliosis in the brain. Genes Dev *15*, 859-876.